



HAL
open science

Mesure de glutamate cérébral chez l'homme et le petit animal par spectroscopie RMN in vivo, application à la maladie de Parkinson

Nils Kickler

► **To cite this version:**

Nils Kickler. Mesure de glutamate cérébral chez l'homme et le petit animal par spectroscopie RMN in vivo, application à la maladie de Parkinson. Biological Physics [physics.bio-ph]. Université Joseph-Fourier - Grenoble I, 2006. English. NNT: . tel-00084812

HAL Id: tel-00084812

<https://theses.hal.science/tel-00084812>

Submitted on 10 Jul 2006

HAL is a multi-disciplinary open access archive for the deposit and dissemination of scientific research documents, whether they are published or not. The documents may come from teaching and research institutions in France or abroad, or from public or private research centers.

L'archive ouverte pluridisciplinaire **HAL**, est destinée au dépôt et à la diffusion de documents scientifiques de niveau recherche, publiés ou non, émanant des établissements d'enseignement et de recherche français ou étrangers, des laboratoires publics ou privés.

Thèse

présentée par

Nils Kickler

pour obtenir le titre de

Docteur de l'Université Joseph Fourier – Grenoble 1
(Arrêtés ministériels du 5 juillet 1984 et du 30 mars 1992)

Spécialité: Physique

Mesure de glutamate cérébral chez l'homme et le petit animal par spectroscopie RMN *in vivo*, application à la maladie de Parkinson

soutenue le 30 juin 2006

Jury

M. von Kienlin	Rapporteur
F. Durif	Rapporteur
C. Segebarth	Directeur de thèse
C. Feuerstein	Examineur
C. Roby	Examineur
V. Lebon	Examineur

Thèse préparée au sein du laboratoire INSERM U594 Neuroimagerie fonctionnelle et métabolique, Grenoble

Remerciements

J'aimerais utiliser cette première page pour remercier tous ceux qui m'ont aidé et accompagné au cours de ces trois dernières années de thèse.

Sans l'énorme soutien de **Christoph Segebarth**, en tant que directeur de thèse, et de **Chantal Rémy**, ce travail n'aurait certainement pas été terminé à ce jour. Je tiens à vous remercier pour votre encouragement, votre patience, vos discussions et corrections, pour l'ensemble de la direction d'un projet que vous avez repris. J'aimerais de même exprimer mon estimation pour **Anne Ziegler**, avec qui le travail commun était d'un grand bénéfice pour moi en ce qui concerne l'apprentissage de la RMN, mais aussi en ce qui concerne le plan personnel.

Ensemble, mais surtout avec l'aide et la grande patience de **Laurent Lamalle**, le travail sur notre imageur corps entier 3T était un vrai plaisir, révélant un appareil fascinant. Je voudrais remercier Laurent également pour sa grande disponibilité.

Les questions de la biologie et de la médecine rencontrées au cours de cette thèse m'inspirent une grande fascination et j'aimerais remercier chaleureusement tous ceux qui m'ont permis d'apprendre un tout petit peu de leur domaine de compétence. **Jonathan Coles** n'a jamais hésité d'abandonner son ordinateur pour se lancer dans des discussions sur la biologie qui étaient certainement basiques pour lui, mais d'un mystère pour moi. Du département de neurologie du CHU de Grenoble je tiens à remercier les professeurs **Pierre Pollak** et **Paul Krack** ainsi que **Valérie Fraix**, avec qui l'étude chez le patient Parkinsonien a été réalisée et qui m'ont permis au cours de ce travail d'apprendre des notions de cette maladie. Egalement, je voudrais remercier leurs patients dont la volonté de participer à notre étude et l'intérêt m'ont inspiré un grand respect. Il n'aurait pas été possible de réaliser nos mesures sans le grand soutien du professeur **Jean-François LeBas** et son équipe du service d'imagerie du CHU de Grenoble, auxquelles je voudrais également adresser mes remerciements.

L'étude sur le petit animal a été réalisée en coopération avec l'équipe de **Marc Savasta**, directeur de l'INSERM U704, et avec **Emilie Lacombe**, qui étaient responsables de tous les aspects « modèle animal ». **Régine Farion** et **Emmanuelle Grillon** assuraient la préparation des animaux pour les examens RMN. Les mesures sur les extraits PCA ont été réalisées au sein de l'équipe du professeur **Franck Durif** à l'INRA de Clermont-Ferrand, par **Carine Chassain**, et j'aimerais leur adresser mes remerciements ainsi que à nos partenaires de l'U704.

Alexandre Krainik était d'une énorme aide pendant l'évaluation des données, surtout de celles issues de l'étude sur le petit animal, et m'a ainsi « débloqué » plus qu'une fois. De même, je voudrais remercier **Roger Dupeyre** pour son soutien tout au long de cette thèse, surtout en ce qui concerne la spectroscopie RMN. Je ne saurais plus les répéter, mais j'aimerais remercier **Peggy Provent** pour son support lors d'à peu près un million

d'occasions, commencé par la commande de produits et allant jusqu'aux manip de RMN *in vivo*. Merci pour trois ans de collégialité et cordialité ! Sans doute, le bureau de Peggy avec ses autres « habitants », **Emmanuel Barbier**, **Olivier Detante**, **Samuel Valable** et **Aktham Asfour**, était une source constante de réponses et d'inspiration. Et même si son bureau se trouvait plus loin, je ne voudrais pas oublier tout le soutien d'**Alban Caporossi** avec le domptage de notre parc informatique. Encore un grand merci à mes collègues de bureau, **Boudewijn van der Sanden** et **Hervé Mathieu**, pour leur support moral et une agréable « collocation » au cours de la dernière année de thèse !

Si cette thèse présente une mise en page acceptable, c'est aussi le mérite de notre secrétaire **Marie-Claude Zanoni** et sa maîtrise de microsoft word.

Permettez-moi à la fin encore un dernier remerciement : J'aimerais remercier ma mère et son marie qui non pas seulement pendant ces trois derniers années mais pendant bien plus longtemps sont un soutien dans toutes les situations de la vie.

Enfin, merci beaucoup à vous tous, aussi à celles et à ceux que je n'ai pas nommé dans ce texte, cette thèse est issue d'un véritable travail d'équipe !

Contents

REMERCIEMENTS	3
1 INTRODUCTION.....	7
1.1 GENERAL INTRODUCTION (ENGLISH AND FRENCH)	7
1.2 BRAIN GLUTAMATE MEASUREMENT USING PROTON MAGNETIC RESONANCE SPECTROSCOPY	9
1.3 BRAIN GLUTAMATE MEASUREMENT IN RESEARCH ON PARKINSON’S DISEASE	14
2 A LOCALIZED DOUBLE QUANTUM FILTER (DQF) SEQUENCE FOR BRAIN GLUTAMATE DETECTION AT 3 TESLA	19
2.1 INTRODUCTION TO DOUBLE QUANTUM FILTERING	19
2.2 SEQUENCE DESIGN OF A DOUBLE QUANTUM FILTER FOR <i>IN VIVO</i> APPLICATIONS	23
2.3 IMPLEMENTATION OF A DQF SEQUENCE ON A 3 T WHOLE BODY IMAGER	24
2.3.1 <i>Radiofrequency pulses</i>	24
2.3.2 <i>Water suppression</i>	26
2.3.3 <i>Voxel positioning and phase calibration</i>	29
2.3.4 <i>Sequence design – Summary</i>	33
2.4 EXPERIMENTAL VALIDATION OF A DQF SEQUENCE ON A 3 T WHOLE BODY IMAGER	34
2.4.1 <i>Validation of the phase calibration procedure</i>	34
2.4.2 <i>Experiments on metabolites in solution</i>	39
2.4.3 <i>In vivo application</i>	41
2.5 CONCLUSION AND PERSPECTIVES	47
3 TE AVERAGED PRESS FOR BRAIN GLUTAMATE DETECTION AT 3 TESLA	49
3.1 INTRODUCTION	49
3.2 EXPERIMENTS ON METABOLITES IN SOLUTION	50
3.2.1 <i>Materials and methods</i>	50
3.2.2 <i>Results</i>	51
3.2.3 <i>Discussion</i>	53
3.3 <i>IN VIVO</i> APPLICATION	54
3.3.1 <i>Materials and methods</i>	54
3.3.2 <i>Results</i>	55
3.3.3 <i>Discussion</i>	59
3.4 CONCLUSION AND PERSPECTIVES	59
4 TE AVERAGED PRESS AND PRESS FOR BRAIN GLUTAMATE DETECTION AT 7 TESLA	61
4.1 INTRODUCTION	61
4.2 EXPERIMENTS ON METABOLITES IN SOLUTION AND <i>IN VIVO</i>	62
4.2.1 <i>Materials and methods in vitro experiments</i>	62
4.2.2 <i>Results of in vitro experiments</i>	64

4.2.3	<i>Materials and methods in vivo experiments</i>	68
4.2.4	<i>Results of in vivo experiments</i>	68
4.2.5	<i>Discussion in vitro and in vivo experiments</i>	69
4.3	CONCLUSION	70
5	STUDY OF GLUTAMATE LEVELS IN HUMAN PARKINSON'S DISEASE	71
5.1	INTRODUCTION	71
5.2	PATIENTS AND METHODS	72
5.3	RESULTS	75
5.4	DISCUSSION	81
5.5	CONCLUSION AND PERSPECTIVES	83
6	STUDY OF GLUTAMATE LEVELS IN A 6-OHDA RAT MODEL OF PARKINSON'S DISEASE	85
6.1	INTRODUCTION	85
6.2	MATERIALS AND METHODS.....	87
6.2.1	<i>Experimental procedure</i>	87
6.2.2	<i>In vivo MRS</i>	89
6.2.3	<i>Postprocessing of in vivo spectra</i>	91
6.2.4	<i>In vitro MRS</i>	92
6.2.5	<i>Postprocessing of in vitro spectra</i>	92
6.2.6	<i>Statistics</i>	93
6.3	RESULTS	93
6.4	DISCUSSION	107
6.5	CONCLUSION AND PERSPECTIVES	109
7	GENERAL CONCLUSION AND PERSPECTIVES (ENGLISH AND FRENCH)	111
8	ANNEX	115
8.1	CHEMICAL SHIFTS AND COUPLING CONSTANTS OF SOME BRAIN METABOLITES	115
8.2	METABOLITE CONCENTRATIONS IN THE RAT BRAIN: LITERATURE VALUES.....	117
8.3	TE AVERAGED PRESS AT 7 TESLA: NUMERICAL SIMULATIONS	118
8.3.1	<i>Materials and Methods</i>	118
8.3.2	<i>Results</i>	119
8.3.3	<i>Discussion</i>	121
8.4	PRESS AT 7 TESLA AND AN ECHO TIME OF 136 MS: EXPERIMENTS ON METABOLITES IN SOLUTION.....	122
8.4.1	<i>Materials and methods</i>	122
8.4.2	<i>Results</i>	122
8.4.3	<i>Discussion</i>	123
9	REFERENCES	124

1 Introduction

1.1 General introduction (English and French)

Français

La résonance magnétique nucléaire (RMN) constitue de nos jours l'un des outils les plus importants pour l'étude de systèmes biologiques. Utilisée *in vitro*, les applications les plus courantes concernent les analyses biochimiques et la détermination de la structure et du dynamique de grandes molécules biologiques comme les protéines. Au cours des dernières vingt années, l'imagerie par résonance magnétique est devenue un outil de routine, tant dans la pratique clinique que dans la recherche médicale et biomédicale, offrant un contraste supérieur entre différents tissus mols sans recours aux radiations ionisantes. La spectroscopie par résonance magnétique a été appliquée *in vivo* dès les premiers jours, mais ce n'est que depuis les années 1980 avec la mise en place des bobines de surface que des techniques optimisées pour une pareille utilisation ont été développées. La mise en place de techniques de localisation du signal et des progrès concernant la suppression du signal de l'eau en spectroscopie du proton (^1H) ont permis d'obtenir une multitude d'informations spectroscopiques, par exemple, concernant le métabolisme énergétique du cerveau ou concernant les acides aminées.

Les signaux de lactate, n-acétylaspartate, créatine et choline sont facilement observés dans des spectres du proton acquis sur le cerveau. La mesure de la plupart des autres molécules présentes dans le cerveau est rendue difficile du fait de leur signature spectrale compliquée, par l'importante largeur des raies habituellement observée *in vivo* et par la présence d'un grand nombre de raies dans une petite largeur spectrale. Ainsi, l'observation du neurotransmetteur glutamate dans des spectres RMN reste difficile malgré sa concentration relativement élevée qui est de l'ordre de 10 mM dans le cerveau humain. La détection de glutamate, l'un des neurotransmetteurs les plus importants du cerveau humain, présente pourtant un grand intérêt, d'autant de plus qu'il est impliqué dans certaines maladies neurodégénératives, comme la maladie de Parkinson.

Le but du présent travail était la mise en place de techniques de spectroscopie RMN permettant la détection de glutamate chez l'homme et le petit animal et l'évaluation de leur potentiel dans le cadre de la recherche sur la maladie de Parkinson.

La suite de ce premier chapitre situe la mesure du glutamate dans le contexte de la méthodologie RMN et dans celui de la recherche sur la maladie de Parkinson. Pour des applications chez l'homme à 3 Tesla, une technique de filtrage à double quanta ainsi qu'une méthode liée à la spectroscopie bidimensionnelle ont été mises en place. L'évaluation de ces techniques est décrite dans les chapitres 2 et 3. La méthode basée

sur la spectroscopie bidimensionnelle a ensuite été comparée à des techniques PRESS conventionnelles à 7 Tesla pour des applications sur le petit animal, voir chapitre 4. Les chapitres 5 et 6 présentent les résultats de deux études faites chez le patient Parkinsonien et sur le modèle animal de cette maladie pour évaluer la possibilité de mesurer des changements pathologiques des concentrations de glutamate.

English

Nuclear magnetic resonance techniques present today one of the most important tools for studies of biological systems. *In vitro*, common applications of magnetic resonance spectroscopy (MRS) concern biochemical analysis as well as the determination of structure and dynamics of large biomolecules such as proteins. During the last two decades, magnetic resonance imaging has developed to a routine tool for medical diagnosis and fundamental research, providing high soft tissue contrast without requiring ionizing radiation. Magnetic resonance spectroscopy has been applied *in vivo* from the early beginning of NMR, but dedicated techniques for *in vivo* MRS were not developed until the 1980s after surface coils had been set up. Especially mono- or multi-voxel localization techniques, using magnetic field gradients, as well as advancements concerning water suppression in proton (^1H) spectroscopy, have permitted *in vivo* MRS to provide a wealth of non-invasive spectroscopic information on, for example, energy metabolism and amino acids.

Signals of lactate, n-acetylaspartate, creatine and choline containing compounds are easily observed in *in vivo* ^1H spectra of brain structures. Detection of other brain metabolites presents difficulties, mainly due to complicated spectral signatures and large linewidths *in vivo*. The neurotransmitter glutamate is present at relatively high concentration in the human brain (about 10 mM) but figures among the metabolites that are not readily observable. As one of the principal neurotransmitters in the brain, its detection *in vivo* is however of high interest in many pathologies, such as Parkinson's disease (PD). Abnormal activation of glutamate systems in the basal ganglia has been recognized to play a central role in the pathophysiology of this disease.

In the present work, we aimed at evaluating the potential of *in vivo* magnetic resonance spectroscopy for the detection of brain glutamate and examine the utility of such measurements for research on Parkinson's disease. The following sections of this first chapter situate the detection of brain glutamate within the methodological context of magnetic resonance spectroscopy and within the medical context of Parkinson's disease. For application in a clinical context, a double quantum filter technique and a technique related to two dimensional MRS were evaluated for glutamate detection at three Tesla field strengths. Results of this methodological evaluation are presented in chapters 2 and 3. The method based on two-dimensional spectroscopy was then examined for use at higher field strengths (7 Tesla) for research applications in a biomedical context and compared to a standard (PRESS) technique (chapter 4). To investigate the possibility to detect pathological abnormalities of glutamate concentrations in Parkinson's disease,

MRS was applied to measurements on patients affected by Parkinson's disease (chapter 5) and to a rat animal model (chapter 6) of PD.

1.2 Brain glutamate measurement using proton magnetic resonance spectroscopy

Proton NMR spectra of the mammalian brain present high information content, as ^1H atoms, of which the magnetic resonance signal is used, are present in almost every brain metabolite. At the same time, because of the small chemical shift range of the proton, the abundance of signals leads to strong overlap between peaks of different molecules and thereby to serious problems of analytical discrimination. At least 35 different brain metabolites give rise to multiple resonances in a spectral range of only 2.4 ppm (Govindaraju, Young et al. 2000). Standard techniques as PRESS or STEAM readily allow the identification of resonances of n-acetylaspartate (NAA) and of choline (cho) and creatine (cr) containing compounds at field strengths of 1.5 T. The identification and quantification of other metabolite resonances often requires a more sophisticated approach. When trying to obtain information about the less concentrated metabolites, which very often present strongly coupled spins giving rise to complicated multiplett structures, three broad options are available *in vivo*:

The most straightforward method to reduce or even eliminate spectral overlap is to increase the magnetic field strength. Higher frequency dispersions due to chemical shift together with higher sensitivity and reduced strong coupling effects increase significantly the number of identifiable metabolites. In combination with very short echo times of about 2 ms, up to 18 molecules can be identified *in vivo* (Pfeuffer, Tkac et al. 1999). High field magnets (7 to 9.4 Tesla) for *in vivo* NMR applications are however very expensive and only very few machines for human applications exist to this day. Full gain in spectral quality may only be obtained if increased susceptibility differences, caused by increased field strengths, are compensated by optimized shimming, as can be achieved for example using the FASTMAP procedure (Gruetter 1993). Strong shimming coil systems, allowing adjustment of at least second order terms, are needed, which until recently were only available as custom made fabrications. Implementation and use of short echo time techniques furthermore demands effective water and macromolecule suppression and precise calibration of the gradient coil system to prevent contamination by eddy currents. In summary, next to high field strengths this approach demands strong gradient coil systems and extensive machine calibrations.

Another approach consists in the acquisition of more information by way of a two-dimensional spectrum (Ziegler, Izquierdo et al. 1995). Some signals of coupled spins overlapping in normal one dimensional spectra become resolved in the second dimension of a 2D spectrum. The acquisition of a two dimensional spectrum is however time consuming, as the second spectral dimension, comparable to the second spatial dimension of an image, is obtained following repeated acquisitions with a parameter varied within the sequence.

Spectral editing techniques that utilize differences in scalar coupling present a third approach. The information content of the one dimensional spectrum is reduced so as to observe only a single spectral shape from a single metabolite ((Shen, Rothman et al. 2002) for example). As usually only one metabolite is targeted, phasing and quantification of an edited spectrum is difficult due to lack of a reference signal. Quantification may for example be achieved using the (singlet-) signal of an unedited reference spectrum acquired from the same region. Phasing problems may be circumvented by evaluating the spectrum in magnitude mode or by comparison to a simulated spectrum. The major drawback of many editing approaches is however their overall signal loss. As a part of this work concerns double quantum filtered editing, further details are discussed in the next chapter.

Together with all approaches of signal acquisition, identification of overlapping resonances is further improved by use of adapted quantification methods.

In some cases, resonance lines may be approximated by Lorentzian peakshapes; these can be fitted directly to the spectrum. Related approaches, instead of working in the spectral domain, rely on adjusting exponentially decaying functions in the time domain (Vanhamme, van den Boogaart et al. 1997). Prior knowledge, such as peak positions and frequency spacing between peaks, may be incorporated in the fitting routine and improve its reliability.

Instead of fitting Lorentzian peakshapes to each resonance line observed, it is also possible to adjust complete spectra of individual metabolites to the *in vivo* spectrum (Provencher 1993). The model spectra may be obtained from simulations or from *in vitro* solutions. Complicated, non-Lorentzian spectral shapes can be evaluated and it is possible to resolve complex spectral pattern (Pfeuffer, Tkac et al. 1999). This approach is laborious, as model spectra using exactly the same parameters as for the acquisition *in vivo* have to be produced for all metabolites.

The task of glutamate measurement is part of the general challenge to gain information about coupled brain metabolites. Glutamate presents five coupled ^1H spins, resonating at 3.7 ppm and in a small region near 2.3 ppm. The molecule and its chemical shifts are displayed in Fig. 1.1, together with the molecules of glutamine, NAA and GABA. In usual *in vivo* spectra, the glutamate signal overlaps strongly with the signals of glutamine, γ -aminobutyric acid (GABA) and the aspartate moiety of NAA (Govindaraju, Young et al. 2000). Fig. 1.2 shows a high resolution spectrum acquired from a PCA extract of a rat brain to demonstrate the proximity of resonances in the spectral area at 2.3 ppm (reproduced from (Govindaraju, Young et al. 2000)).

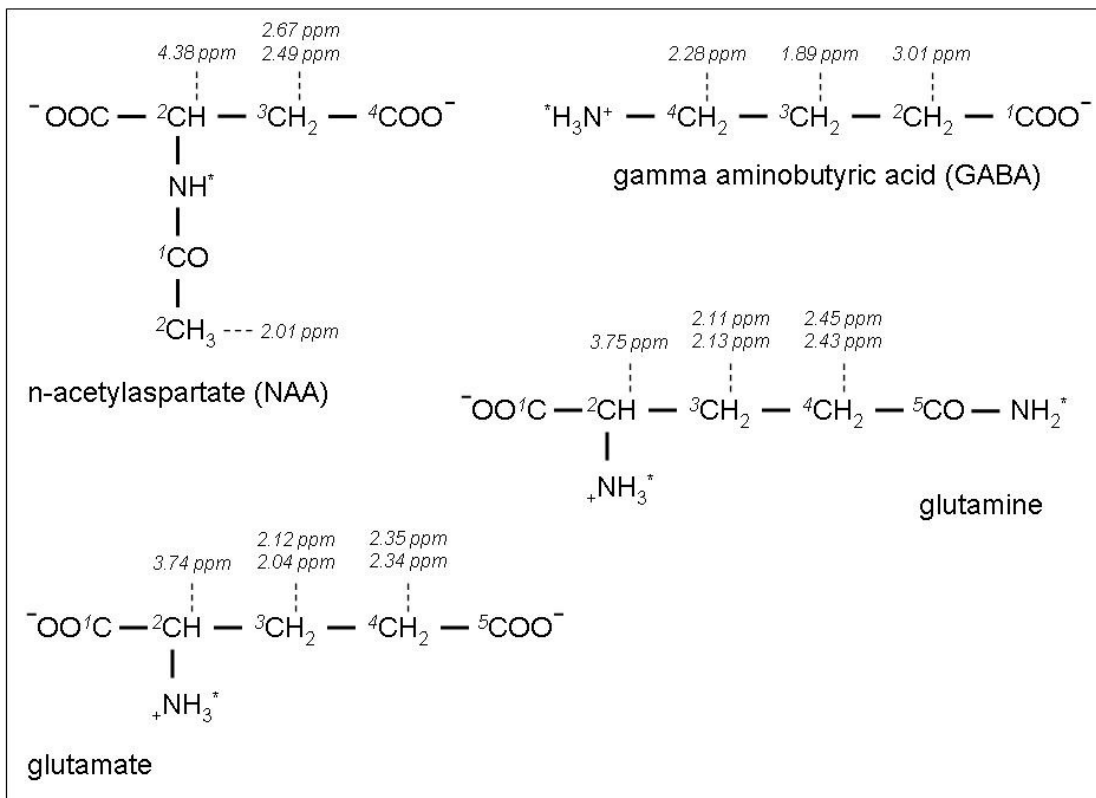


Fig. 1.1: Molecular structure of n-acetylaspartate (NAA), gamma aminobutyric acid (GABA), glutamate and glutamine. In the targeted chemical shift range for *in vivo* glutamate measurement, near 2.3 ppm, the resonance lines of these four molecules overlap. Chemical shifts were taken from (Govindaraju, Young et al. 2000). Protons marked by an asterisk are in rapid exchange with water.

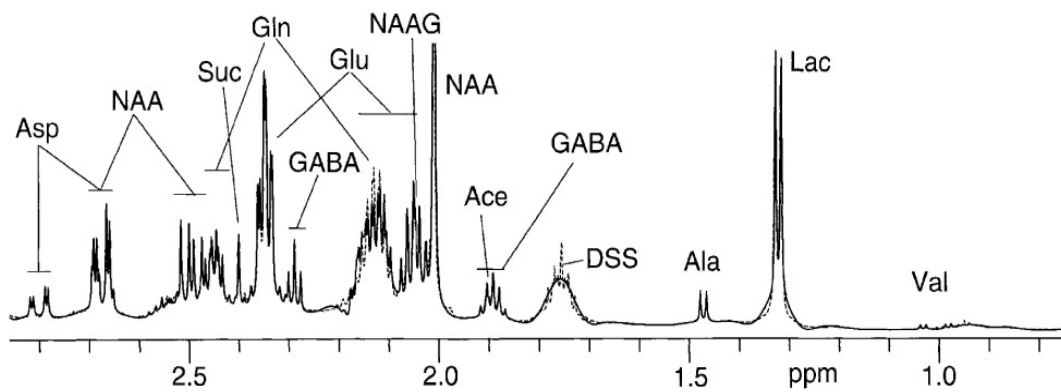


Fig. 1.2: High resolution ^1H spectrum of a PCA extract from a rat brain obtained at 600 MHz (dashed line) and results of spectral analysis (solid line). The vertical scale has been increased, resulting in truncation of the NAA singlet resonance. Figure reproduced from (Govindaraju, Young et al. 2000).

Efforts to measure glutamate unobstructed from contributions of other metabolites usually target the chemical shift range near 2.3 ppm, because glutamate overlaps inseparably with glutamine at 3.7 ppm. The challenge of glutamate measurement stems from four principal difficulties.

First, the spectral pattern of glutamate in the 2.3 ppm region is highly complicated and analytically difficult to predict because of strong coupling effects at most field strengths that are available for *in vivo* experiments. At 3 Tesla, all spin groups resonating in the 2.3 ppm region have to be considered as strongly coupled, as can be seen in Table 8.1, annex. At 7 T, most spin groups are at the limit where strong coupling effects may be neglected.

A second difficulty is the low intensity of glutamate pattern *in vivo*. As the signal intensity is split on a multitude of peaks (see (Govindaraju, Basus et al. 1998), the signal amplitude of each peak remains low in spite of the relatively high glutamate concentration in the human brain (6 mmol/kg_{ww} to 12 mmol/kg_{ww}). The spectrum shown in Fig. 1.2 has been acquired at a field strength, where glutamate, glutamine, NAA and GABA may be described as weakly coupled system. At 2.15 ppm and 2.35 ppm, the numerous peaks of glutamate are well visible. The maximal amplitude of glutamate remains far below the amplitude of the (cropped) NAA singlet at 2.0 ppm. NAA is present in the rat brain in concentrations of about 9 mmol/kg_{ww}.

Glutamate and glutamine present a highly similar molecular structure, leading to almost equal chemical shifts and coupling constants in the proton spin groups of both metabolites. Separating glutamate from glutamine presents a third major difficulty. The spin groups of glutamine, NAA and GABA giving rise to resonances in the targeted chemical shift range for glutamate measurements, near 2.3 ppm, present strong coupling features themselves, complicating further all approaches for glutamate measurement. At 3 Tesla field strength the respective spin groups have to be considered strongly coupled, as for glutamate. At 7 Tesla, glutamine (as glutamate) is at the limit to weak coupling behavior for most of its spins. GABA may be considered weakly coupled, but the two spins of NAA present in the targeted chemical shift range, resonating at 2.5 ppm and 2.7 ppm, remain strongly coupled.

Several studies concerning glutamate measurement may be found in the literature. A very successful approach combines high fields (7 T, 9.4 T), short echo time (2 ms to 6 ms) and high performance shimming (FASTMAP, (Gruetter 1993)) and uses a fit of model spectra (LC model, (Provencher 1993)) for quantification (Pfeuffer, Tkac et al. 1999; Tkac, Andersen et al. 2001). Glutamate and glutamine may be resolved from each other and from the resonances of NAA and GABA and can be quantified by this technically and instrumentally highly demanding technique.

At lower field strengths, at 3 Tesla, short echo time spectra do not display a visually distinguishable glutamate signal (Zhong and Ernst 2004). In this case, some authors propose to rely on fitting procedures, fitting model spectra to the *in vivo* spectrum, in

order to obtain information about glutamate concentrations (Boumezbeur, Besret et al. 2005; Jang, Lee et al. 2005).

At these field strengths, editing techniques present another promising approach. Double quantum filter sequences and J-refocused (Lee, Yaman et al. 1995) spectral editing techniques have been applied to *in vivo* glutamate measurement at 3 Tesla (Thompson and Allen 1998; Schubert F 2001) and 4.1 Tesla (Pan, Mason et al. 1996) field strengths. Double quantum filtering will be further detailed in the following chapter. J-refocused editing relies on suppression of J-coupling evolution, assuring that spectra acquired at different echo times present similar spectral shapes for coupled spin systems (for details, see (Lee, Yaman et al. 1995; Pan, Mason et al. 1996)). Glutamate and glutamine have shorter transverse relaxation times than the other metabolites as NAA, creatine and GABA. Glutamate (glu) and glutamine (gln) can therefore be differentiated from the other metabolites using their T_2 relaxation rate: Two measurements with different TE values are performed and subtracted in the J-refocused editing technique. The difference spectrum contains mainly glutamate and glutamine, whereas other metabolites are reduced by subtraction.

Only recently, two-dimensional spectroscopy techniques have been successfully applied to glutamate measurement at 3 Tesla field strengths. These techniques rely on J-resolved acquisitions (Hurd, Sailasuta et al. 2004) or constant time PRESS (CT-PRESS) (Mayer and Spielman 2005; Schulte, Trabesinger et al. 2005) sequences, that have been optimized for glutamate detection. Not the whole two dimensional spectrum is used for evaluation but only one dimensional cuts, fixing one of the two frequency dimensions. For example, TE averaged PRESS uses the central trace of a 2D spectrum ($f_1 = 0$). J-resolved acquisitions of this type will be described in a later chapter. CT-PRESS uses signal preparation as PRESS. Spectra with different echo times are acquired; the acquisition window starts however always at a fixed delay after the first PRESS excitation pulse. The different spectra display identical J coupling evolutions but differing chemical shift evolutions. A Fourier transformation as a function of the echo time therefore gives a two dimensional spectrum where the usual frequency domain contains J and chemical shift information, the additional dimension, corresponding to the echo time, however displays only chemical shift information. After optimization of the sequence parameters, spectra displaying a glutamate signal almost free of contamination by other metabolites can be acquired (Mayer and Spielman 2005).

The present work concerns glutamate measurement at low field (3 T) in a clinical environment and at high field (7 T) for biomedical research. In the clinical environment, we have first followed an editing and later a 2D approach for glutamate measurement. At high field, satisfactory results for biomedical research were obtained with a standard point resolved spectroscopy (PRESS) method.

1.3 Brain glutamate measurement in research on Parkinson's disease

Parkinson's disease (PD) was first described by James Parkinson in the year 1817 as a single disease entity. PD is a chronic, progressive neurodegenerative brain disease, afflicting about 1 in 1000 persons of the population and about 1 in 100 persons older than 60 years. Principal clinical symptoms are tremor, rigidity and akinesia (loss or impairment of voluntary activity, as of a muscle). Between 15 and 30 % of the patients develop psychological problems as depression or dementia in an advanced disease state. Eighty percent of all patients suffer from idiopathic Parkinson's disease for which no cause is known.

Degeneration of the melanized neurons in the substantia nigra pars compacta (SNc), which contain the chemical dopamine as neurotransmitter, is one of the most important neuropathological features of Parkinson's disease. The reduction of dopamine affects functioning of the basal ganglia, implied in the control of movement. A model of the functional organization of the basal ganglia and alterations in the case of Parkinson's disease is shown in Fig. 1.3 (Obeso, Rodriguez-Oroz et al. 2000). Fig. 1.4 and Fig. 1.5 situate the implied brain structures in the human and in the rat brain. In this (simplified) model, the putamen is the "input" structure, receiving inhibitory projections (blue) from the cortical areas implied in movement control. In a more developed model of the same reference (Obeso, Rodriguez-Oroz et al. 2000), these projections are assumed as excitatory. The "output" structure are the internal segment of the globus pallidus (GPi) and the reticular part of the substantia nigra (SNr). These send inhibitory projections to the ventral anterior – ventral lateral thalamus (VL), which send back excitatory (red) projections to the cortical motor areas. Input and output structures are connected via two pathways, the direct pathway, projecting from putamen to GPi and SNr and the indirect pathway. The indirect pathway links the putamen with the "output structure" via projections to the external part of the globus pallidus (GPe) and from there to the subthalamic nucleus (STN). The arrangement of excitatory and inhibitory projections is such that stimulation of the direct pathway facilitates thalamocortical excitatory activity and stimulation of the indirect pathway exerts an inhibition. The role of nigrostriatal dopamine is to balance these two functionally opposing systems. Different dopamine receptors, D1 and D2, of the neurons projecting to GPe (D2) and GPi (D1) from the putamen make that dopamine enhances the activity of the direct pathway and inhibits the indirect pathway.

In the case of Parkinson's disease, the degeneration of the melanized neurons in the substantia nigra pars compacta (SNc) leads to reduction of dopamine concentration in the putamen and thereby to a reduction of the balancing dopamine influence on the two pathways. The end result of this misbalance is a reduction of the thalamocortical excitatory projection and thereby an inhibition of the cortically initiated movement.

As can be seen in Fig. 1.3, right, dopamine reduction stimulates the inhibitory projection of the external part of the globus pallidus (GPe) and thereby releases the

subthalamic nucleus (STN) from its inhibition. This release leads to hyperactivity of the glutamatergic (excitatory) projections from the subthalamic nucleus to the internal part of the globus pallidus and the reticular part of the substantia nigra (SNr). Inhibition of the thalamus is thereby increased and feedback to the cortical motor areas decreased.

Most current treatments of the symptoms of Parkinson's disease rely on replacement of dopamine by administration of its precursor, L-DOPA (levodopa), which is transformed to dopamine in the striatum. About 90% of patients respond to levodopa treatment. Whereas in the first years of treatment, levodopa administration strongly reduces Parkinson symptoms, side effects appear after several years. Probably because of loss of storage capacity of the formed dopamine, action duration of an administered levodopa dose becomes shortened. Dyskinesias (impairment of voluntary movements resulting in fragmented motions) may appear at any time during chronic levodopa treatment. They may be due to relative overdosage or development of supersensitivity of dopamine receptors.

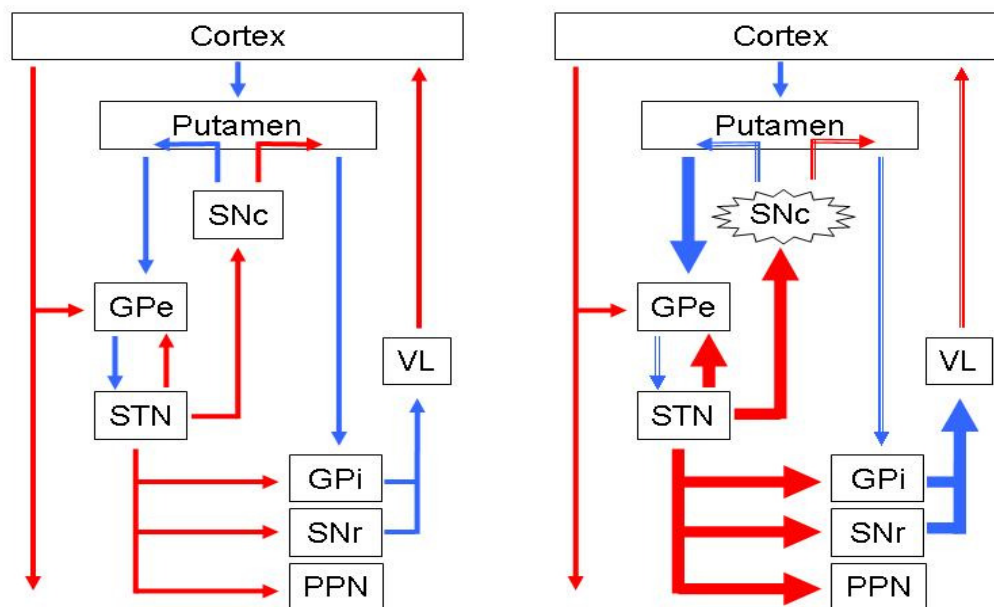


Fig. 1.3: Schematic of the classic model of the basal ganglia, reproduced from (Obeso, Rodriguez-Oroz et al. 2000). The left figure displays the normal state, the right figure the case of Parkinson's disease. Blue arrows indicate inhibitory projections and red arrows excitatory projections. In the parkinsonian state (right figure), thick arrows indicate hyperactivity of the representative projection and double lines hypoactivity. For further descriptions please refer to the text, for a placement of the anatomical structures in human and rat brain to Fig. 1.4 and Fig. 1.5. Abbreviations: GPe: globus pallidus pars externa, GPi: globus pallidus pars interna, SNc: substantia nigra pars compacta, STN: subthalamic nucleus, SNr: substantia nigra pars reticularis, VL: ventralis lateralis (of thalamus), PPN: pedunculopontine nuclei.

The existence of animal models allows the study of specific aspects of Parkinson's disease, as functional organization of the basal ganglia and its alteration following dopamine depletion. A widely used model, in the rat, relies on administration of the neurotoxin 6-hydroxydopamine (6-OHDA). Injection of 6-OHDA in the substantia

nigra of the rat brain leads to degeneration of the dopaminergic neurons and thereby to lesion of the nigrostriatal pathway. The mechanisms of toxicity of 6-OHDA rely on introduction of oxidative stress via inhibition of mitochondrial respiration.

Functional organization and interaction of different brain structures as the basal ganglia are far from being understood and remain a field of intensive research. The model shown in Fig. 1.3 certainly represents a strong simplification and may only explain specific facts. It demonstrates however how the loss of striatal dopamine via the interaction between different structures may give rise to changes in other basal ganglia neurotransmitter systems.

Several results demonstrate increase of striatal glutamatergic activity in case of Parkinson's disease or in the animal model. Increased glutamate concentrations as compared to a control group have been measured post-mortem in the putamen of PD patients (subgroup of three from nine patients) (Kish, Rajput et al. 1986) using high performance liquid chromatography (HPLC). Anatomical studies in the 6-OHDA rat model have demonstrated an increase in the density of synapses associated with glutamatergic activity one month following the lesion of the nigrostriatal pathway (Meshul, Emre et al. 1999; Meshul, Cogen et al. 2000). *In vivo* microdialysis allows the direct assessment of extracellular glutamate levels. In the same animal model, increases of striatal extracellular glutamate as compared to control rats have been demonstrated by several groups. Measured increases vary from 45% (Jonkers, Sarre et al. 2002) and 56% (Bruet, Windels et al. 2003) up to 146% (Meshul, Emre et al. 1999). However, also contradictory results have been found by other groups (Robelet, Melon et al. 2004).

Changes in striatal glutamatergic activity caused by dopamine depletion present a central point in Parkinson's disease. It has been hypothesized that agents acting to restore normal glutamatergic function may provide therapeutic interventions improving current levodopa therapies (Chase, Oh et al. 2000; Marino, Valenti et al. 2003). The ability to measure glutamate in the framework of research on Parkinson's disease is therefore of strong interest.

Most studies concerning glutamate measurement in Parkinson's disease have been performed post-mortem or using invasive techniques as microdialysis. Magnetic resonance spectroscopy (MRS) is non invasive, permitting the measurement of principal brain metabolites. Clinical studies involving patients are possible without major problems. Animal studies may profit from the possibility to follow long term disease developments on the same animal (Brownell, Jenkins et al. 1998). Compared to microdialysis techniques, MRS brings in a complementary point of view. Microdialysis assesses extracellular glutamate concentrations, which are on the scale of nanomol (Fillenz 2005). Glutamate concentrations measured by MRS are on the order of millimol and stem mainly from an intracellular origin (see Table 8.3).

In the clinical environment, Parkinson's disease has been extensively studied using MRS (Bowen, Block et al. 1995; Davie, Wenning et al. 1995; Holshouser, Komu et al. 1995; Clarke, Lowry et al. 1997; Cruz, Aminoff et al. 1997; Ellis, Lemmens et al. 1997;

Federico, Simone et al. 1997; Tedeschi, Litvan et al. 1997; Hoang, Bluml et al. 1998; Hu, Taylor-Robinson et al. 1999; Ross, Hoang et al. 1999; Taylor-Robinson, Turjanski et al. 1999; Abe, Terakawa et al. 2000; Clarke and Lowry 2000; Lucetti, Del Dotto et al. 2001; O'Neill, Schuff et al. 2002; Baik, Choe et al. 2003; Camicioli, Korzan et al. 2004). The strong peaks of choline, creatine and n-acetylaspartate have been investigated to detect differences between healthy subjects and PD patients or to distinguish between forms of Parkinsonism. Because of different experimental protocols, results are difficult to compare (Clarke and Lowry 2001; Firbank, Harrison et al. 2002) and are contradictory. For the NAA to creatine or NAA to choline ratios for example, some groups find decreased values in PD whereas others state no difference between healthy subjects and PD patients (Clarke and Lowry 2001).

Only very few investigators have so far addressed the problem of glutamate measurement (Clarke, Lowry et al. 1997; Taylor-Robinson, Turjanski et al. 1999; Clarke and Lowry 2000). Alterations of the glutamate level in patients affected by PD could not be demonstrated in these studies, using however MRS techniques not optimized for glutamate measurement.

Magnetic resonance spectroscopy has as well been used for studies on the animal model (Brownell, Jenkins et al. 1998; Podell, Hadjiconstantinou et al. 2003). Only a recent study addresses the specific problem of glutamate measurement, using carbon-13 MRS at 4.7 Tesla field strengths (Chassain, Bielicki et al. 2005). Using the carbon-13 nucleus for MR spectroscopy facilitates resolution of glutamate from other metabolites. However, it is dependant on the infusion of an agent enriched in ^{13}C , such as $[2-^{13}\text{C}]$ sodium acetate in the study of Chassain et al. The authors demonstrate that significant increase of ^{13}C label incorporation into glutamate occur in the rat Parkinson model. These changes are normalized by L-DOPA administration. The information obtained from ^{13}C experiments is different from the one obtained with proton spectroscopy, as the incorporation of the marker in the molecule to be studied is observed, not solely the (static) molecule content.

It was therefore interesting to address the problem of glutamate measurement in Parkinson's disease using proton magnetic resonance spectroscopy. Proton MRS was chosen for its high sensitivity and as the equipment, as opposed to the one necessary for carbon spectroscopy, is usually available with any MR machine. Furthermore, proton-MR spectroscopy techniques present higher potential for transfer to the clinical environment.

With this work, we would like to add a study addressing the problem of glutamate measurement in human PD, using a new MRS technique (TE averaged PRESS (Hurd, Sailasuta et al. 2004)) optimized for glutamate detection. Complementary to the study on the patient, we have performed MRS experiments on the 6-OHDA rat model of PD.

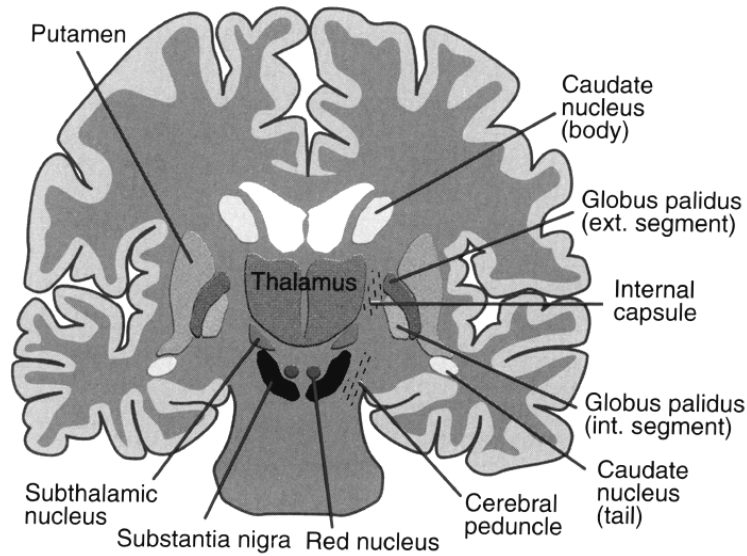


Fig. 1.4: Schematic picture of the basal ganglia (striatum (putamen and caudate nucleus), globus pallidus (internal and external segment), subthalamic nucleus and substantia nigra) and other structures in the human brain. The combined structure of putamen and globus pallidus is sometimes called lentiform nucleus.

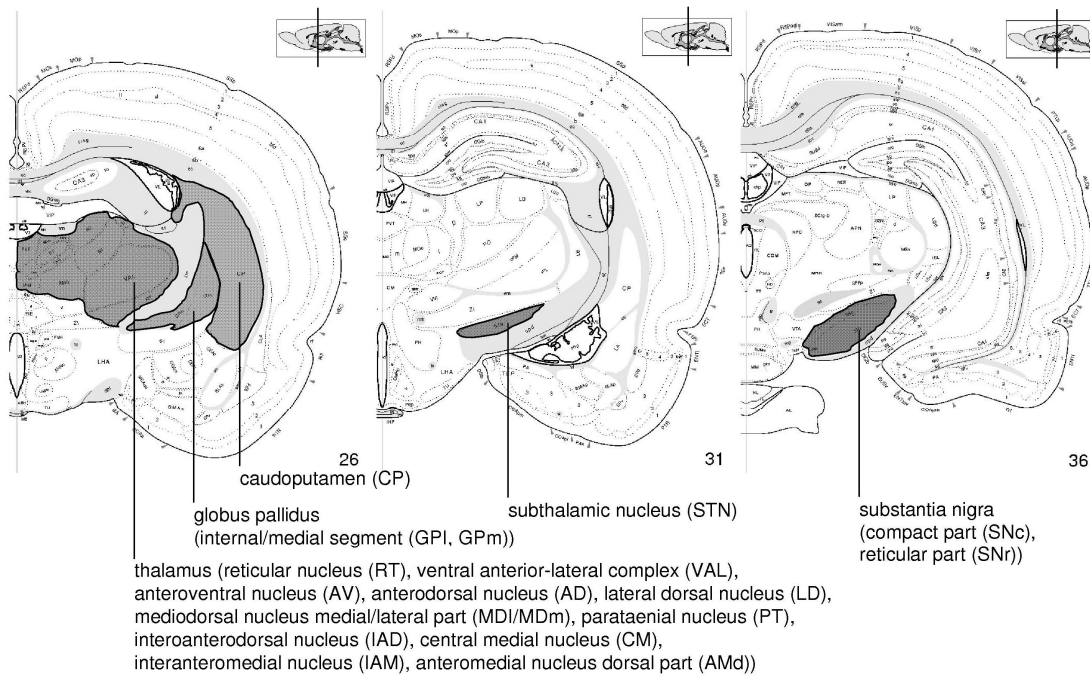


Fig. 1.5: Map of the rat brain (single hemisphere) as taken from (Swanson 1998/1999). Structures implied in the basal ganglia motor cycle as described in Fig. 1.3 have been indicated. The small insert on the top-right of each picture situates the position of the cut in the rat brain. The caudoputamen in the rat brain corresponds to the striatum in the human brain, as caudate nucleus and putamen are not distinguished in the rat.

2 A localized double quantum filter (dqf) sequence for brain glutamate detection at 3 Tesla

Les séquences de filtrage à plusieurs quanta offrent des propriétés intéressantes pour les applications in vivo. Une bonne suppression du signal de l'eau indépendamment de sa fréquence de résonance est autant un facteur clé que la possibilité de filtrer un signal sans la nécessité d'ajouter plusieurs acquisitions. Le filtrage à deux quanta avec localisation spatiale du signal a été proposé pour la mesure de glutamate cérébral (Thompson and Allen 1998).

Ce chapitre présente une introduction aux principes de filtrage à deux quanta. Ensuite, une séquence optimisée pour la détection de glutamate cérébral est présentée (Thompson and Allen 1998). Son implémentation sur un imageur corps entier à 3 Tesla est décrite en détail.

Double and multiple quantum coherence editing sequences present properties interesting for *in vivo* applications. Of advantage are good, frequency independent water suppression and single-scan editing capability. Localized double quantum filtering (dqf) has for example been proposed for the *in vivo* detection of cerebral glutamate at field strengths of 3 Tesla (Thompson and Allen 1998).

This chapter begins with an introduction to the principles of double quantum editing. Then, a sequence optimized for brain glutamate detection (Thompson and Allen 1998) is described. Its implementation and test on a 3 Tesla whole body MRI is in the following reported in detail.

2.1 Introduction to double quantum filtering

Multiple quantum coherence editing sequences use selective preparation of multiple quantum coherences (mqc) on a targeted molecule to distinguish it from the overlapping signals of its vicinity. Subgroups of this type of sequences are double quantum filters using magnetic field gradients. This sequence type, as used for homonuclear spectral editing, will be described in this section.

Double and multi quantum coherence editing has been applied targeting different brain metabolites such as GABA (Du, Chu et al. 2004), glucose (Keltner, Wald et al. 1997), taurine (Lei and Peeling 1999) or glutathione (Trabesinger, Weber et al. 1999). But also other regions of the body (Jouvensal, Carlier et al. 1996) have been examined using this type of sequence. The scheme of a double quantum filter sequence is shown in Fig. 2.1.

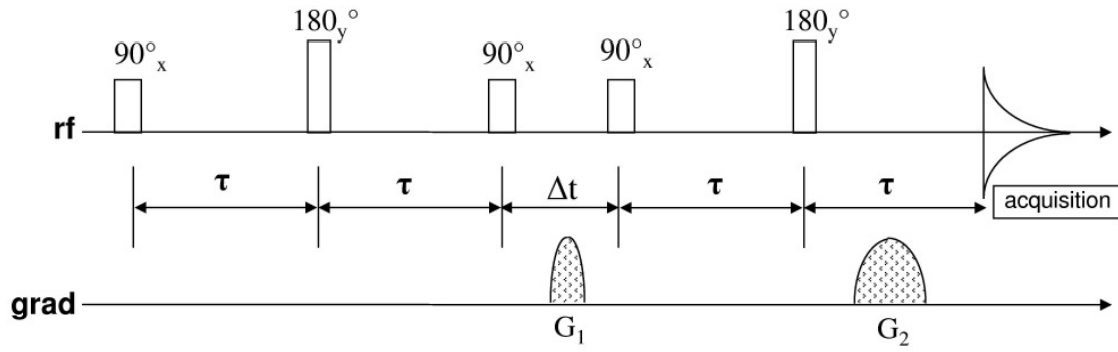


Fig. 2.1: Radiofrequency and gradient pulse scheme of a double quantum filter (dqf) sequence. Double quantum coherences are created by the second 90_x pulse and converted back to observable single quantum coherences by the third 90_x pulse.

For a weakly coupled two spin system (I-S), the delay τ is ideally chosen to $1/(4J)$, with J the coupling constant between I and S. At the end of the first evolution period (2τ) and before the second 90_x pulse, the state of the spin system can then be written as (Ernst, Bodenhausen et al. 1987; de Graaf 1998)

$$\sigma(2\tau-) = 2I_x S_z \quad (2.1)$$

In this description we only look at the I part of the spin system. The symbol σ designates the systems density operator and I and S are the product operators of the respective spins. Application of the second 90_x pulse, called “double quantum coherence” (dqC) pulse, generates double and zero quantum coherences:

$$\begin{aligned} \sigma(2\tau+) &= -2I_x S_y \\ &= \frac{i}{2}(I^+ S^+ - I^+ S^- + I^- S^+ - I^- S^-) \end{aligned} \quad (2.2)$$

A corresponding contribution arises from the S spin. In the gradient field of G_1 each product operator accumulates a phase shift Φ proportional to its coherence order. The delay Δt in this example is considered short enough to neglect chemical shift and coupling evolution. At the time $t = 2\tau + \Delta t$, before the third 90_x pulse, the system state is characterized by

$$\sigma(2\tau + \Delta t) = \frac{i}{2}(I^+ S^+ e^{-i2\phi_1} - I^+ S^- + I^- S^+ - I^- S^- e^{+i2\phi_1}) \quad (2.3)$$

with $\Phi_i = \Phi_i(\vec{r}) = \gamma \vec{r} \cdot \int_0^{\Delta t} \vec{G}_i(t) dt$. The vector \vec{r} designates the localization of the considered spin group; γ is the proton gyromagnetic ratio. The phase Φ is determined by the gradient amplitude and duration of its application. Often, these are summarized in the variable k so that one may write $\Phi_i = \Phi_i(\vec{r}) = 2\pi \vec{r} \cdot \vec{k}_i$ with $\vec{k}_i = \frac{\gamma}{2\pi} \cdot \vec{r} \int_0^{\Delta t} \vec{G}_i(t) dt$.

The third 90_x pulse, called “read pulse”, converts double quantum coherences back to observable single quantum coherences (sqc), and only those will be written in the

following. This is justified because dqc present in the system after the third 90_x pulse will not -in the weak coupling approximation and assuming ideal rf pulses- develop into observable coherences. Other single quantum coherences produced will be dephased by the second gradient G_2 . At the beginning of the signal detection period, the chemical shift evolution has been refocused by the second 180° pulse and the spins have acquired an additional phase shift due to the second gradient pulse G_2 . The system state is written as

$$\begin{aligned}\sigma(4\tau + \Delta t) = & \frac{i}{8} I^+ e^{i(2\phi_1 - \phi_2)} - \frac{i}{8} I^- e^{-i(2\phi_1 - \phi_2)} \\ & + \frac{i}{8} I^+ e^{-i(2\phi_1 + \phi_2)} - \frac{i}{8} I^- e^{+i(2\phi_1 + \phi_2)} \\ & + \frac{i}{4} I^+ e^{-i\phi_2} - \frac{i}{4} I^- e^{+i\phi_2}\end{aligned}\quad (2.4)$$

For double quantum filtering, as in our case, k_2 equals $2k_1$ and therefore Φ_2 becomes equal to $2\Phi_1$. Integrated over the sample volume, only operators without phase term give a resulting signal. The resulting signal is therefore determined by

$$\sigma = \frac{i}{8} (I^+ - I^-) = -\frac{1}{4} I_y \quad (2.5)$$

The same contribution arises from the S spin, which has not been observed since the beginning of this calculation.

Uncoupled spin groups, giving rise to strong singlet signals in NMR spectra, are unable to produce double quantum coherences that follow the process described above. Transverse magnetization produced on these spin groups by the first pulse of the sequence is still present as observable transverse magnetization after the second 180° pulse, but then dispersed by the second gradient pulse G_2 . This is not only useful for effective water suppression, but also for the elimination of singlet resonances that may cover the signal of coupled spins in *in vivo* NMR spectra. An example is the detection of GABA at 3 ppm which is covered by the singlet peaks of creatine / phosphocreatine and choline in unedited spectra (McLean, Busza et al. 2002). Also the unwanted contribution of coupled spin groups other than the one targeted can be attenuated. Differentiation is done by the differing J couplings constants of the different molecules. The sequence timing assures optimal production of double quantum coherences only for molecules with a coupling constant of $J = 1/(2t)$. In the example of our sequence t equals 2τ , see Fig. 2.1. The magnetization of molecules with differing J values will remain partially in a single quantum state and be suppressed, leading to an attenuation of the signal from this molecule.

The disadvantage of the filtering approach presented in this section is an overall signal reduction of about (exactly only in our example) 75% for the signal coming from the targeted molecule. This signal loss is caused by the only partial transformation of single

quantum coherence to double quantum coherence, as can be seen in equation (2.2), and the fact that, using gradient filtering, only one coherence transfer pathway is refocused.

Designing and using double quantum filter sequences for *in vivo* applications presents several difficulties.

The strong reduction of the signal from the targeted molecule is an important drawback, as the concentration of brain metabolites is low, around 8 mMol / kg w.wt *in vivo*. Reliable signal quantification using dqf sequences therefore needs large acquisition volumes or long acquisition durations.

The dqf sequence shown in this chapter is a very strong simplification of a sequence useable for *in vivo* spectroscopy. Efficient *in vivo* spectroscopy needs spatial localization of the acquisition volume, demanding either a preparation module before the dqf sequence or volume selective pulses within the dqf sequence. It has been shown that the use of shaped pulses and the process of volume selection has an important influence on the evolution of coupled spin systems (Slotboom and Mehlkopf 1994; Thompson and Allen 2001). Optimization of sequences incorporating spatial localization is therefore more difficult as described in the preceding paragraph.

Molecules that present an interest in medical or biomedical research have more than two observable spins, as it was the case in the calculation of an I-S system. An example is glutamate or GABA, having five and six observable spins. At the currently available field strengths for medical research (up to 3 T), most molecules of interest can not be considered in the weak coupling approximation, as has been done for the calculation presented in this section. Optimal timing parameters are therefore difficult to determine.

Several authors show the optimization of localized dqf sequences, adjusting the sequence timing (Wilman and Allen 1995; Trabesinger, Weber et al. 1999), the read pulse flip angle (Wilman and Allen 1993; Lei and Peeling 1999) or even the dqc pulse phase (Kim and Allen 2003) and using an experimental approach or simulations. A major improvement can be achieved using read pulses that are selective only on the coupling partner of the spin to be observed. In our example such a read pulse would be frequency selective on the S spin, if we wanted to observe signal from the I spin. A recovery of 50% of the signal amplitude instead of only 25% can be achieved. The suppression of contributions from other coupled spins than the one targeted may be improved as the double quantum coherences of these spins are not transformed back into single quantum coherences by the read pulse. In the literature binomial pulses (Trabesinger, Weber et al. 1999), shaped pulseforms (Lei and Peeling 1999), block pulses (Keltner, Wald et al. 1998) or even composite pulses (DANTE pulse train) (Trabesinger and Boesiger 2001) can be found for the realization of frequency selective read pulses. More recently developed filter sequences use refocusing pulses pulses that are selective on certain resonances of the targeted molecule (Shen, Rothman et al. 2002; Choi, Lee et al. 2004; Choi, Lee et al. 2005). These sequences thereby achieve a further improvement in resolving the targeted molecule from its overlapping background.

2.2 Sequence design of a double quantum filter for *in vivo* applications

The pulse sequence evaluated in this work is based on a proposition of Thompson *et al* (Thompson and Allen 1998). The rf and gradient pulse scheme is reproduced in Fig. 2.2.

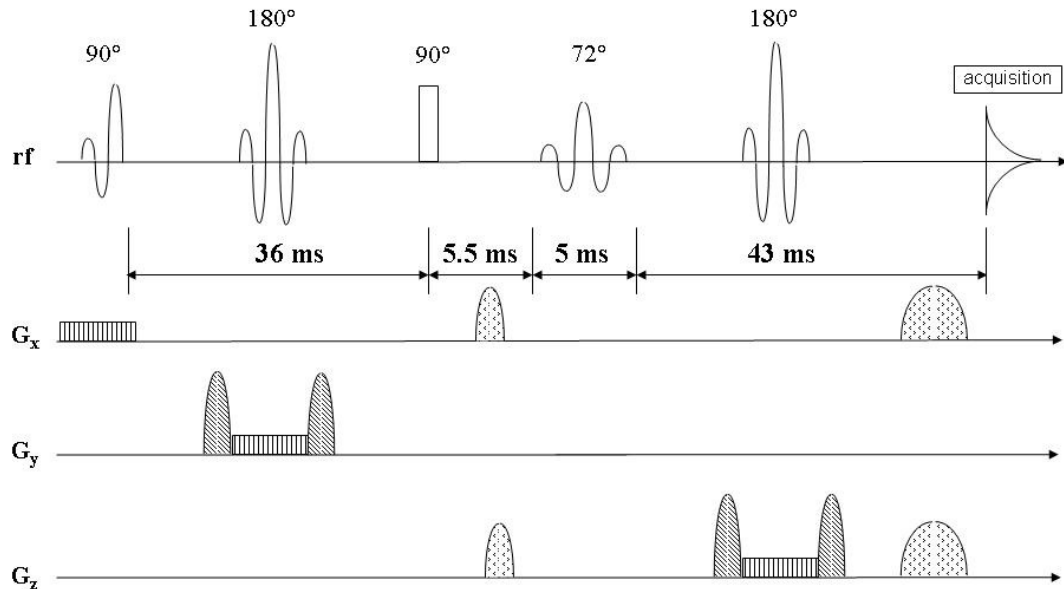


Fig. 2.2: Sequence design of a localized double quantum filter (Thompson and Allen 1998). Sequence timings and the flip angle of the fourth pulse (called “read” pulse) have been determined numerically to optimize glutamate detection at 2.3 ppm at a field strength of 3 Tesla.

The sequence design incorporates spectral editing into a PRESS localization module by making the excitation pulse and the two refocusing pulses slice selective. A self refocusing BURP pulse (Geen and Freeman 1991) of 4 ms length is used for excitation in order to begin the evolution period with completely refocused magnetization. Optimized sinus cardinal pulses of 4 ms length are used for refocusing and slice selection in the two directions perpendicular to the excitation slice. The authors emphasize to use optimized pulses, as the slice profile is not only important for proper localization, but also plays a role in coherence transfer (Thompson and Allen 1999). The second 90° pulse, which has the function of producing multiple quantum coherence orders is realized as a rectangular shaped pulse of 250 μ s length. Its length is kept short in order to achieve as well as possible the behavior of an ideal pulse that would be infinitely short. The read pulse is a sinus cardinal shape multiplied with a Gaussian function. This apodization renders its frequency profile stable to a range of flip angles differing from 90° at the cost of a larger transition band. The pulse is applied with a flip angle of 72°. Filtering gradients of 2 ms and 4 ms length are used, oriented at the “magic angle” (see section 2.3.2).

The target of this dqf sequence is the glutamate resonance in the 2.3 ppm region. While a maximum of glutamate signal should be produced, the close and underlying resonances of glutamine, NAA and GABA should be suppressed. Furthermore, the aim is to keep only one single peak from the complicated glutamate lineshape (Govindaraju, Basus et al. 1998).

Optimal sequence parameters are difficult to determine. Glutamate, glutamine, NAA and GABA present strong coupling behavior at field strengths of 3 Tesla. The evolution of the spin systems can therefore not be described easily. Furthermore, the influence of shaped pulses has to be taken into account. Depending on their length and shape, coherences in the spin systems are produced and redistributed (Thompson and Allen 1999). As already mentioned, some dqf sequences use pulses that are selective on certain resonances of the targeted molecule. Multiple quantum coherences are prepared only on the targeted molecule (for example GABA or glutathione (Trabesinger and Boesiger 2001; Shen, Rothman et al. 2002)). This way to proceed is not possible for targeting glutamate while suppressing glutamine, NAA and GABA. Coupled resonances of glutamate, glutamine, NAA and GABA overlap in a small spectral area of only 0.2 ppm. Separating glutamate from its background with double quantum filtering therefore relies on an adapted timing of the sequence. The coherence transfer properties of the pulses used for slice selection and the read pulse may be used.

In the dqf sequence proposed by Thompson *et al* (Fig. 2.2), several sequence parameters have been optimized numerically. A density matrix description of the spin system has been used to predict the spectral shape in dependence of the sequence delays, the read pulse length and the read pulse flip angle. Optimal parameters are derived for these parameters from the simulations.

2.3 Implementation of a dqf sequence on a 3 T whole body imager

In this section the implementation and parameterization of the dqf sequence, especially with respect to water suppression and rf pulses, will be detailed. A procedure assuring optimal results from freely positioned voxels will further be described.

2.3.1 Radiofrequency pulses

All radiofrequency pulses are applied with the carrier frequency set to the glutamate resonance at 2.3 ppm. The position of the volume selected for the spins resonating at 2.3 ppm thereby coincides exactly with the chosen position. Voxels for differing resonance frequencies will be slightly displaced.

2.3.1.1 Excitation and refocusing pulses

For excitation and refocusing, 3-lobe sinus cardinal (sinc) pulses have been chosen. The excitation profile of a BURP pulse (Geen and Freeman 1991) is very sensible to small rf

power maladjustments. During *in vivo* tests, time consuming fine adjustments were necessary to achieve an acceptable slice selection. Still, the profile stayed improper compared to that of a normal sinc pulse. In simulations (Smith, Levante et al. 1994), no difference in the lineshape of a glutamate and glutamine dqf spectrum using a BURP or a sinc pulse could be found. The refocusing profile quality as produced by a normal sinc pulse was estimated to be sufficient.

An improvement of the glutamate peak intensity could be achieved shortening the excitation and refocusing pulse lengths from 4 ms to 2 ms. Experiments on phantoms containing only glutamate in solution show an increase of the 2.3 ppm glutamate resonance of about 15%. The excitation and refocusing pulses that are used for spatial localization interfere with the coherence transfer (Thompson and Allen 1999). Shorter pulses approximate better the behavior of ideal pulses. Shorter pulses used for voxel localization therefore interfere less with the double quantum filtering and lead to improved performance. Also, the relative displacement of the volumes selected for the glutamate resonances near 2.3 ppm and 3.7 ppm is reduced, increasing the volume in which double quantum coherence between these two spin groups can be produced. Even shorter pulses could possibly further improve the performance. Due to rf power limitations a duration of 2 ms is although the experimental limit for the moment on our system.

2.3.1.2 DQC pulse

The dqc pulse (second 90° rf pulse of the sequence) is realized as block shaped pulse. The length of this pulse was kept as short as possible to approximate the behavior of an ideal pulse. A duration of 250 μ s presents the minimum length with respect to rf power limitations of our system. First *in vivo* and *in vitro* tests on centered voxels were conducted with dqc pulse lengths of 250 μ s. In later experiments on freely positioned voxels, it was necessary to match the length of the dqc pulse with the length of a 180° block shaped pulse. This pulse was used in a complementary sequence necessary for calibration purposes, see section 2.3.3. As minimal common pulse duration, we chose a length of 350 μ s.

2.3.1.3 Read pulse

A sinus cardinal shape with two lobes (two zero passages to each side) was used for the read pulse. This sinc shape has been multiplied with a Gaussian profile cut off at 25% of its maximal amplitude. Fig. 2.3 shows the calculated excitation profile of this pulse to illustrate its characteristics. A flip angle of 72° and a length of 5 ms, as used in the dqf sequence, have been simulated. A solid line indicates the real part, a dotted line the imaginary part of the magnetization. The Gaussian apodization of the sinc shape allows the pulse to have a flat excitation band for flip angles differing from 90°. The spectral region, near 2.3 ppm, is homogeneously excited. The water resonance is situated slightly next to the excitation band; its content in the spectrum is only slightly reduced in this way.

2.3.2 Water suppression

Double quantum filtered spectroscopy sequences have intrinsic water suppression, as the water molecule presents only uncoupled resonances. Under certain circumstances it is however possible to create multiple quantum coherences between separate water molecules. These can pass the filter and give rise to relatively strong water signals in the spectrum. A qualitative description of this circumstance known as “intermolecular multiple quantum coherences (iMQC)” will be given in the following. In this work, the objective was to circumvent this effect in order to completely eliminate the water signal from the spectrum.

Multiple quantum coherences between water molecules are created by the dqc and read pulse together with the two filter gradients. This sequence part is shown in Fig. 2.4. A review of the fundamental principles of how multiple quantum coherences are formed by this sequence has been given Richter *et al* (Richter and Warren 2000).

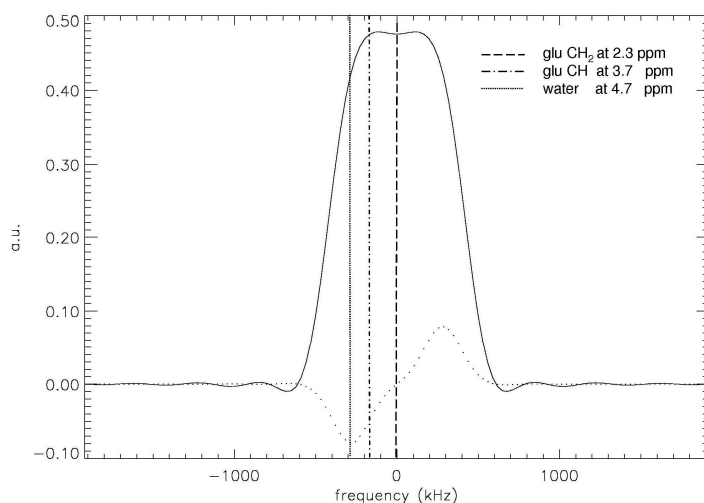


Fig. 2.3: Excitation profile of the read pulse as used in our sequence implementation. Frequency positions of the glutamate and water resonances are indicated, assuming the pulse carrier frequency centered on the glutamate 2.3 ppm multiplet. The simulated pulse is a two lobe sinc shape (two zero crossings to each side) multiplied with a Gauss form. The Gauss shape has a cutoff factor of 25%, the simulated flip angle was 72° and the pulse length 5 ms. The solid line indicates the real part, a dotted line the imaginary part of the magnetization. The Gaussian apodization assures a flat excitation band at a flip angle below 90° . All glutamate resonances are homogeneously excited.

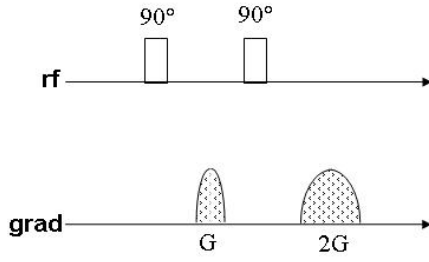


Fig. 2.4: Radiofrequency and gradient pulse scheme for the generation of intermolecular multiple quantum coherences (“CRAZED” (Richter and Warren 2000)). The dqc pulse, read pulse and the filter gradients of a double quantum filter sequence correspond to the “CRAZED” scheme. Intermolecular multiple quantum coherences can be created on the water molecules and lead to a strong water signal in the spectrum.

Two generally made assumptions have to be revised to explain the formation of iMQC. The first assumption is the “high temperature approximation” for the density operator. This assumption says that the general density operator given by

$$\rho = \frac{\exp(-\hbar\omega/kT) \sum_i I_{zi}}{\text{tr}(\exp(-H/kT))} \quad (2.6)$$

may be approximated by a Taylor series that is cut after the linear term, giving

$$\rho = \frac{1 - (\hbar\omega/kT) \sum_i I_{zi}}{\text{tr}(\exp(-H/kT))} \quad (2.7)$$

This simplification is not justified for macroscopic samples, as, because of an important number of spins, higher order terms in the Taylor series are not small compared to one and therefore not negligible. A valid description has to consider higher order terms, that make appear two spin operators as $I_{z1}I_{z2}$ not present in (2.7).

The second assumption concerns dipolar couplings between spins. The dipolar coupling Hamiltonian for the spin system may be written in polar coordinates as

$$H_d = \sum_{k=0}^N \sum_{l=0}^N D_{kl} (3I_{kz}I_{lz} - \vec{I}_k \cdot \vec{I}_l) \quad (2.8)$$

with the “dipolar coupling constant” D that evaluates to

$$D_{kl} = \frac{\mu_0}{4\pi} \frac{\gamma_k \gamma_l \hbar}{4r_{kl}^3} (1 - 3\cos^2 \theta_{kl}) \quad (2.9)$$

In the equation for D, θ_{kl} indicates the angle between the internuclear vector and the main magnetic field.

In liquid samples, dipolar couplings add to zero. To demonstrate this, equation (2.8) and (2.9) are evaluated looking at two limits, the interaction of a two spins at a close distance (short range dipolar interactions) and the interaction of a spin with a great number of other spins situated at a fixed, large radial distance (long range dipolar

interactions). For the formation of iMQC, long range dipolar couplings are of importance. Integrating (2.8) for a fixed distance r we obtain the following expression:

$$H_d \sim \int_{\Theta=0}^{\pi} \int_{\varphi=0}^{2\pi} (3I_{kz}I_{lz} - \vec{I}_k \cdot \vec{I}_l)(1 - 3\cos^2\theta) \sin\theta d\theta d\varphi \quad (2.10)$$

If the sample is homogeneously magnetized, the term in the first parenthesis of (2.10) is independent of θ and φ . In the vector model, one can imagine that all magnetization vectors are parallel. H_d is therefore proportional to

$$\int_{\Theta=0}^{\pi} \int_{\varphi=0}^{2\pi} (3\cos^2\Theta - 1) \sin\Theta d\Theta d\varphi \quad (2.11)$$

which is zero. If magnetic field gradients have been present at a time during the sequence (after excitation of the spin system), the sample is not homogeneously magnetized. The magnetic moments of the spins in the sample are no longer aligned but wound up in a helix characterized by the gradient strength. The expression in the first parenthesis of (2.10) becomes a function of θ and φ and H_d no longer adds to zero. The spins evolve under the influence of spin-spin dipolar coupling between distinct molecules.

Longitudinal two spin terms in the equilibrium density matrix and the presence of dipolar couplings together explain the production of a signal from the sequence displayed in Fig. 2.4. The first pulse transforms longitudinal two spin operators as $I_{z1}I_{z2}$ to transverse spin operators as $I_{x1}I_{x2}$ for example. These represent a mixture of zero and double quantum coherence. Chemical shift evolution makes appear terms as $I_{x1}I_{y2}$, which are being transformed to $I_{z1}I_{y2}$ by the second pulse. The first and the second gradient have introduced inhomogeneous magnetization in the sample; terms of the form $I_{z1}I_{y2}$ evolve under dipolar couplings to I_{x1} , which is measurable magnetization. It can be shown that the strength of the signal S is proportional to

$$S \sim 3\cos^2\Theta - 1 \quad (2.12)$$

where θ is the angle between the B_0 field axis and the magnetic field gradient axis. Along the dqc and read pulse of the double quantum filter sequence together with the two filter gradients produce detectable signal. These pulses are non selective, they act on the whole sample volume. Intramolecular multiple quantum coherence signal from the water is therefore produced from almost the whole volume. The last refocussing pulse of the dqc sequence however reduces the contributing volume, as a slice is selected. At the start of the acquisition, two major signal contributions are present: A double quantum filtered signal from the voxel, which is the signal of interest, and water iMQC signal originating from the whole slice that has been selected by the last rf pulse. As the volume of the voxel is much smaller than the slice volume, and as the water concentration is much higher than the metabolite concentration *in vivo*, iMQC signal from the water strongly contaminates the spectrum.

To suppress the formation of water iMQC signals, the orientation of the filter gradients in the dqc sequence has to be set to the magic angle of $\theta = 54.7^\circ$. At this gradient angle, as can be verified in equation (2.11), the dipolar interaction vanishes and no iMQC signal is produced. The water signal reacts very sensitively to the gradient orientation and careful fine adjustment was necessary to minimize the water contamination in the dqf spectrum. Additionally it was necessary to use long filter gradient durations of 4 ms for the first and 8 ms for the second filter gradient. Further improvement of the water suppression was necessary and could be achieved by phase cycling and a water suppression module preceding the dqf sequence. As phase cycle, an eight step cycle (Henning 1992) has been used. The dqc and read pulse are cycled as the excitation pulse. The cycling assures that only signal excited by the first and refocused by the two 180° pulses remains in the spectrum, whereas signal produced by the dqc and read pulse is efficiently eliminated. Further reduction of the water signal is achieved by a VAPOR water suppression module (Tkac, Starcuk et al. 1999; Tkac, Andersen et al. 2001). A hermitian pulse shape of 160 Hz bandwidth has been used for selective excitation of the water resonance.

Magic angle filter gradient orientation together with phase cycling and water suppression by VAPOR assure that in the dqf spectra acquired *in vivo* no residual water signal is visible.

2.3.3 Voxel positioning and phase calibration

Free positioning of the volume of interest is necessary for *in vivo* applications of NMR spectroscopy and can be achieved by adding offsets to the excitation and refocusing pulses. To obtain optimal filtering results, it is however necessary to adjust the relative pulse phases of dqc and read pulse in the dqf sequence. In this section we will first demonstrate the necessity of this phase adjustment and then describe a procedure for the determination of the optimal pulse phases.

2.3.3.1 The necessity of phase calibration and phase calibration procedures

As may be deduced from the introduction to double quantum filtering, a maximum of double quantum coherence is produced if the dqc pulse and the magnetization on which it acts have a phase difference of 90° . The read pulse needs to be applied with the same phase as the dqc pulse. For non-localized dqf sequences, as treated in the introduction to double quantum filtering, the phase relation between dqc pulse and magnetization is assured by application of the same phase for the excitation and dqc pulse. In the case of localized dqf sequences, the excitation and refocusing pulses are applied with a frequency offset to position the voxel in the region of interest. The magnetization phase at the first echo time, the time of the application of the dqc pulse, depends on the phase of the excitation and refocusing pulses and on their frequency offsets. Fig. 2.5 illustrates this effect.

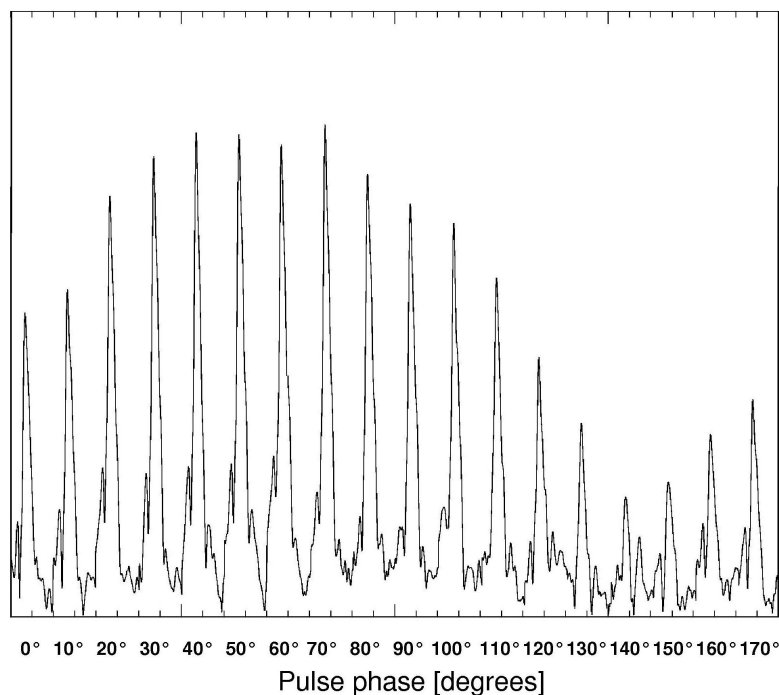


Fig. 2.5: Glutamate signal at 2.3 ppm (magnitude mode) in dependence of the read and dqc pulse phase angle to demonstrate the necessity of phase calibration for acquisition volumes positioned off-center. The first signal to the left has been acquired from a voxel shifted in x by 3.2 cm, in y by 3 cm and in z by 1.8 cm and with the excitation pulse, dqc pulse and read pulse applied with the same phases. The following signals to the right were acquired with the read and dqc pulse phase set to the value indicated in the legend. Optimal signal intensity at this voxel position is obtained for a dqc and read pulse phase of about 70°.

The peaks in Fig. 2.5 are the glutamate peak at 2.3 ppm acquired *in vitro* with the localized dqf sequence in different acquisitions, as will be described at once. All signals are shown in the magnitude mode; a phantom containing a high concentrated glutamate solution (100 mM) has been used to achieve good SNR. A $(25 \text{ mm})^3$ voxel, shifted in x by 3.2 cm, in y by 3 cm and in z by 1.8 cm was selected by application of the necessary frequency offsets to the excitation and refocusing pulses. The pulse phases of the slice selective pulses were set to x for the excitation and to y for the refocusing pulses. The first signal in Fig. 2.5 has been obtained with the dqc and read pulse phase set to x, as the excitation pulse. With this phase setting, the dqf sequence should produce optimal signal, if the magnetization at the first echo time, when the dqc pulse is applied, had really y-phase, as supposed by the excitation pulse phase. For the acquisition of the second peak from the left and the following peaks, the dqc and read pulse phase have been increased in steps of 10 degrees without changing any other sequence parameter. Maximal signal intensity is obtained if the dqc read and pulse are applied with a phase of about 70 degrees. To achieve maximal signal intensity, an adjustment of the dqc and read pulse phase is therefore necessary. This phase adjustment has to be performed for every position of the volume of interest, as the optimal dqc and read pulse phase depends on the phase of the magnetization at the first echo time, when the dqc pulse is

applied. The magnetization phase changes with the frequency offsets used for the excitation and first refocusing pulse.

Different approaches to obtain optimal filter performance for freely chosen voxel positions have been described in the literature. Some authors (Jouvensal, Carlier et al. 1996) restrain the voxel placement to certain positions, where maximum filter output is achieved. This procedure restricts voxel placements to positions where the correct phase relation between magnetization and dqc pulse is fulfilled. Other authors (Keltner, Wald et al. 1997; Keltner, Wald et al. 1998; Trabesinger, Weber et al. 1999; McLean, Busza et al. 2002) adjust the dqc and read pulse phase. Mc Lean *et al* calibrate the phase in phantom experiments for different voxel positions and use this calibration *in vivo*. Trabesinger *et al* and Keltner *et al* perform phase calibration *in vivo* before starting the dqf sequence.

2.3.3.2 Implementation of a phase calibration procedure

For the double quantum filter implementation in this work we chose to perform phase calibration of the dqc and read pulse before each experiment, as proposed in (Keltner, Wald et al. 1997; Keltner, Wald et al. 1998; Trabesinger and Boesiger 2001). This approach allows maintaining the free choice of voxel positioning, as compared to (Jouvensal, Carlier et al. 1996), and direct control of successful phase adjustment, as compared to (McLean, Busza et al. 2002). Function and use of this procedure will be detailed in the following.

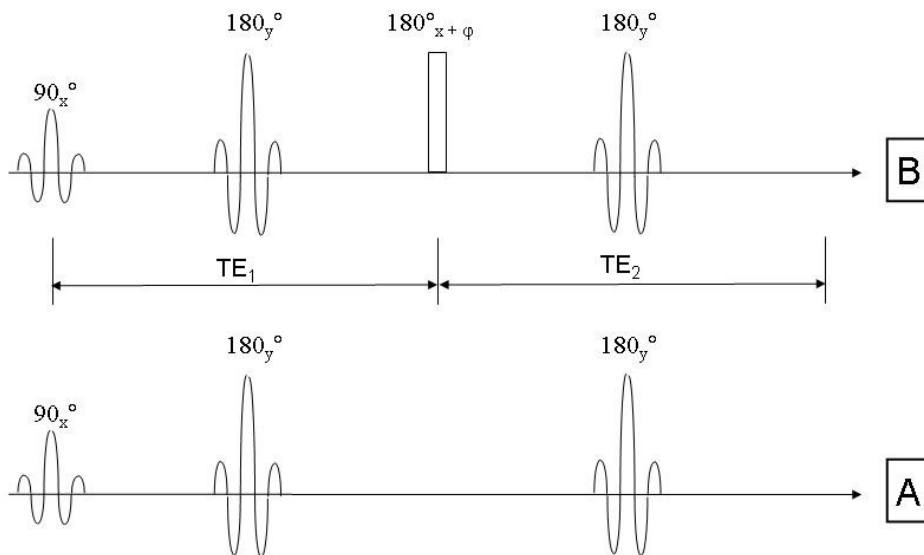


Fig. 2.6: Radiofrequency pulse scheme used for determination of the optimal dqc and read pulse phase for acquisition from volumes positioned off-center (Keltner, Wald et al. 1997). The phase angle ϕ of the second 180° pulse in B is adjusted to obtain a signal phase difference of 180° comparing the signals acquired with sequence A and B.

The calibration procedure is based on comparison of the two signals acquired with the sequences shown in Fig. 2.6. Slice selection and crusher gradients have not been drawn

for simplicity. The additional 180° block pulse in sequence B, Fig. 2.6, is as well surrounded by spoiler gradients. The aim of the calibration procedure is the determination of the block pulse phase angle correction φ . This correction should be determined to apply the blockpulse with a phase difference of 90° to the magnetization phase at the end of the first echo time, TE_1 . The correction φ will then be used for the dqc and read pulse phase in the dqf sequence to achieve optimal signal intensity. The calibration procedure starts with signal acquisition using sequence A and B, with φ set to zero in B. The correction angle φ is then determined from the signal phases as follows:

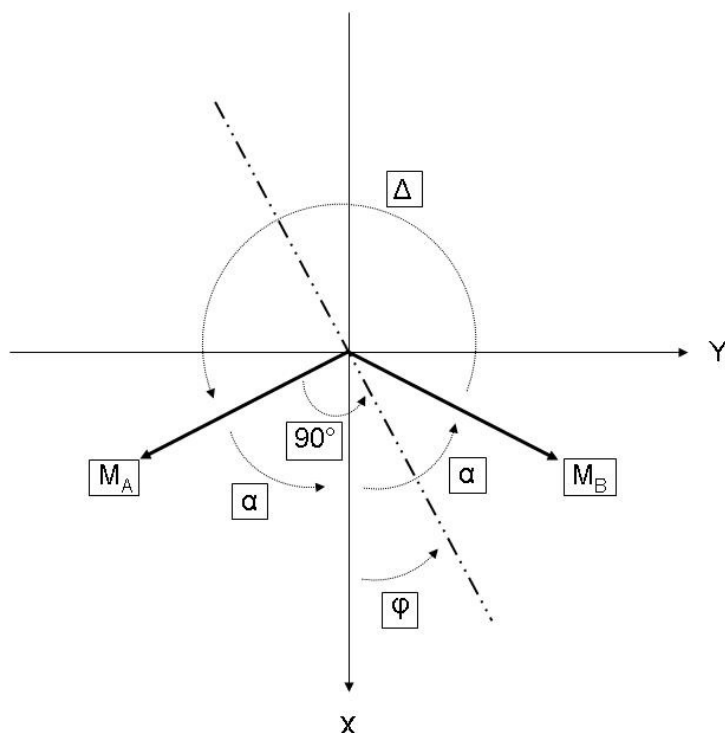


Fig. 2.7: Calculation of the phase correction angle φ from the signals acquired with the phase calibration sequence A and B of Fig. 2.6. M_A corresponds to the signal phase produced by sequence A, M_B to the phase produced by the sequence B. The pulse phase of the second 180° pulse of sequence B, which should present a phase difference of 90° with respect to M_A for correct adjustment of φ , is indicated by a dash-dotted line.

Consider the magnetization produced with sequence A, Fig. 2.6., at $t = TE_1$, denoted M_A in Fig. 2.7. As the excitation and first refocusing pulse were applied with a frequency offset determined by the voxel position, M_A has an unknown phase α within the rotating frame reference system (x-y coordinate system). In Sequence B, a 180°_X block pulse is applied at exactly this point of time. As this pulse is applied without any frequency offset, its phase is reliably situated on the x-axis of the rotating frame. After the application of this blockpulse, M_B will be the mirror image of M_A with respect to the x-axis at $t = TE_1$. The second refocusing pulse acts in the same way on M_A and M_B in sequence A and B. The phase difference of the signal acquired with sequence A and sequence B is Δ , as indicated in Fig. 2.7. Our aim is to add an angle φ to the phase of

the 180°_x block pulse in order to apply this pulse with 90° phase difference to the magnetization phase M_A . The phase desired for the blockpulse is indicated by a dash-dotted line in Fig. 2.7. To calculate φ we pose $90^\circ = \alpha + \varphi$. With the measured phase difference Δ and knowing that $360^\circ = \Delta + 2\alpha$ we can determine the phase correction angle φ to

$$\varphi = \frac{1}{2}(\Delta - 180^\circ) \quad (2.13)$$

In the experiment, M_A and M_B are acquired with a common phase error of 0^{th} order. Therefore, calculating the difference of the phases of M_A and M_B may give Δ as indicated in Fig. 2.7 or $\Delta' = -(360^\circ - \Delta)$, depending on this global phase error. For simplicity we use the absolute value of the phase difference Δ in equation (2.13). It has to be determined experimentally if φ needs to be added or subtracted from the phase of the 180°_x block pulse. If the phase correction angle of the block pulse has been correctly set, the phase difference Δ of the signals acquired with sequence A and B is determined to 180° .

2.3.4 Sequence design – Summary

This section summarizes and complements the sequence parameters discussed in the preceding sections to give an overview of the dqf implementation used in this work.

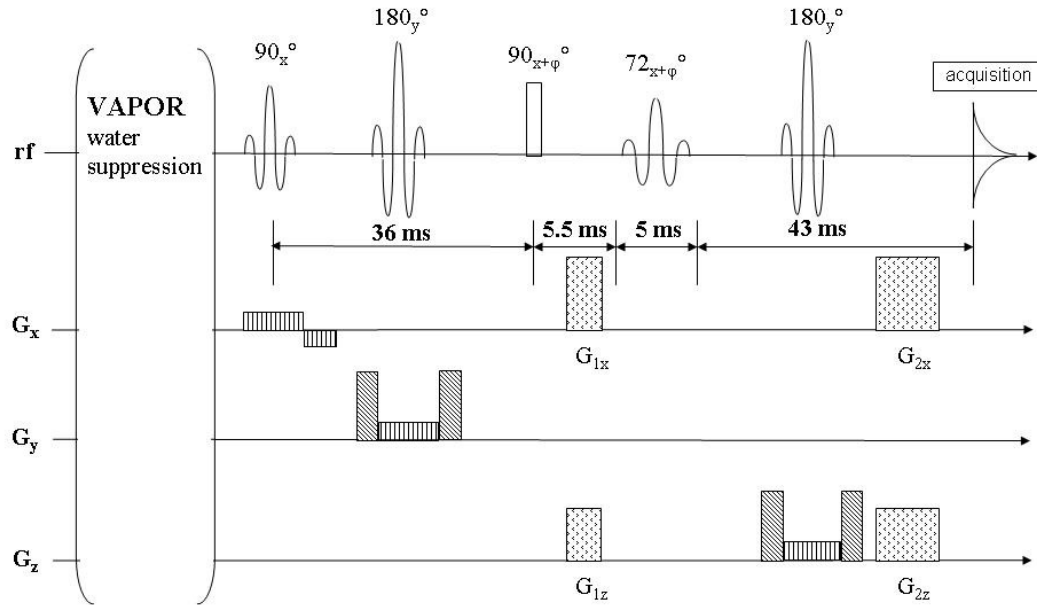


Fig. 2.8: Radiofrequency and gradient pulse scheme of the double quantum filter sequence used for glutamate detection in this work. Compared to the original design (Thompson and Allen 1998) VAPOR water suppression was added. The excitation pulse is a usual sinus-cardinal shape, the phase correction angle φ for dqc and read pulse is determined with the phase calibration procedure detailed above.

The sequence starts with a VAPOR module for water suppression, shown in Fig. 2.8. VAPOR uses hermitian pulses of 160 Hz bandwidth and gradients on the x, y and z axis of 16 mT/m strength and 1.5 ms length. As excitation and refocusing pulses 3 lobe sinc shaped pulses are used. Pulse lengths of 4 ms and 2 ms have been tested. The pulse phase of the excitation pulse is set to x, whereas the refocusing pulses are applied with y phase. For the dqc pulse a length of 250 μ s and 350 μ s has been tested, depending on whether or not phase calibration for the dqc and read pulse had been performed. This point will be further detailed in section 2.4.1. A two lobe sinc shaped pulse multiplied with a Gaussian shape cut off at 25% of its main amplitude is used for the read pulse, calibrated to a flip angle of 72°. This pulse has a length of 5 ms. DQC and read pulse have x phase with a phase correction angle ϕ added for off-center positions, determined with the phase calibration procedure. During accumulations an eight step phase cycling is applied to all pulses. DQC and read pulse are cycled as the excitation pulse. The carrier frequency for all pulses is set to the glutamate resonance frequency at 2.3 ppm. For voxels shifted from the magnet isocenter, offsets are applied to the excitation and refocusing pulses. No changes were made to the sequence timing with respect to the proposition of the original sequence design. Spoiler- and filter gradients use rectangular shapes. For the spoiler gradients, a length of 3 ms / amplitude of 24 mT/m is sufficient. Good water suppression was obtained only with relatively strong filter gradients of 4 ms length for the first pair of gradients (G_{1x} , G_{1z}) and 8 ms for the second pair of gradients (G_{2x} , G_{2z}) together with amplitudes of 34 mT/m for G_{1x} and G_{12x} and 22.4 mT/m for G_{1z} and G_{12z} . The filter gradient amplitudes are calibrated to orient the resulting gradient at the magic angle.

2.4 Experimental validation of a dqc sequence on a 3 T whole body imager

First tests *in vitro* are shown to validate the phase calibration procedure and the ability to distinguish glutamate from its background signal. Further tests evaluate the dqc sequence for glutamate detection *in vivo*.

2.4.1 Validation of the phase calibration procedure

Experiments to verify the accuracy of the phase correction angle determined with the phase calibration procedure are described in this section. First, the phase correction angle ϕ is determined for a voxel positioned at an off-center position. By systematic variations of ϕ around the determined value, as seen in section 2.3.3.1, its accuracy is then verified.

2.4.1.1 Materials and methods

The experiments have been performed on a 3 T whole body imager (Medspec, Bruker, Ettlingen, Germany), equipped with a gradient system allowing gradients of up to 40 mT/m. An 8 kW rf amplifier was used for rf pulse generation. Signal excitation and

reception were performed using a birdcage head coil. A solution of 100 mM glutamate in 2.2 liter PBS buffer served as sample, its pH value adjusted to the physiological value of 7.3 ppm. In order to circumvent the problem of partial signal saturation when short repetition times are used, a contrast agent (chelated gadolinium complex, Dotarem, Guerbet, France, 0.5 mMol/ml) was added at a concentration of 0.5 ml per liter sample volume. Sodium azide (NaN_3) was added to the sample to prevent bacterial growth. The sample solution was contained in a glass sphere, placed at the center of the birdcage resonator.

The phase calibration sequence was realized as shown in Fig. 2.6. For the selective pulses, the same pulseshapes and lengths as later in the dqf sequence have been used (sinus cardinal shaped pulses of 2 ms length). As in the dqf sequence, the excitation pulse is applied with x-phase and the two selective refocusing pulses with y-phase. A pulse length of 350 μs was used for the rectangular shaped 180° pulse of sequence B. Due to rf power limitations, a shorter pulselength was not possible. Care was taken with respect to the placement of the frequency switch command before each pulse in the pulse program (Jouvensal, Carlier et al. 1996). The delay between the issue of the switch command and the middle of the following rf pulse was strictly the same for the corresponding pulses of the phase calibration sequence and the dqf sequence (excitation pulse, first refocusing pulse and block shaped pulse). As has been shown in (Jouvensal, Carlier et al. 1996), this delay determines the effective pulsephase of the shaped pulses. TE_1 was set to 36 ms and TE_2 to 48 ms. Data acquisition started directly at the end of TE_2 . A voxel of $(2.5 \times 2.5 \times 2.5) \text{ cm}^3$, shifted from the magnet isocenter (x-shift = 1.5 cm, y-shift = 2.8 cm and z-shift = 2.1 cm), but well contained within the sample volume, was chosen. A spectral width of 4960 kHz on 4096 points was acquired, performing 8 dummy scans before the start of the acquisition and accumulating the signal from the 8 following scans. All pulses were phase cycled during these accumulations following the same phase cycling scheme used for the dqf sequence (see section 2.3.2). The rectangular shaped pulse of sequence B was cycled as the excitation pulse.

Using these parameters, the water signal was acquired from the voxel, using sequence A and sequence B with the phase angle φ of the added 180° block pulse in B set to zero. Both signals were Fourier transformed and phased to absorption, performing 0th order phase correction. We used the Bruker supplied software "XWINNMR" for this purpose, determining always positive angles to phase to absorption mode. The phase correction PH0_A determined from the signal acquired with sequence A corresponds to the phase of M_A , displayed in Fig. 2.7, the phase correction PH0_B determined from the signal acquired with sequence B to the phase of M_B .

From PH0_A and PH0_B , the phase difference Δ is determined to $\Delta = \text{PH0}_A - \text{PH0}_B$. Using the absolute value of Δ and equation (2.13), φ was calculated. With the phase correction angle φ added to the phase of the rectangular shaped 180° pulse of sequence B, Fig. 2.6, the water signal was acquired a third time. After Fourier transformation, as for the

preceding acquisitions, the 0th order phase correction for an absorption mode peak was determined, called PHO'_B in the following. The phase difference Δ was calculated from PHO_A and PHO'_B . For a correctly adjusted φ , Δ should be determined to $\Delta = 180^\circ$. If this is not the case, the value of φ has to be subtracted.

In order to verify the accuracy of the result found for φ , a dqf spectrum was acquired from the same voxel. As for the phase calibration sequence Fig. 2.6 B, φ was adjusted for the phase of the dqc and read pulse (see section 2.3.1.2, 2.3.1.3). DQC and read pulse need to have the same phase. The dqf sequence was realized as described in 2.3.4, using 2 ms pulselengths for the selective excitation and refocusing pulses and a length of 350 μs for the dqc pulse. A spectral width of 4960 kHz on 4096 points was acquired, performing 8 dummy scans before the start of the acquisition and accumulating the signal from the 64 following scans.

Twelve further dqf spectra were acquired from the same voxel position, using the parameterization described above, but varying the phase added to the dqc and read pulse from one spectrum to the next. Six spectra were acquired using a phase varying from $(\varphi + 10^\circ)$ to $(\varphi + 60^\circ)$, six further spectra using a phase from $(\varphi - 10^\circ)$ to $(\varphi - 60^\circ)$, where φ is still the value determined by the phase calibration procedure described above.

Line broadening of 8 Hz was applied to all dqf spectra before zero-filling and Fourier transformation. No further posttreatment as phase correction was used, as the spectra were evaluated in magnitude mode. All posttreatment was performed using the IDL programming language (RSI, Boulder).

Further tests were performed in order to investigate the influence of different parameters of the phase calibration sequence on the calibrated phase φ . For a given voxel position, the phase angle φ was determined once using a 500 μs block pulse and once using a 300 μs block pulse with all other parameters left unchanged. Furthermore, φ was determined once setting the spoiler gradients surrounding the block pulse to 16 mT/m (40% of the maximum value of the gradient system), once doubling them to 32 mT/m (80%). Also, φ was determined applying the gradients of the VAPOR water suppression module at the beginning of the sequence, without using the VAPOR rf pulses.

2.4.1.2 Results

Fig. 2.9 shows the voxel position inside the spherical phantom. From the signals acquired with the two sequences used for phase calibration (Fig. 2.6, A, B) as described above, PHO_A and PHO_B were determined, showing a phase difference of $\Delta = -2^\circ$. With the absolute value of Δ , the phase correction angle φ was determined to $\varphi = -89^\circ$. This phase correction angle subtracted from the phase of the rectangular shaped 180° pulse of sequence B, the acquisition of the signal with sequence B, Fig. 2.6, was repeated. As expected, Δ determined from PHO_A and PHO'_B (see above, methods section) was now close to 180° , being $\Delta = 179^\circ$ (spectra not shown).

Fig. 2.10 shows the glutamate peak at 2.3 ppm as acquired with the localized dqf sequence in different acquisitions. The signal marked by an arrow has been acquired with ϕ set to the value determined with the phase calibration procedure. The signals to the left and to the right of this peak have been acquired changing the phase correction ϕ from the determined value in steps of 10° . All signals are shown in the magnitude mode. It can be seen in Fig. 2.10 that maximal signal amplitude is acquired with ϕ set to the calibrated value (signal marked by an arrow). Acceptable signal strengths can still be acquired for ϕ values varying up to 15° from the calibrated value.

Altering the length of the block pulse of the calibration sequence from $500 \mu\text{s}$ to $300 \mu\text{s}$ changed the determined value for ϕ by 21° . Doubling the amplitude of the spoiler gradients that surround this pulse changed ϕ by 15° . The same value was determined for ϕ with the gradients of the VAPOR module preceding the calibration sequence set or switched off.

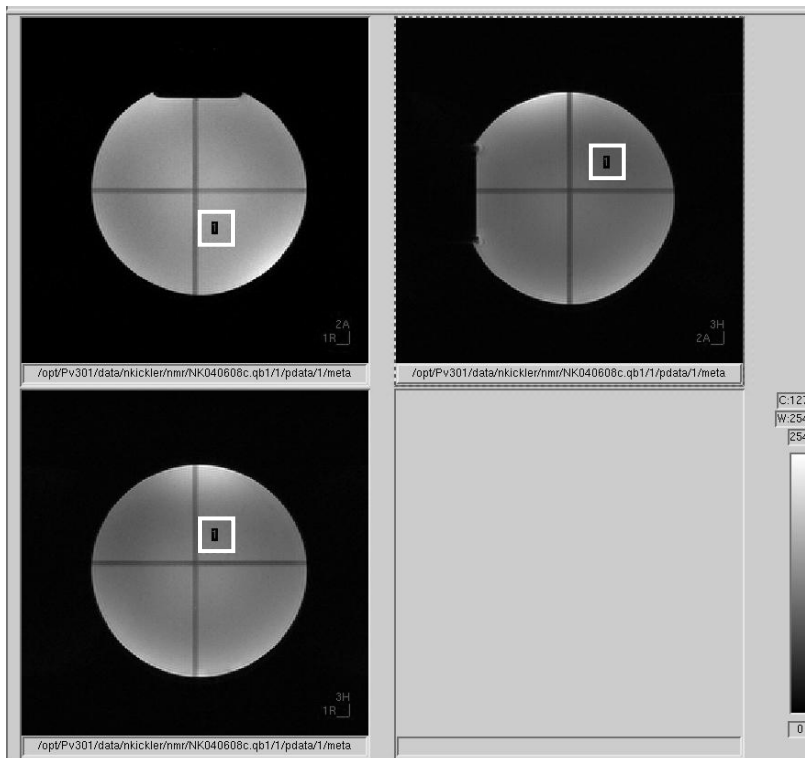


Fig. 2.9: Voxel position inside a spherical phantom used for acquisitions to verify the phase calibration procedure. A voxel of $(2.5 \times 2.5 \times 2.5) \text{ cm}^3$, shifted from the magnet isocenter in x, y and z direction (x-shift = 1.5 cm, y-shift = 2.8 cm and z-shift = 2.1 cm) was chosen.

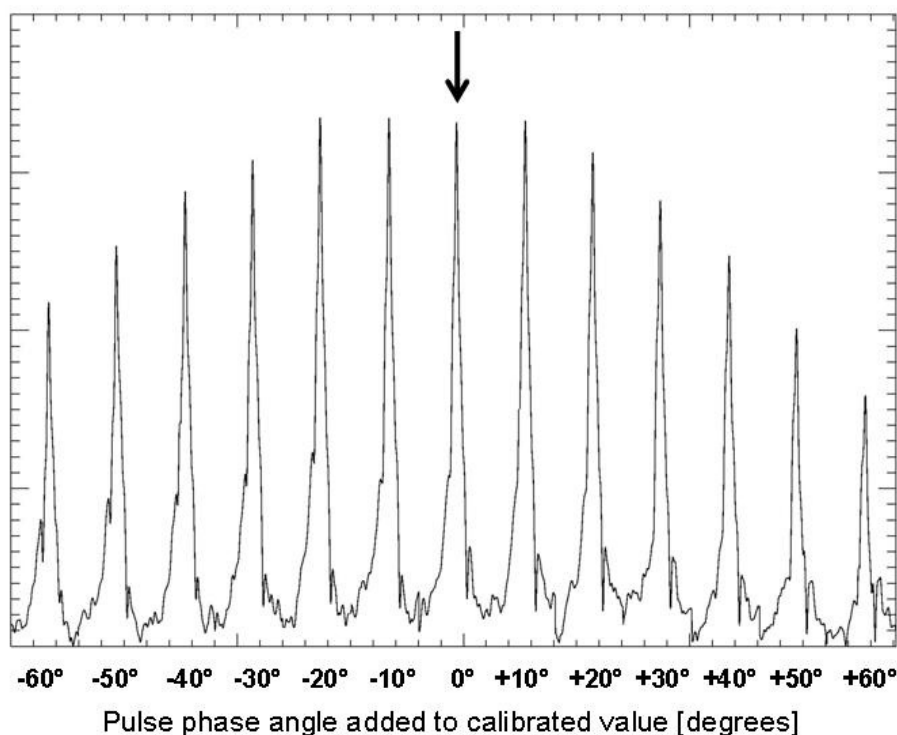


Fig. 2.10: Glutamate signal at 2.3 ppm (magnitude mode) as acquired with the localized dqf sequence in different acquisitions from the voxel position shown in Fig. 2.9. The signal marked by an arrow has been acquired with the dqc and read pulse phase corrected by φ as determined with the phase calibration procedure. The signals to the left and to the right of the peak marked by the arrow have been acquired changing φ from the determined value in steps of 10° . As demonstrated, the implemented phase calibration procedure allows determination of φ to obtain optimal signal intensity from off-center voxel positions.

2.4.1.3 Discussion

Using the phase calibration sequence described in this chapter, the phase correction of dqc and read pulse, as it is necessary for acquisitions from off-center voxel positions, can be reliably determined. Fig. 2.10 demonstrates that the calibrated φ value is optimal.

We observed that the length of the 180° block pulse of the phase calibration sequence had an influence on the value determined for φ . The blockpulses in calibration- and filter sequence should therefore have the same duration. We choose a duration of $350 \mu\text{s}$ as this is the shortest pulse length with which a flip angle of 180° can be realized on our system. As well, the amplitude of the spoiler gradients surrounding the blockpulse in the phase calibration sequence has an influence on the value determined for φ . Not completely refocused magnetization due to gradient imperfections, depending on the gradient amplitude, may explain this shift in phase. As these gradients do not exist in the dqf sequence, their amplitude should be kept as small as possible. The same influence on the signal phase could have residual gradients of the VAPOR module used in the dqf sequence. It might be necessary, in order to assess this influence, to use these gradients at the beginning of the phase calibration sequence, in the same way as they

precede the dqf sequence. In our case, the influence of these gradients was however negligible.

2.4.2 Experiments on metabolites in solution

In order to assess the ability to acquire spectra containing mainly glutamate signal with the double quantum filter sequence, experiments on samples, each containing only one metabolite, were performed. Samples contained either glu, gln, NAA or GABA, as these present resonances in the chemical shift range targeted by spectral editing, near 2.3 ppm. The superposition of the individual metabolite spectra gives an indication about the composition of the signal observed *in vivo*.

2.4.2.1 Materials and methods

The same spectrometer configuration as described in 2.4.1.1 has been used. Samples containing glu, gln, NAA and GABA at 50 mM in a phosphate buffer were prepared. The samples contained about 0.25 mmol/l chelated gadolinium complex (0.5 ml/l Dotarem, Guerbet, France) as relaxant. The pH value of each sample was adjusted to a value typical for the brain, about 7.3, after having added all components. A sample volume of 270 ml, enclosed in spherical glass containments, was used for the experiments. The sample was placed in the middle of the birdcage resonator, surrounded by four 500 ml plastic bags containing physiological serum, in order to ensure correct loading of the resonator. The dqf sequence was realized as summarized in 2.3.4, using 4 ms pulses for voxel localization and a dqc pulse of 250 μ s length. No phase calibration for the dqc and read pulse phase was performed as the voxel was chosen in the magnet isocenter; the phase correction angle ϕ was set to zero. A spectral width of 4960 Hz was acquired on 4096 points. For referencing purposes, the unsuppressed water signal was acquired from the same voxel as the dqf spectrum for the different samples.

A line broadening giving a linewidth of about 7 Hz on the water signal was determined for each reference spectrum. This broadening was then applied to the corresponding dqf spectrum, in order to account for differing field homogeneities in the different experiments. A common line broadening was then applied to all spectra, giving a linewidth of about 12 Hz on the water signal. This is the linewidth typically found after posttreatment for the *in vivo* experiments presented in this work. All dqf spectra were normalized with respect to the water peak amplitude in order to account for further differences in signal intensity. The spectra were then multiplied with the typical concentration for the respective metabolite in the brain, as taken from the literature (Govindaraju, Young et al. 2000). We assume a concentration of 9.25 mmol/kg w.wt. for glutamate, 4.4 mmol/kg w.wt. for glutamine, 12.25 mmol/kg w.wt. for NAA and 1.6 mmol/kg w.wt. for GABA. Phasing of the spectra is difficult as there is no singlet signal present that could serve as reference. The water signal originating from the same volume was therefore used: The same 0th order phase correction as for the water peak was applied to the dqf spectra. The sum of the different metabolite signals was then

phased to present a signal in absorption mode. This global phase correction was then applied to each individual metabolite dqf spectrum in order to plot the peak decomposition. A common frequency shift was applied to all individual spectra together in order to position the sum peak at 2.3 ppm.

2.4.2.2 Results

Fig. 2.11 shows the dqf spectra acquired on the samples containing either glutamate, glutamine, NAA or GABA. The spectra have been superposed and their sum has been calculated. The sum is displayed as solid line, glutamate as dotted-, glutamine as dashed- and NAA as dash-dotted line. GABA is printed as dash-dot-dot-dot line.

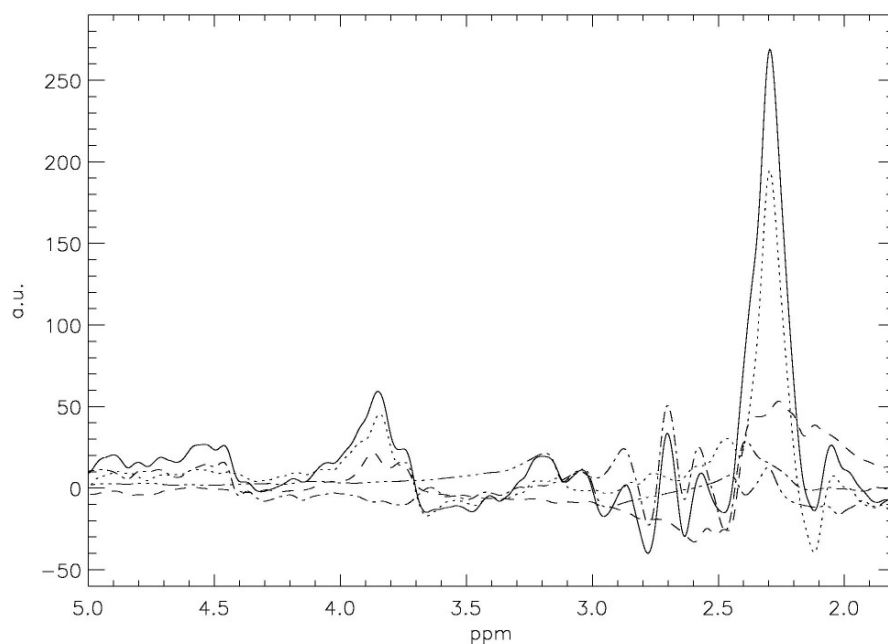


Fig. 2.11: Superposition of dqf spectra acquired on a solution containing either glutamate (dotted), glutamine (dashed), NAA (dash dot) or GABA (dash dot dot dot). The sum of the different signals has been drawn as solid line. For the plot, assumed concentrations were: glutamate 9.25 mmol/kg w.wt., glutamine 4.4 mmol/kg w.wt., NAA 12.25 mmol/kg w.wt. and GABA 1.6 mmol/kg w.wt. About 72% of the sum signal amplitude is due to glutamate, 16% due to glutamine.

The sum of glu, gln, NAA and GABA, as they are acquired with the dqf sequence, displays one preeminent peak that is dominated by glutamate. The second strongest component in the peak is glutamine. From Fig. 2.11 it can be estimated that about 72% of the sum signal amplitude is due to glutamate, 16% due to glutamine. NAA and GABA contribute less than gln to the main peak. Singlet signals, as they would be visible in a non edited spectrum from NAA at 2 ppm and from water at 4.7 ppm, are not present.

2.4.2.3 Discussion

The aim of spectral editing is to acquire a well formed signal from glutamate with as few as possible contamination from other metabolites. As can be seen in Fig. 2.11, the signal contains principally glutamate but also a non negligible amount of glutamine. Contributions of NAA and GABA are less important. The glutamate signal that can present a highly complicated lineshape (Govindaraju, Basus et al. 1998) has been simplified by spectral editing to a single peak. How much the content of other metabolites than glutamate in the measured signal is disturbing depends on the intended application. If strong glutamate changes are to be measured and if it can be assured that the levels of gln, NAA and GABA remain constant, changes of glu will be well reflected by changes of the peak acquired with the dqf sequence. Small changes may however become masked. As the roles of glutamate and glutamine are connected in brain metabolism, a rise of one of the components may in some cases bring along a decrease in the other. In this case, the combined glutamate+glutamine signal observed with dqf filtering may remain unchanged.

2.4.3 *In vivo* application

The double quantum filter sequence is used for acquisitions on the human brain to show the validity of this approach. First, a spectrum from a centered voxel position is presented. Then, to demonstrate the feasibility of *in vivo* phase calibration, acquisitions from a voxel in an off-center position are shown.

2.4.3.1 Materials and methods, acquisition from a voxel in the magnet isocenter

The same spectrometer configuration as described in 2.4.1.1 has been used. The dqf sequence was realized as summarized in 2.3.4, using 4 ms pulses for voxel localization and a dqc pulse length of 250 μ s.

Acquisitions start with scout images of the head, acquiring an axial, frontal and transverse view (machine coordinate system). We used an imaging protocol based on a FLASH method preinstalled on our spectrometer. According to the scout images, the patient bed is moved in z-direction to position the upper half of the patient's brain in the magnet isocenter. Local adjustments of the resonance frequency and the rf power (via BRUKER reference gain) are performed in a (39 mm)³ voxel in the isocenter, using procedures implemented with the BRUKER supplied PRESS sequence. Preliminary tests showed that no further fine adjustment of the rf power is necessary, the implemented automatic adjustment performs well. A larger voxel size than the one chosen for later acquisitions is used for calibrations to account for voxel displacements due to differing chemical shifts of the brain metabolites. Automatic first and second order localized shimming is performed using FASTMAP (Gruetter 1993). The voxel size is then reduced to a (25 mm)³ voxel. For referencing purposes, the unsuppressed water signal is acquired from this voxel, using PRESS. Before starting dqf acquisitions, the rf power of the VAPOR pulses is fine adjusted by hand. Spectra using the dqf sequence were acquired with the resonance frequency set to the glutamate peak at 2.3

ppm. The voxel position for this chemical shift is exactly at the specified position in this way. A spectral width of 4960 Hz on 4096 points was acquired. Acquisitions used 256 accumulations with a repetition time of 3 seconds and started with dummy scans in order to establish equilibrium magnetization. Total acquisition time for one spectrum was about 14 minutes. Posttreatment was performed with the IDL programming language (RSI, Boulder). Six Hertz exponential broadening was applied to improve the signal to noise ratio, the spectra were zero-filled to 8192 points to smooth the lineshape. Necessary zero order phase correction was determined to phase the signal visible near 2.3 ppm to absorption mode.

2.4.3.2 Results, acquisition from a voxel in the magnet isocenter

Fig. 2.12 shows the voxel from which the double quantum filtered spectrum has been acquired, positioned on the axial, frontal and transverse scout images. The two black lines on each image, intersecting in the middle of the voxel, are due to saturation effects that originate from the acquisition of the images. Their intersection point indicates the magnet isocenter. The image contrast does not allow for gray matter / white matter distinction, but is sufficient to recognize the major brain structures. The brain region where the voxel is positioned is unproblematic with respect to shimming, resulting in a linewidth of about 7 Hz for the water signal of this voxel size.

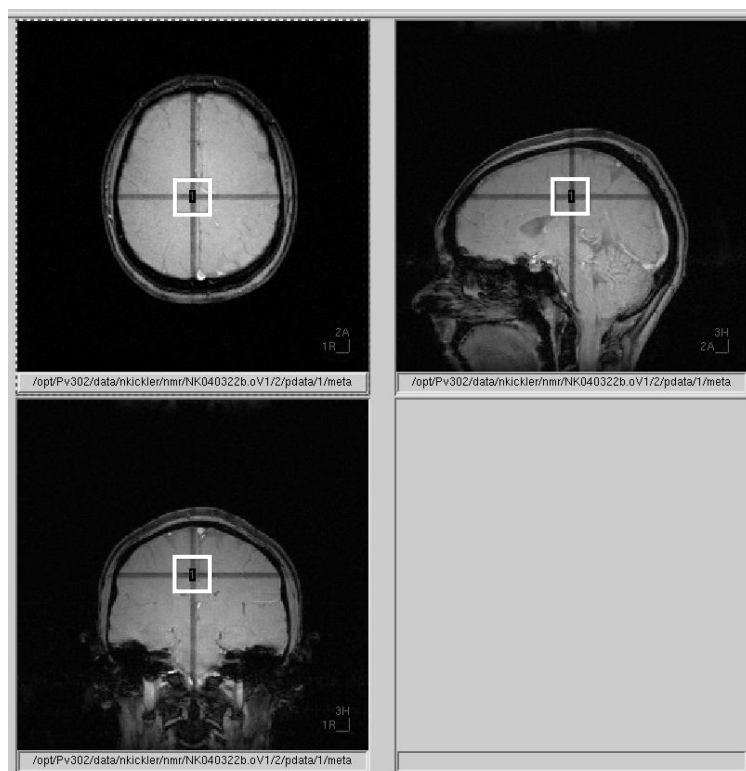


Fig. 2.12: Voxel of $(25 \text{ mm})^3$ size, positioned on the parietal lobe of a volunteer for acquisition of a dqf spectrum. The volume is situated in the magnet isocenter, as indicated by the intersection of the two black lines on each image (originating from saturation effects during acquisition of the two perpendicular images). The dqf spectrum acquired from this position is shown in Fig. 2.13.

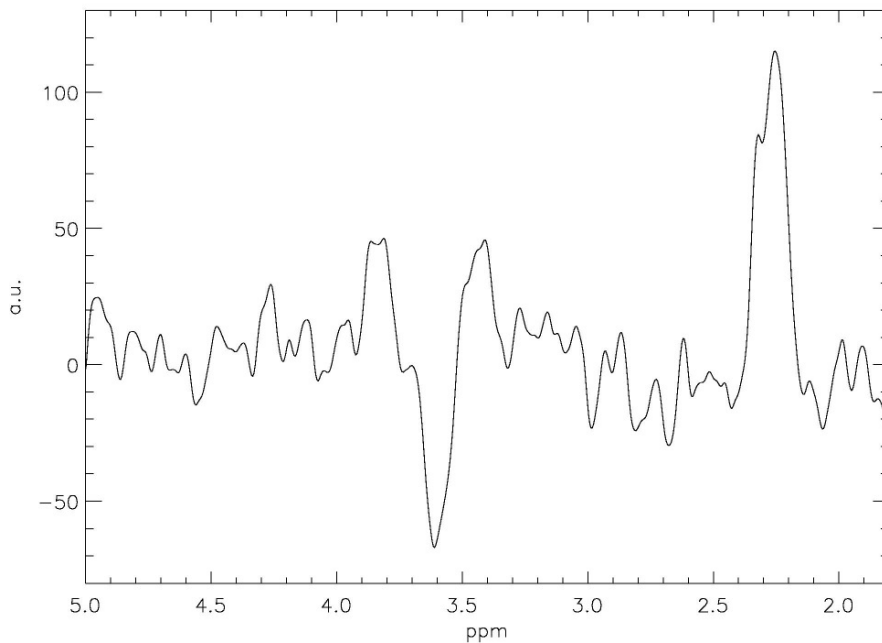


Fig. 2.13: DQF spectrum acquired from a $(25 \text{ mm})^3$ voxel positioned on the parietal lobe of a volunteer, indicated in Fig. 2.12. The peak at 2.3 ppm originates mainly from glutamate, as demonstrated *in vitro*. No water signal is visible in the spectrum and the baseline is essentially flat. DQF spectra of good quality can be acquired *in vivo*.

Fig. 2.13 shows the dqf spectrum acquired from the $(25 \text{ mm})^3$ voxel, positioned as indicated in Fig. 2.12. One single peak is visible at about 2.25 ppm, a further less important signal near 3.7 ppm. Referencing of the ppm scale has been performed setting the middle of the spectrum, corresponding to the water peak position, to 4.7 ppm. The baseline is essentially flat; no water signal contaminates the spectrum. The signal to noise ratio of the peak at 2.25 ppm is about nine. Singlet signals from metabolites present in the human brain, as for example creatine or choline, are efficiently suppressed. In this acquisition, distortions appeared below 1.6 ppm. They are excluded from the picture of this spectrum.

2.4.3.3 Materials and methods, acquisition from a voxel not positioned in the magnet isocenter

The spectrometer configuration as described in 2.4.1.1 has been used. The dqf sequence was realized as summarized in 2.3.4, using 2 ms pulses for voxel localization and a dqc pulse of 350 μs length. A 100 μs longer dqc pulse was necessary to match the pulse length of the blockpulse in the phase calibration sequence, as has been explained before. As for the experiments described above, acquisitions start with scout images of the head, acquiring an axial, frontal and transverse view (machine coordinate system). The voxel position is then freely chosen on the images. For the present experiments we chose a position in the right parietal lobe. In this region good field homogeneity via shimming can be achieved. Local adjustments of the resonance frequency and the rf power (via the BRUKER reference gain) were performed in a $(39 \text{ mm})^3$ voxel. As for the former experiments automatic first and second order localized shimming was done.

The voxel size is then reduced to $(25 \text{ mm})^3$ and the unsuppressed water signal is acquired. As the voxel is not positioned in the magnet isocenter, the phase of the dqf and read pulse have to be calibrated. The procedure described in section 2.4.1.1 has been performed *in vivo*, with the pulse carrier frequency adjusted to the glutamate resonance at 2.3 ppm. Running the dqf sequence in setup mode, VAPOR pulse gains were fine adjusted. The same acquisition parameters for the dqf sequence as described in 2.4.3.1 and the same posttreatment, using 6 Hz exponential broadening, have been used.

2.4.3.4 Results, acquisition from a voxel not positioned in the magnet isocenter

Fig. 2.14 shows the voxel position chosen for the acquisition of the dqf spectrum. The two black lines on each image indicate the magnet isocenter. The $(25 \text{ mm})^3$ voxel is approximately shifted 1.6 cm to the right, 1.3 cm upwards and 1.9 cm in the anterior direction. As can be seen on the images, the voxel is distant from problematic regions as the ventricles or the scalp. A linewidth of about 6Hz has been achieved for the water peak after automatic 1st and 2nd order shimming.

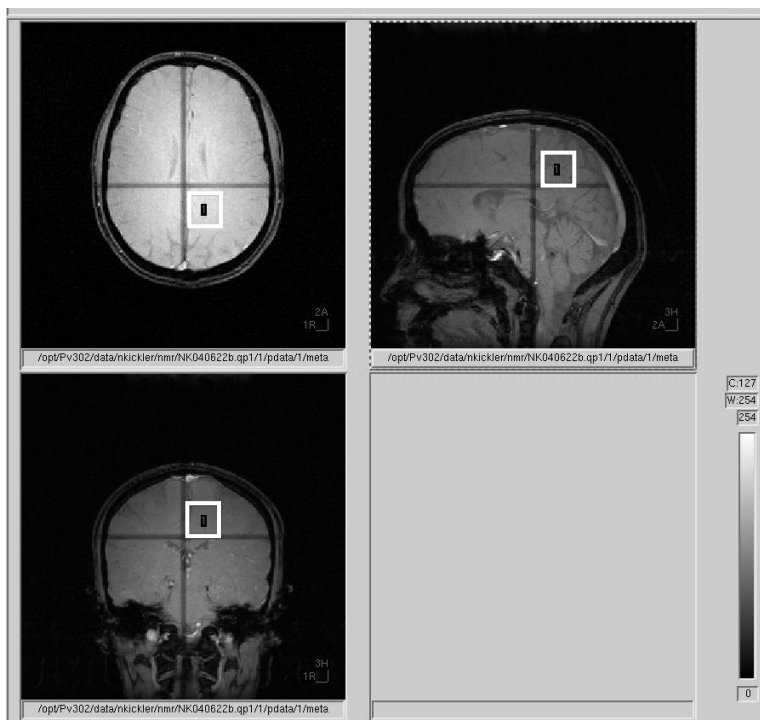


Fig. 2.14: Voxel of $(25 \text{ mm})^3$ size, positioned on the parietal lobe of a volunteer for acquisition of a dqf spectrum. The voxel is approximately shifted 1.6 cm to the right, 1.3 cm upwards and 1.9 cm in the anterior direction with respect to the magnet isocenter (situated at the intersection of the two black lines on each image). The dqf spectrum acquired from this position is shown in Fig. 2.15.

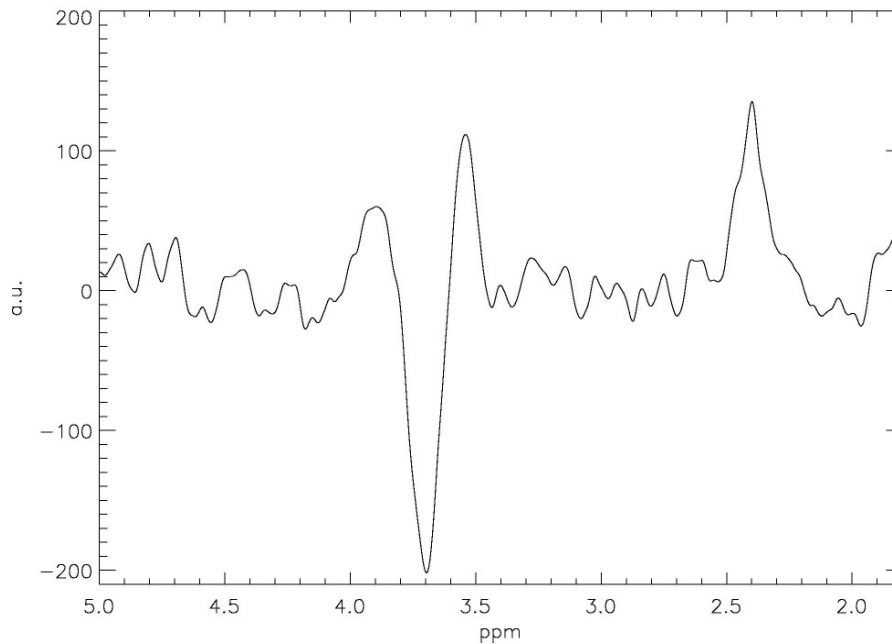


Fig. 2.15: DQF spectrum acquired from a $(25 \text{ mm})^3$ voxel positioned in the parietal lobe of a volunteer, as shown in Fig. 2.14. The voxel was not situated in the magnet isocenter and phase calibration of dqf and read pulse was performed prior to acquisition of the spectrum. The signal at 2.3 ppm contains principally glutamate, the signal at 3.7 ppm glutamate and glutamine. No water is visible in the spectrum and the baseline is essentially flat. Spectra of good quality can be obtained from off-center positions.

Fig. 2.15 shows the dqf spectrum acquired from the voxel position indicated in Fig. 2.14. A phase correction of $\phi = 83^\circ$ for the read and dqc pulse was necessary. The spectrum essentially displays one peak at 2.4 ppm. Referencing of the ppm scale has been performed setting the middle of the spectrum, corresponding to the water peak frequency, to 4.7 ppm. The signal at 2.4 ppm has a signal to noise ratio a bit better than nine. A further strong signal is visible at near 3.7 ppm. This signal can not be phased to absorption mode. No water peak is visible in the spectrum, resulting in a flat baseline. At lower or higher frequencies near the spectral range displayed, no line distortions or signals are visible. The total duration of the measurement protocol was about 45 minutes.

2.4.3.5 Discussion

Double quantum filtered spectra can be acquired *in vivo* from the human brain, as is demonstrated by Fig. 2.13. and Fig. 2.15. The editing approach is successful as one single peak remains in the spectrum. The suppression of uncoupled singlet signals, as for example of total creatine or total choline, leads to a highly simplified spectrum with a single well visible peak remaining. The very strong *in vivo* water signal was completely eliminated, using VAPOR and taking advantage of implicit water suppression of double quantum filter sequences. A completely flat baseline was achieved. The signal to noise ratio of the peak of interest in both spectra, about nine, is quite low considering voxel size and acquisition duration. Uncomplicated spectral pattern and flat baseline simplify signal quantification; integration between fixed

frequency limits for example could readily furnish acceptable results. Normalization of the measured peak although has to be done via an external signal, as there is only one peak of known origin in the edited spectrum. The water signal, acquired in a separate acquisition, could be used. Calculating ratios between distinct acquisitions may although add variability to quantification. The low signal to noise ratio, in spite of the relatively big voxel size (about 16 ml) and in spite of the good field homogeneity (about 6 Hz for the water peak) achieved at this voxel position, is a very strong drawback. Compared to brain structures, the voxel volume is very large. Precise measurements are thereby difficult to perform.

Further signals in both spectra are present near 3.7 ppm. These signals originate partially from the glu and gln ^2CH resonances, as can be determined by comparison with the *in vitro* acquisitions, Fig. 2.11. The size of these signals in the shown spectra is although stronger than predicted. Coupled resonances of other molecules present in this spectral area, as myo-inositol, may contribute. In the spectrum shown in Fig. 2.15 signals appear near 1.6 ppm. In spectra from comparable voxel positions, these signals are not always present. Their origin could be residual lipid signals, whose suppression partially depends on the use of phase cycling. Accidental head movement could lead to small signal alterations, reducing efficiency of the phase cycling. The presence of lipid signals indicates contamination from areas external to the voxel volume. Outer volume suppression (OVS) could be used to reduce this contribution. The residual signal near 3.7 ppm and the one near 1.6 ppm are however distant enough to not disturb the signal of interest, situated at 2.3 ppm.

The composition of the peak at 2.3 ppm may be assessed by comparison with the *in vitro* acquisitions shown in Fig. 2.11. *In vitro* acquisitions used the same sequence configuration as for the spectrum shown in Fig. 2.13. The spectrum from an off-center voxel in Fig. 2.15 used 2 ms shorter excitation / refocusing pulses and a 100 μs longer dqc pulse than the *in vitro* acquisitions. The peak composition shown in Fig. 2.11 should still however be a very good approximation. As stated before, the major contribution to the peak of interest at 2.3 ppm is given by glutamate. A further more precise comparison of the peakform obtained *in vitro* and *in vivo* is difficult because of the low signal to noise ratio *in vivo*.

Double quantum filtered spectra can be acquired *in vivo* from freely positioned voxel positions. Phase calibration of the dqc and read pulse is indispensable. For the acquisitions shown in Fig. 2.15 a phase correction of more than 80° was necessary. Omitting this correction would have led to almost complete signal extinction, as may be estimated looking at the influence of the phase on the signal amplitude, Fig. 2.5.

2.5 Conclusion and perspectives

In this chapter we have demonstrated the feasibility of using double quantum filtering for detection of glutamate in the human brain at field strengths of 3 Tesla. The double quantum filtered spectrum contains foremost glutamate. Residual signals of other metabolites, mainly glutamine, persist however (comparing Fig. 2.11 and Fig. 2.15). The spectra are easily interpretable, presenting mainly one signal peak, a flat baseline and no water signal. Normalization of the spectrum for comparison between different exams and quantification has to be done with the signal from another acquisition. The water peak or easily measured singlet signals as those of NAA or creatine may be used, or even model spectra (Provencher 1993). The glutamate content in the dqf spectrum as well as the *in vivo* signal to noise ratio achieved in this work is comparable to that of earlier studies (Thompson and Allen 1998; Schubert F 2001). It would be interesting to continue the process of numerical optimization, as proposed by (Thompson and Allen 1998), to examine whether improvements in glutamate/glutamine distinction are possible simulating the exact pulseshapes and the exact magnetic fieldstrength of our system. For positions outside the magnet isocenter, calibration of the relative pulse phases has to be performed. The calibration procedure is complicated and increases significantly the protocol duration. Acquiring only low quality images for voxel positioning, the protocol duration was about 45 minutes. For medical studies, this duration is lengthened by the necessary acquisition of more precise images for exact voxel placement. The application of a protocol with this duration for clinical research could be difficult. Most spectrometers offer however the possibility to program automations of complex processes. Programming of a macro for phase calibration would significantly reduce user interaction and time consumption, so that the use on patients could be possible. During *in vitro* experiments, using larger voxel displacements than in section 2.4.3, strong variations in the signal intensity have been observed, leading in some cases to strong signal reduction. The acquisition sensitivity of a birdcage resonator is best in its coil center and reduced in the surrounding area. This may account for reduced signal to noise ratios. Furthermore, less well formed slice profiles produced by the excitation and the refocusing pulses have been observed in these spatial regions. Given the complexity of signal preparation in the filter sequence, asymmetric voxel shapes may have a negative influence on the filtering efficiency. Of strong concern is the low signal to noise ratio, achieved in spite of the large voxel size and the good field homogeneity. The higher the variability, the more exams are needed in clinical studies to verify or dismiss the hypothesis to be tested. Large variability of the measuring method therefore leads to long, expensive studies. In brain regions difficult to shim, as the profound structures of basal ganglia (an area of interest for research on Parkinson's disease), the signal to noise ratio will be still lower. The possibility to achieve exact results from small brain structures is limited by the large voxel size. The double quantum filter method should therefore preferably be used when important concentration changes of glutamate are to be expected in relatively large structures.

Only few methods allowing glu detection at field strengths of 3 Tesla or below have been proposed so far. Among these the double quantum filter method presented in this work offers a technically demanding but interesting approach. The performance of this technique will be compared to another method for glutamate detection in the following chapter.

3 TE averaged PRESS for brain glutamate detection at 3 Tesla

Ce chapitre décrit l'évaluation de la méthode « TE averaged PRESS » (Hurd, Sailasuta et al. 2004) pour la mesure de glutamate cérébral à 3 Tesla. Des expériences en amont sur des métabolites en solution permettent d'estimer la contribution du glutamate par rapport à d'autres métabolites. La méthode est ensuite évaluée pour des acquisitions in vivo. Les résultats obtenus sont comparés à des spectres PRESS acquis à des temps d'écho de 80 ms et de 136 ms.

3.1 Introduction

In J-resolved spectra, the multiplet structure of coupled molecules is resolved in two frequency dimensions, called f_1 and f_2 . The dimension f_2 is related to the acquisition time, called t_2 . To introduce an additional dimension, several PRESS spectra with linearly increased echo times are acquired, providing a second time dimension t_1 . By Fourier transformation with respect to t_1 , one obtains the second spectral dimension f_1 . A TE averaged PRESS spectrum (Hurd, Sailasuta et al. 2004) is the $f_1 = 0$ trace of such a two dimensional J-resolved spectrum.

As certain resonance lines from coupled molecules appear at frequencies of $f_1 \neq 0$, signal overlap is reduced in a TE averaged spectrum as compared to normal PRESS spectra. In the case of glutamate, resonance lines of glutamine, NAA and GABA overlap with glutamate in usual PRESS spectra. In two dimensional J-resolved spectra, some of these overlapping signals are moved in the f_1 direction and glutamate may thereby be observed almost unobstructed (Hurd, Sailasuta et al. 2004) on the central trace.

An important influence on the overlap of the glutamate signal with the other resonances has the f_1 resolution. If the resolution is not sufficient, the t_1 acquisition window too small, contributions of gln, NAA and GABA become increased. At three Tesla field strengths, a glutamate signal with only minor contributions of other resonances may be acquired using a t_1 acquisition window length of 165 ms. The f_1 resolution of about 6 Hz per point is however not sufficient to use the information content of the whole two dimensional spectrum. It is advantageous to be able to work with relatively small t_1 acquisition windows. For a given number of total scans, determining the experiment duration, more time per t_1 step can be used for signal acquisition as compared to larger t_1 windows. The signal to noise ratio of the individual PRESS spectra is improved, allowing individual shift and phasing corrections.

A TE averaged spectrum is easily obtained by adding all individual spectra of the 2D acquisition. The following notation will be used from now on: A scan corresponds to a

single acquisition with a fixed echo time. The accumulation of several scans will be called experiment. All experiments with their individual echo times together are called J-resolved acquisition.

3.2 Experiments on metabolites in solution

As for the double quantum filter sequence, *in vitro* acquisitions on samples containing a single metabolite were performed. Samples contained one of the metabolites of glu, gln, NAA or GABA. These metabolites present resonances in the region of interest, near 2.3 ppm. The superposition of the single metabolite spectra gives information about the composition of the signal observed *in vivo* and allows to assess possibilities of glutamate detection.

3.2.1 Materials and methods

The same spectrometer and configuration as for the double quantum filter experiments, described in the preceding chapter, has been used (3 T whole body imager, 8 kW rf amplifier, birdcage head coil for signal excitation and reception). As well, the same samples containing glu, gln, NAA or GABA have been used (50 mM metabolite solution in phosphate buffer, 0.25 mmol/l chelated Gadolinium (0.5 ml/l Dotarem, Guerbet) as relaxant, pH adjusted to 7.3, 270 ml sample volume enclosed in spherical glass containments). TSP (3-(Trimethylsilyl)- Propionic acid), was added to each sample as frequency and phase reference. For the experiments, the sample was placed in the middle of the birdcage resonator, surrounded by four 500 ml plastic bags containing physiological serum, in order to ensure correct coil loading. A PRESS and a TE averaged PRESS spectrum were acquired from each sample.

The BRUKER supplied source code of a PRESS implementation on our machine was modified to allow acquisitions of 2D J-resolved spectra. Half of the echo time augmentation from one scan to the next was added to the first echo time, half to the second echo time. Hermitian pulseshapes of 2 ms length were used for PRESS, water suppression was achieved by VAPOR (Tkac, Starcuk et al. 1999). VAPOR used hermitian pulses for selective water excitation. A (25 mm)³ volume, well contained within the sample, was chosen for acquisition. After local adjustments of resonance frequency and rf gain and after local shimming, the unsuppressed water signal was acquired for referencing purposes. For comparison with TE averaged PRESS, a PRESS spectrum with an echo time of TE = 136 ms was performed, accumulating 128 scans. The total echo time was divided symmetrically between the first and the second echo time. An echo time of 136 ms is usually used in clinical applications as lactate presents a fully inverted doublet at this evolution time. Lactate presence can thereby be discriminated from lipid signals. For TE averaged PRESS, 17 experiments starting at TE = 35 ms were acquired and stored in a 2D data matrix. TE was increased in steps of 10 ms, 8 scans per experiment were accumulated. PRESS and TE averaged PRESS acquisitions started with eight dummy scans to achieve steady state. A spectral width of

5000 Hz on 4096 points was acquired using repetition time of 3 seconds. Eight step phase cycling (Henning 1992) was used during accumulations.

Posttreatment used the IDL programming language (RSI, Boulder). Each single experiment of the TE averaged PRESS acquisition was corrected for frequency shift and 0th order phase using the TSP signal as reference. Differences in field homogeneity (shim) achieved on the different samples were assessed via the frequency width of half max of the water reference scan. The water linewidths were similar for the acquisitions on the different samples. Exponential broadening was applied to achieve a linewidth of about 7 Hz on the NAA singlet signal. This is the linewidth we usually find for good *in vivo* spectra after posttreatment. The same broadening was then applied to the spectra of glu, gln and GABA. To simulate signal decay caused by T₂ relaxation over different experiments in TE averaged PRESS acquisitions, a decaying exponential was applied in t₁. A decay characterized by a T₂ of 200 ms (Traber, Block et al. 2004) was adjusted on the singlet signal of NAA and then applied to the spectra of glu, gln and GABA. Finally, TE averaged spectra were calculated by summing up the experiments of the 2D J-resolved acquisition.

PRESS spectra acquired at TE = 136 ms were as well phased and frequency shift corrected using the TSP reference signal. The same line broadening as determined for the TE averaged PRESS acquisitions was applied.

The spectra of the different metabolites were multiplied with the typical concentration for the respective metabolite in the brain, as taken from the literature (Govindaraju, Young et al. 2000). We assume a concentration of 9.25 mmol/kg w.wt. for glutamate, 4.4 mmol/kg w.wt. for glutamine, 12.25 mmol/kg w.wt. for NAA and 1.6 mmol/kg w.wt. for GABA.

3.2.2 Results

Fig. 3.1 shows the TE averaged spectra acquired on the samples containing glutamate, glutamine, NAA or GABA. The spectra have been superposed and their sum has been calculated. The sum is displayed as solid line, glutamate as dotted-, glutamine as dashed- and NAA as dash-dotted line. GABA is printed as dash-dot-dot-dot line.

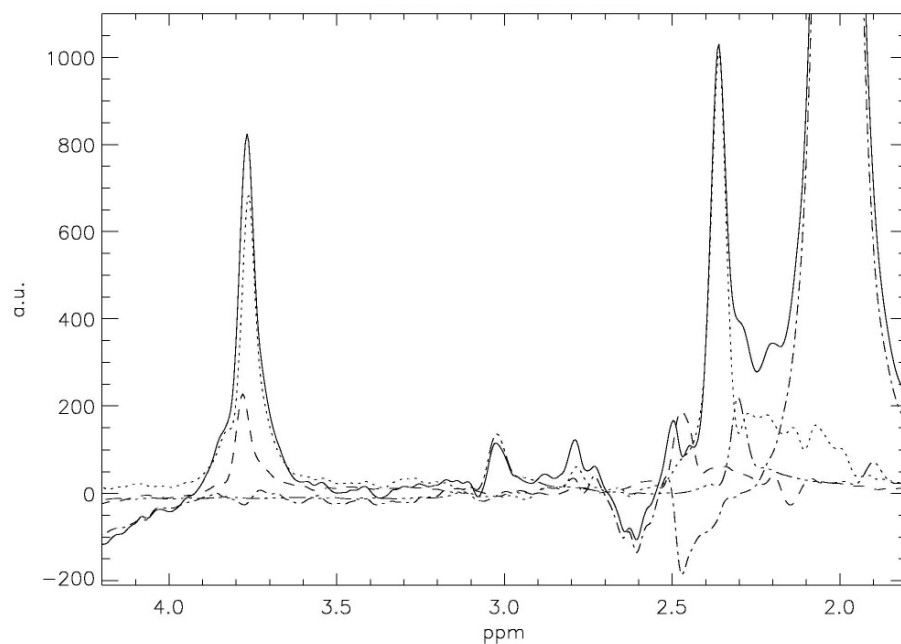


Fig. 3.1: TE averaged spectra acquired on samples containing in solution either glutamate, glutamine, NAA or GABA. The sum of the individual metabolite spectra is displayed as solid line, glutamate as dotted-, glutamine as dashed- and NAA as dash-dotted line. GABA is printed as dash-dot-dot-dot line. TE averaged PRESS allows the acquisition of a signal at 2.3 ppm containing almost exclusively glutamate.

Fig. 3.2 shows the PRESS spectra acquired on the samples containing glutamate, glutamine, NAA or GABA, using an echo time of 136 ms. The same linestyles as in Fig. 3.1 have been used to trace the spectra of the different metabolites and their sum.

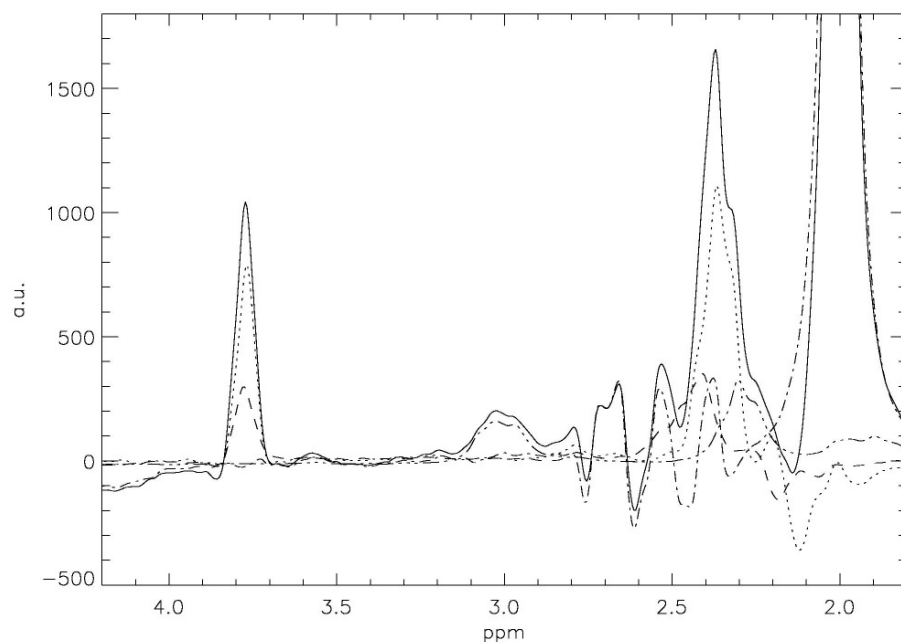


Fig. 3.2: PRESS spectrum using an echo time of 136 ms acquired on solutions containing either glutamate, glutamine, NAA or GABA. The sum of the individual metabolite spectra is displayed as solid line, glutamate as dotted-, glutamine as dashed- and NAA as dash-dotted line. GABA is printed as dash-dot-dot-dot line. The signal situated at 2.3 ppm is a mixture of glu, gln, NAA and GABA, with the glu part being the strongest component.

The PRESS as well as the TE averaged PRESS spectrum show a strong singlet signal of NAA at 2 ppm. The spectral shape in the region of interest, near 2.3 ppm, is strongly simplified in TE averaged PRESS. TE averaged PRESS spectra show a single peak containing almost exclusively glutamate left of NAA. The PRESS spectrum displays as well a marked signal at 2.3 ppm, that is however a mixture of glutamate, glutamine, NAA and GABA. The glutamate content of the signal in the PRESS spectrum may be estimated to be about 70% of the total peak area. At 3.7 ppm, as well in the PRESS as in the TE averaged PRESS spectrum, a single peak representing the sum of glutamate and glutamine is visible.

3.2.3 Discussion

TE averaged PRESS allows improved glutamate observation as compared to PRESS using an echo time of 136 ms. In PRESS spectra, the region near 2.3 ppm is characterized by overlapping multiplet signals. In the TE averaged PRESS spectrum, the glutamate signal dominates the sum of all metabolites (solid line of Fig. 3.1, Fig. 3.2) near 2.3 ppm. This improvement is not only achieved because contributions of gln, NAA and GABA are reduced, but also because the spectral shape of glutamate is simplified to a single line. As the TE averaged PRESS spectrum is the sum of PRESS spectra at different echo times, one can imagine how positive and negative signal contributions present at different echo times, add to zero and provide as sum a simplified spectrum. The signal at 2.3 ppm representing almost only glutamate in TE averaged PRESS may be easily quantified by peak integration or by fit of a Lorentzian lineshape.

Our results obtained *in vitro* concerning the resonances visible at 2.3 ppm in TE averaged PRESS are comparable to the ones published in the literature (Hurd, Sailasuta et al. 2004). Hurd *et al* find however equal glutamate peak amplitudes at 2.3 and 3.7 ppm, whereas in our experiments the 3.7 ppm resonance line is less intense. We have chosen to compare TE averaged PRESS to PRESS using an echo time of 136 ms because this echo time is usually used in clinical application, as it corresponds to complete inversion of the lactate doublet. Other groups (Schubert F 2001) use an echo time of 80 ms for glutamate detection, which they determined to be optimal. *In vivo* acquisitions at 80 ms will be presented later in this chapter and compared with TE averaged PRESS.

3.3 *In vivo* application

Experiments have been performed to assess the performance of TE averaged PRESS *in vivo*. PRESS spectra with an echo time of 136 ms and 80 ms have been acquired for comparison with TE averaged PRESS.

3.3.1 Materials and methods

The same spectrometer and configuration as used before, described in the preceding chapter, has been used (3 T whole body imager, 8 kW rf amplifier, birdcage head coil for signal excitation and reception). PRESS and TE averaged PRESS were parameterized as for the *in vitro* experiments in section 3.2.1 (2 ms hermitian pulseshapes for PRESS, VAPOR using hermitian pulses). For PRESS at 136 ms and TE averaged PRESS, longer pulses were used for VAPOR to improve selectivity of water suppression.

Experiments started with the acquisition of scout images in the frontal, axial and sagittal planes (machine coordinate system), using a FLASH based method. Slice packages oriented according to patient position were then acquired using an MDEFT sequence. Sagittal images were oriented parallel to the inter-hemispherical plane, transverse images perpendicular to the sagittal images and parallel to the axis defined by anterior and posterior commissures (ac and pc). Orientation of frontal images was thereby defined as orthogonal to the sagittal and transverse images. A voxel measuring 20 mm x 20 mm in the left-right and head-foot direction and 30 mm in the anterior-posterior direction was placed in the parietal lobe. This region was chosen as very good shim results may be achieved. The voxel axes were oriented parallel to the patient coordinate system. The voxel dimensions were chosen as for later studies in research on Parkinson's disease (see following chapter). Resonance frequency, rf gain and shim were adjusted locally in a voxel measuring (35 mm)³. This larger voxel was chosen to account for chemical shift displacements of the acquisition volume. Localized shimming used FASTMAP, localized rf gain and resonance frequency adjustments used procedures implemented in the BRUKER PRESS method of our machine. Before the start of acquisitions, the VAPOR pulse gains were fine adjusted by hand to obtain optimal water suppression. All acquisitions started with eight dummy scans to achieve equilibrium magnetization and used a repetition time of 3 seconds. A TE averaged PRESS spectrum using echotimes from 35 ms to 195 ms and steps widths of 10 ms was acquired. Eight scans per echo time were averaged, we used a spectral width of 5000 Hz and 4096 points for acquisition. A PRESS spectrum with an echo time of 136 ms was then acquired from the same voxel, accumulating 128 scans, using a spectral width of 2500 Hz and 2048 points for acquisition. Acquisition time for PRESS and TE averaged PRESS was about seven minutes per spectrum. The unsuppressed water signal was as well acquired from the same volume for referencing purposes. Posttreatment used the IDL programming language (RSI, Boulder). Two Hertz linebroadening was applied to improve the signal to noise ratio. Each single experiment of the TE averaged PRESS

acquisition was corrected for frequency shift and 0th order phase using the NAA signal as reference. The TE averaged PRESS spectrum was then calculated by adding the different experiments of the 2D acquisition.

Further experiments, performed on another volunteer, are presented to demonstrate PRESS at 80 ms (Schubert F 2001). The experimental protocol and posttreatment were the same as described above for PRESS using 136 ms echo time. For voxel positioning, an axial, frontal and transverse view (machine coordinate system) were acquired, using a FLASH based imaging method. A voxel of (25 mm)³ was positioned in the right parietal lobe. A repetition time of 3 seconds was used, accumulating 128 scans after having performed 8 dummy scans. A spectral width of 5000 Hz was acquired on 4096 points.

3.3.2 Results

Fig. 3.3 shows the voxel from which the 136 ms PRESS and the TE averaged PRESS spectrum have been acquired. The voxel has been positioned on the axial and frontal MDEFT images, it extends equally to both sides of the shown image slice. White and gray matter are present in the acquisition volume.

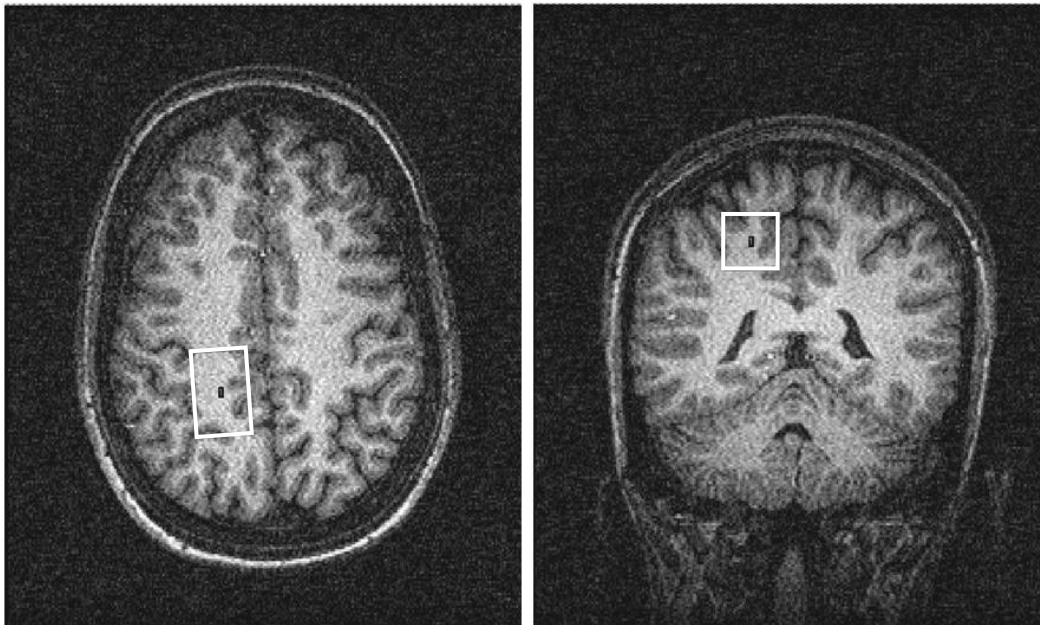


Fig. 3.3: Voxel measuring 20 mm x 20 mm in the left-right and head-foot direction and 30 mm in the anterior-posterior direction positioned on the left parietal lobe of a volunteer. The volume extends equally to both sides of the image. This volume was used for acquisition of the PRESS and TE averaged PRESS spectra of Fig. 3.4 and Fig. 3.5.

Fig. 3.4 shows the PRESS spectrum, acquired using an echo time of 136 ms from the position indicated in Fig. 3.3. A linewidth of about 6 Hz in the acquisition volume for the water peak was achieved by shimming. Fig. 3.5 shows the TE averaged PRESS spectrum, acquired from the same voxel as the PRESS spectrum of Fig. 3.4.

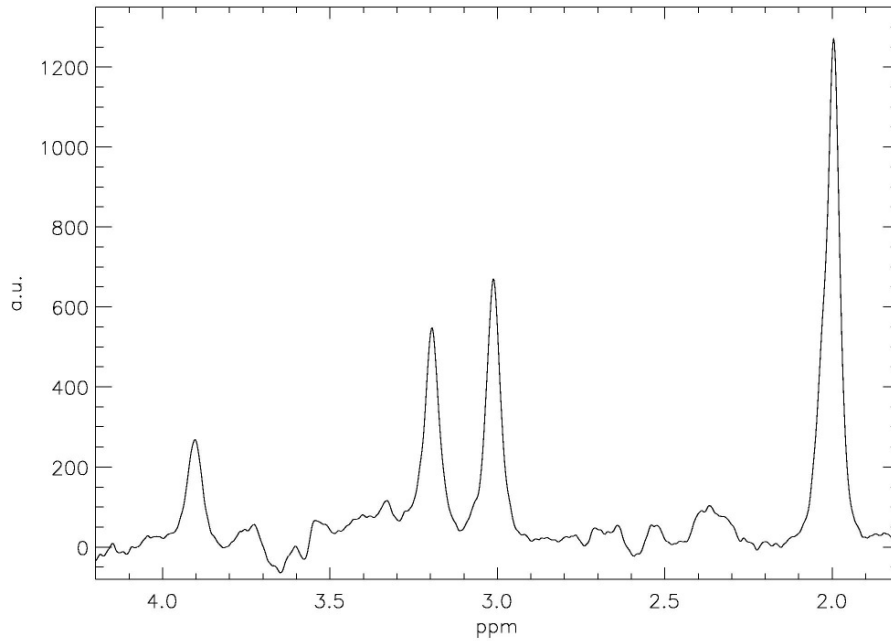


Fig. 3.4: PRESS spectrum, acquired from a $(20 \times 20 \times 30)$ mm³ volume positioned the parietal lobe of a volunteer, as shown in Fig. 3.3. An echo time of 136 ms was used. NAA, total creatine and total choline are well visible at 2.0 ppm, 3.0 ppm and 3.2 ppm. Another resonance of total creatine is visible at 3.9 ppm. At 2.3 ppm, no clear signal shape can be distinguished.

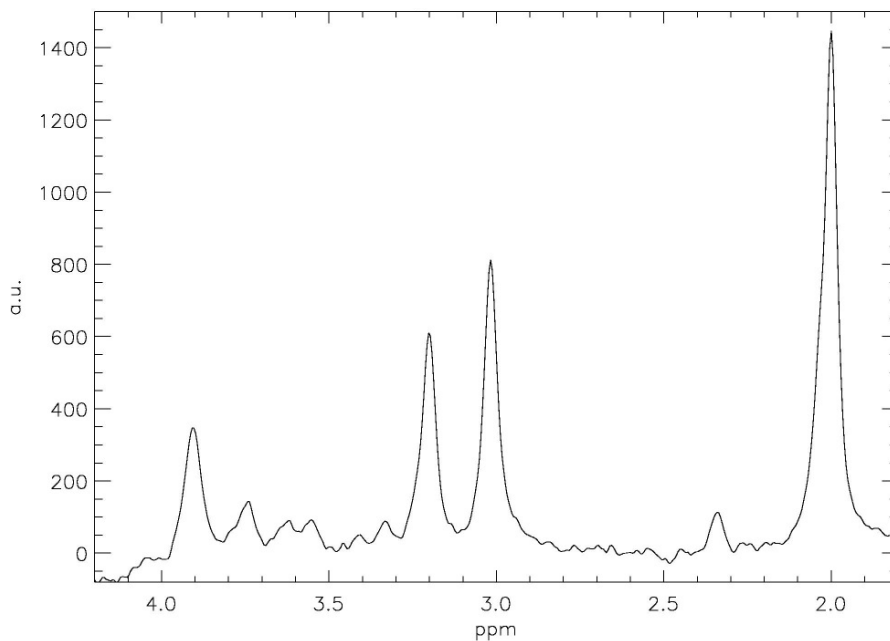


Fig. 3.5: TE averaged PRESS spectrum, acquired from from a $(20 \times 20 \times 30)$ mm³ volume positioned the parietal lobe of a volunteer, as shown in Fig. 3.3. The same signals as described for Fig. 3.4 can be identified. Additionally, a well formed peak is visible at 2.35 ppm and at 3.75 ppm. These can be identified as almost exclusively glutamate signal (2.3 ppm) and combined glutamate+glutamine (3.75 ppm).

Fig. 3.6 shows the images used for positioning of a $(25 \text{ mm})^3$ voxel in another experiment. This voxel was used for acquisition of a PRESS spectrum at 80 ms echo time. The two black lines on each image are due to saturation effects that originate from the image acquisition. The image contrast does not allow for gray matter / white matter distinction, but was sufficient for voxel positioning in these experiments.

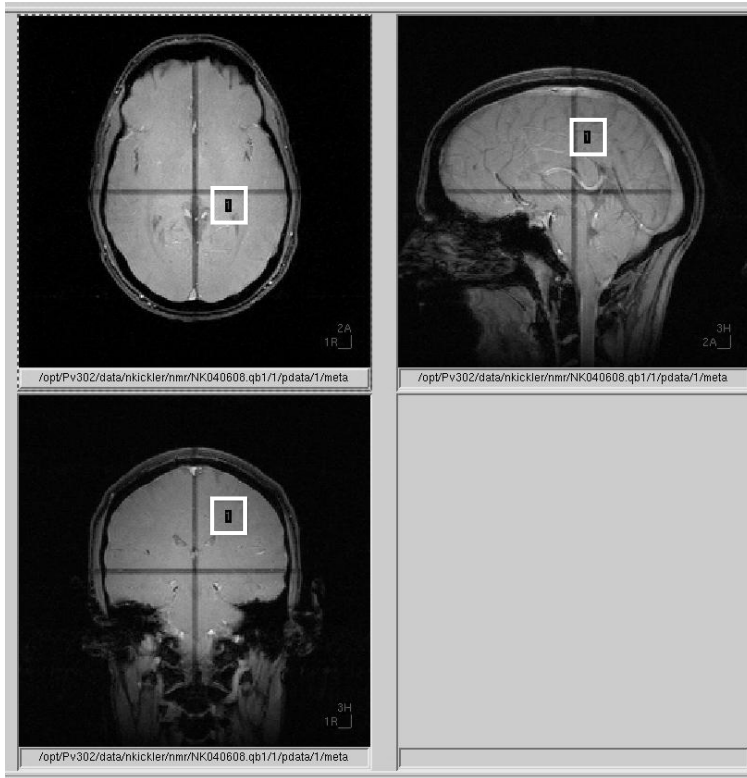


Fig. 3.6: Voxel of $(25 \text{ mm})^3$ situated in the right parietal lobe of a volunteer. This volume was used for acquisition of a PRESS spectrum using an echo time of 80 ms.

Fig. 3.7 shows the PRESS spectrum acquired using an echo time of 80 ms from the volume indicated in Fig. 3.6. Linewidths in this spectrum are comparable to the preceding spectra.

In all three spectra, signals of NAA, total creatine and total choline are well visible at 2.0 ppm, 3.0 ppm and 3.2 ppm. In the spectra of the first session, Fig. 3.4 and Fig. 3.5, another resonance of total creatine appears at 3.9 ppm. In the spectrum of the second session, Fig. 3.7, no signal is visible left of choline due to less well parameterized water suppression. The most interesting differences between PRESS at 80 ms, at 136 ms and TE averaged PRESS take place in the spectral region where coupled spins have their resonances, near 2.3 ppm and left of choline, between 3.3 and 3.8 ppm. Using an echo time of 136 ms, no clear signal shape is visible in a simple PRESS spectrum in the region of 2.3 ppm. At an echo time of 80 ms, a signal corresponding more or less to a peakshape appears at 2.3 ppm. To the left and to the right, other signals are present, although not as well formed peak shape. In TE averaged PRESS, a well formed peak

with a linewidth comparable to NAA is visible at 2.3 ppm. To the left and to the right of this signal, the baseline is essentially flat.

The PRESS spectrum at 136 ms shows no clearly visible signal in the spectral region from 3.3 to 3.8 ppm. In TE averaged PRESS, a well formed peak appears at 3.75 ppm and a further, smaller signal contribution is visible near 3.6 ppm. These can be associated with combined glutamate+glutamine (3.75 ppm) and myoInositol (3.6 ppm).

The brain regions chosen for the demonstrations of PRESS and TE averaged PRESS are very homogeneous compared to other parts of the brain and allow obtaining very small linewidths. The NAA signal, after having applied exponential filtering of 2 Hz, displays a frequency width at half max of about seven Hertz in all spectra (Fig. 3.4, Fig. 3.5, Fig. 3.7, compare to Fig. 3.1, Fig. 3.2). The high field homogeneity achieved after shimming can be seen by the very good resolution of total choline and total creatine.

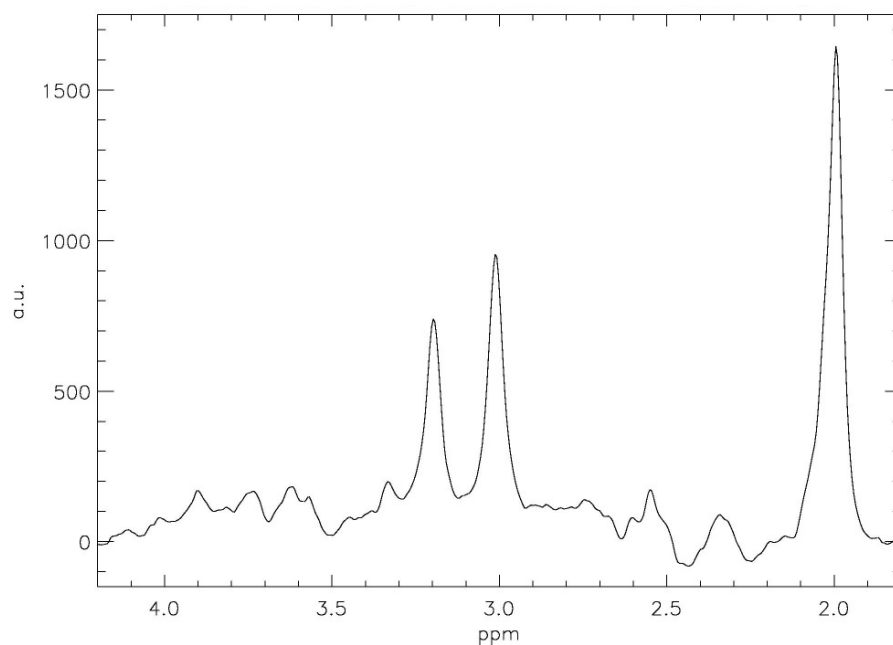


Fig. 3.7: PRESS spectrum, acquired from the volume shown in Fig. 3.6 using an echo time of 80 ms. NAA, total creatine and total choline are well visible at 2.0 ppm, 3.0 ppm and 3.2 ppm. Signals above 3.4 ppm were attenuated by water suppression (compare to Fig. 3.4). At 2.3 ppm, a relatively large peak may be distinguished, which is dominated by glutamate (Schubert, Gallinat et al. 2004).

3.3.3 Discussion

Among the three approaches presented (PRESS at 80 ms, at 136 ms and TE averaged PRESS), TE averaged PRESS shows the most clear signal shape near 2.3 ppm, where glutamate resonances are situated. The metabolite contributions to this signal may be estimated by comparison with the *in vitro* TE averaged PRESS spectrum of Fig. 3.1. The signal at 2.3 ppm is almost exclusively glutamate with very low contributions of glutamine, GABA and NAA. PRESS at 136 ms shows no clearly distinguishable peak in the spectral area of 2.3 ppm *in vivo*. Signals of glutamate, glutamine, NAA and GABA strongly overlap, as may be assessed comparing to Fig. 3.2.

No *in vitro* experiments have been performed with PRESS using an echo time of 80 ms. Comparing the *in vivo* acquisitions of Fig. 3.5 (TE averaged PRESS) and Fig. 3.7 (PRESS 80 ms), TE averaged PRESS spectra seem the preferable approach because of a flatter baseline and a more clearly distinguishable signal at 2.3 ppm. The results achieved with PRESS at 80 ms and TE averaged PRESS are comparable to the ones published by Schubert et al (Schubert, Gallinat et al. 2004) and Hurd et al (Hurd, Sailasuta et al. 2004).

We compare spectra acquired from not exactly the same brain region and using not exactly the same acquisition volume and duration. Because of different voxel sizes, the overall signal to noise ratios of the spectra is certainly not comparable. Because of different voxel placements, glutamate concentration in the volume may differ slightly because of different gray matter and white matter contents. The linewidths of the signals of NAA, tCr and tCho are comparable for all spectra, and we may therefore compare the spectral shape of the signal near 2.3 ppm used for glutamate measurement, as has been done above. The signal saturation to the left of 3.5 ppm in the PRESS spectrum at 80 ms, caused by water suppression, could possibly influence the spectral shape of the glutamate signal at 2.3 ppm because of coupling effects. As our spectra compare well to those of Schubert et al, this influence seems negligible.

3.4 Conclusion and perspectives

TE averaged PRESS is an easy to use and easy to implement technique allowing almost unobstructed glutamate detection at field strengths of 3 Tesla. Concerning the acquisition of a glutamate signal, better results than with standard PRESS acquisitions, using a fixed echo time of 136 ms or 80 ms, can be achieved. The glutamate signal of TE averaged spectra may be quantified using simple peak integration or fit of a Lorentzian lineshape. TE averaged PRESS spectra with good signal to noise ratio can be acquired in durations of about 7 minutes.

Better results for the detection of glutamate have been achieved using TE averaged PRESS than using the double quantum filter sequence, presented in the preceding chapter. In the double quantum filtered spectra, relatively strong glutamine contributions remained in the signal. This is not the case in TE averaged spectra. A

much higher signal to noise ratio for glutamate can be achieved with TE averaged PRESS in a shorter acquisition time. Handling of this sequence is much easier, as no phase calibration procedure is necessary. Quantification of glutamate may be done referring to other signals from the same spectrum as for example the peak of NAA, total creatine or total choline. This is an advantage compared to the use of an external reference signal as referencing between different spectra may add variability.

For future developments it would be interesting to compare TE averaged PRESS to other recently proposed 2D techniques for glutamate detection (Mayer and Spielman 2005; Schulte, Trabesinger et al. 2005). These techniques rely as well on the PRESS sequence and on the acquisition of spectra with different echo times. Different as in TE averaged PRESS however, the acquisition window in these approaches begins at a fixed delay after the first excitation pulse. Traces at $f_1 \neq 0$ of the two dimensional spectrum are evaluated. TE averaged PRESS spectra, CSSF (Schulte, Trabesinger et al. 2005) spectra and CT PRESS (Mayer and Spielman 2005) spectra could possibly be reconstructed from the same data set.

4 TE averaged PRESS and PRESS for brain glutamate detection at 7 Tesla

Ce chapitre décrit l'évaluation de la séquence « TE averaged PRESS » à un champ de 7 Tesla pour la mesure de glutamate cérébral chez le petit animal. Les paramétrages des séquences « TE averaged PRESS » et « PRESS » sont optimisés utilisant des mesures sur des métabolites en solution. Les performances respectives des deux méthodes optimisées sont ensuite comparées in vivo, à 7 Tesla.

4.1 Introduction

Numerical simulations suggest that TE averaged PRESS could be a useful technique for glutamate detection at seven Tesla field strength (Hurd, Sailasuta et al. 2004). J-coupling evolution of glutamate, glutamine, NAA and GABA at seven Tesla is different than at three Tesla, as well as relaxation times and linewidths. The acquisition parameters of TE averaged PRESS therefore have to be examined. In this chapter, TE averaged PRESS will be examined at 7 Tesla field strength and be compared a standard PRESS sequence. As TE averaged PRESS is the sum of PRESS spectra acquired at different echo times, PRESS and TE averaged PRESS can be compared using the same data set.

For the terms of “scan”, “experiment” and “J-resolved acquisition” please refer to chapter 3. The principal parameters to be chosen for TE averaged PRESS are the echo time to start the J-resolved acquisition with (TE_{init}), the number of experiments, the echo time increment (Δt) and the number of scans to be accumulated per experiment.

TE_{init} is determined by the mid-position of the t_1 acquisition window and its length. The position of the acquisition window should be chosen to contain a maximum of glutamate signal to assure optimal signal to noise ratio. T_2 relaxation and J-coupling evolution determine this optimal position (Ziegler, Izquierdo et al. 1995).

In a first step, the echo time for which the glutamate signal is maximal will be determined experimentally. The t_1 acquisition window for TE averaged PRESS experiments will then be centered on this echo time to achieve maximal signal intensity for glutamate. Increasing t_1 acquisition windows will be tested. Long t_1 acquisition windows assure good TE averaged PRESS spectra because of high spectral resolution in f_1 . At the same time, for a fixed number of total scans (a fixed experiment duration), longer t_1 acquisition windows lead to reduced signal to noise ratio because of T_2 relaxation and coupling effects. T_2 relaxation limits as well the achievable resolution in f_1 . For a given total number of scans and a given t_1 acquisition window length, Δt should be chosen short enough to assure correct sampling of the glutamate signal evolution in dependence of the echo times within the acquisition window. The number

of scans accumulated per experiment should however assure a sufficient signal to noise ratio in each experiment to apply individual shift and phasing corrections.

4.2 Experiments on metabolites in solution and *in vivo*

PRESS and TE averaged PRESS experiments have been performed *in vitro* on samples of glutamate, glutamine, NAA and GABA. The results give an impression of the precision of glutamate measurement to be expected *in vivo*. Further experiments have been conducted to assess the signal quality of PRESS and TE averaged PRESS spectra *in vivo*.

4.2.1 Materials and methods *in vitro* experiments

Acquisitions

Experiments were performed using a 7 Tesla horizontal bore magnet (Magnex Scientific, Abington, UK) dedicated to biomedical research. The bore diameter of the magnet is 20 cm, of which 12 cm are usable inside the gradient coil tube. The system is interfaced to a SMIS console (MRRS, UK). A house made surface coil of 2.5 cm in diameter was used for signal excitation and acquisition. Samples containing glu, gln, NAA or GABA at 100 mM were prepared in a phosphate buffer. The samples contained about 0.2 mmol/l chelated Gadolinium complex (0.4 ml/l Dotarem, Guerbet) as relaxant. As reference, TSP (3-(Trimethylsilyl)- Propionic acid) in a constant quantity of 37 mmol/l was added to all samples. Added at this quantity, the preeminent TSP signal has roughly twice the amplitude of the glutamate signal at 2.3 ppm. To prevent bacterial growth, 0.5 ml (1% of the sample volume) of penicillin streptomycin (5000 units/ml, Gibco) was added. The sample pH was adjusted to the typical brain value of 7.3 after having added all components. Glass cylinders of about 2 cm in diameter and 1.5 cm in height were used as containments; correct coil loading was assured with this sample volume. The sample was placed directly under the surface coil.

Acquisitions used a standard PRESS sequence, modified to automate J-resolved 2D acquisitions (for the notations of scan and experiment and J-resolved acquisition refer to chapter 3). Only the second echo time was increased, the first echo time is kept to a minimal value of 12 ms. Gradient commutations for the crusher gradients surrounding the second refocusing pulse can thereby be kept far from the acquisition window, minimizing the influence of residual eddy currents on the spectrum. PRESS used 3 lobe sinc pulses of 6.6 kHz bandwidth for volume localization, water suppression was performed by a preceding VAPOR module (Tkac, Starcuk et al. 1999). Our VAPOR implementation used 2 lobe sinc pulses of 500 Hz bandwidth for selective water excitation. A (4 mm)³ volume was chosen for acquisition, resonance frequency, rf gain and shim were adjusted locally in this voxel. Forty PRESS experiments with linearly increased echo time were acquired from each sample and stored independently in a 2D data matrix for later signal processing. Acquisitions started at an echo time of 35 ms,

divided into 12 ms for the first and 23 ms for the second echo time. An echo time of 35 ms is the actual minimum echo time achievable on our system. Eight scans with a fixed echo time were accumulated, using exorcycle phase cycling. The second echo time was increased by 10 ms from one experiment to the next. Acquisitions started with eight dummy scans to achieve steady state, repetition time was 3 seconds. A spectral width of 5000 Hz was acquired on 4096 points.

Postprocessing

Postprocessing was performed using the IDL programming language (RSI, Boulder). Spectra were zero-filled to 8192 points to smooth the lineshape and to facilitate treatments such as frequency shift correction in the spectral domain. Each single experiment of the TE averaged PRESS acquisition was corrected for frequency shift and 0th order phase using the TSP signal as reference. Individual amplitude scaling and exponential broadening was applied to the spectra acquired from the different samples to produce always the same linewidth and amplitude for the TSP signal. Differing linewidths due to shimming and differing signal intensities (due to rf calibration for example) have thereby been accounted for, as well as T₂ decays in the t₁ acquisition dimension differing from one sample to another. The same additional linebroadening was then applied to all spectra, giving a frequency width of 19 Hz on the NAA signal at 2.0 ppm. This is a typical value found *in vivo* under our experimental conditions. In the t₁ acquisition dimension, spectra were apodized to produce an exponential decay corresponding to a T₂ of 170 ms on the NAA signal (de Graaf 1998). The spectra of the different metabolites were multiplied with the typical concentration of the respective metabolite in the rat brain, as taken from the literature (see annex Table 8.2). We assume a concentration of 11.3 mmol/kg w.wt for glutamate, 5.5 mmol/kg w.wt for glutamine, 8.9 mmol/kg w.wt for NAA and 1.7 mmol/kg w.wt for GABA.

The result of acquisitions and postprocessing so far is a 2D data matrix for each sample of glu, gln, NAA or GABA, containing PRESS spectra acquired with an echo time ranging from 35 ms to 425 ms. Linewidths, concentrations and T₂ decay have been adapted as well as possible to simulate *in vivo* conditions. These experiments now allow the comparison of PRESS at different echo times and TE averaged PRESS for glutamate measurements at 7 Tesla.

To determine the echo time for which maximal glutamate signal can be acquired, the glutamate peak intensity at 2.3 ppm was determined in all spectra acquired from the glutamate sample. TE averaged spectra for different t₁ acquisition window lengths, always centered on the echo time yielding maximal glutamate intensity, were calculated from the data sets acquired on the different samples. To be able to compare signal intensities between PRESS and TE averaged PRESS with respect to the same acquisition duration, TE averaged spectra have been normalized with the number of experiments contained in their sum. The signal intensity displayed in the TE averaged spectra is therefore an intensity “per unit time”.

4.2.2 Results of *in vitro* experiments

Fig. 4.1 shows the evolution of the glutamate peak amplitude at 2.3 ppm in PRESS acquisitions as a function of the echo time. For better visualization, the connecting line in Fig. 4.1 has been traced “smoothed” as offered by MS Excel. Only the results of the first 27 experiments have been displayed. The sinusoidal oscillations are due to J-coupling effects, the overall intensity decrease is caused by simulated T_2 relaxation. Indicated by a dashed line at 115 ms is the maximum of the glutamate signal at 2.3 ppm, by dashed lines at 65 ms and 165 ms the minimal and maximal echo time for the longest t_1 acquisition window used for TE averaged PRESS (compare to Fig. 4.3 right).

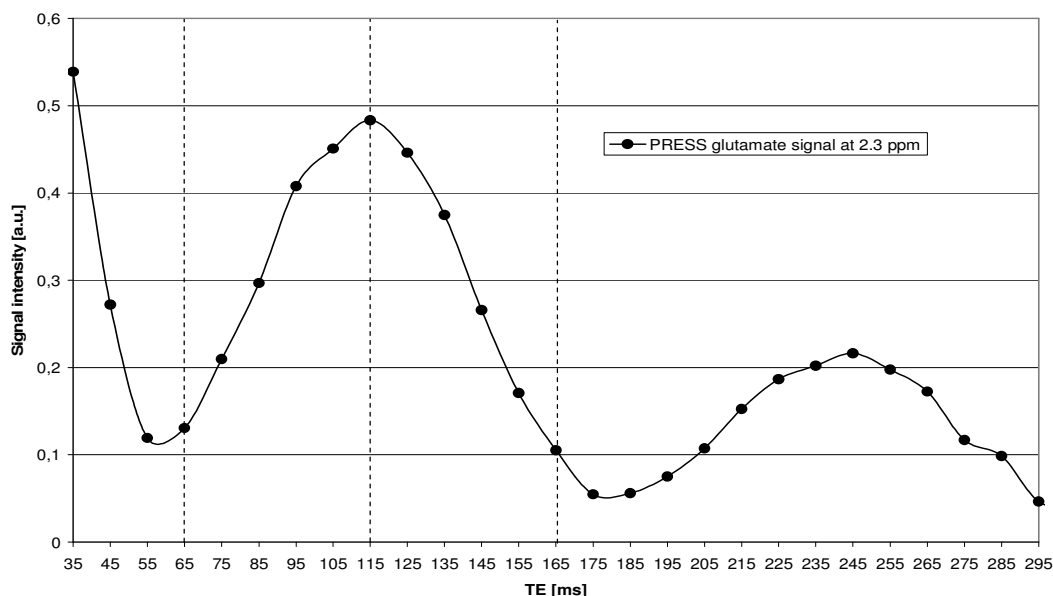


Fig. 4.1: Evolution of the glutamate peak amplitude at 2.3 ppm in PRESS spectra as a function of the echo time at seven Tesla field strength. Acquisitions were performed on a phantom containing glutamate in solution, a T_2 of 170 ms was simulated during posttreatment. Indicated by a dashed vertical line at 115 ms is the maximum of the glutamate signal, by dashed lines at 65 ms and 165 ms the minimal and maximal echo time for the longest t_1 acquisition window used for TE averaged PRESS acquisitions. For visualization, the connecting line in has been traced “smoothed” as offered by MS Excel.

In order to choose optimal parameters for PRESS and TE averaged PRESS, singular spectra have been plotted for both methods additionally to Fig. 4.1.

Fig. 4.2 shows PRESS spectra acquired on the samples containing glutamate, glutamine, NAA or GABA at echo times ranging from 95 ms to 135 ms. These echo times have been chosen symmetrically around the echo time of 115 ms, where the glutamate signal found at 2.3 ppm is maximal. Glutamate has been plotted as dotted, glutamine as dashed and NAA as dash-dotted line. GABA has been printed as dash-dot-dot line and the sum of all metabolites as solid line. The same linestyles have been used for the TE averaged PRESS spectra of Fig. 4.3. Different TE averaged PRESS spectra have been calculated using t_1 acquisition windows lengths from 20 ms to 100 ms, always centered on an echo

time of 115 ms. Parameters are as indicated on top of the spectra. PRESS and TE averaged PRESS spectra have been plotted using the same y-scale.

PRESS at an echo time of 115 ms shows the highest glutamate peak intensity at 2.3 ppm. The signal expected *in vivo* (solid line, sum of all metabolites) contains mostly glutamate with small contaminations of gln, NAA and GABA. At longer or shorter echo times, the signal intensity is reduced but the content of gln, NAA or GABA in the sum peak is not much higher than at 115 ms.

The TE averaged PRESS spectra displayed in Fig. 4.3, using different t_1 acquisition window lengths, show all approximately the same composition of the sum peak (solid line). No significant improvements for glutamate measurement can be achieved by further increasing the t_1 acquisition window length. The signal intensity acquired per unit time is largely reduced using a t_1 window of 100 ms (spectrum to the right) as compared to using a window of 20 ms (spectrum to the left).

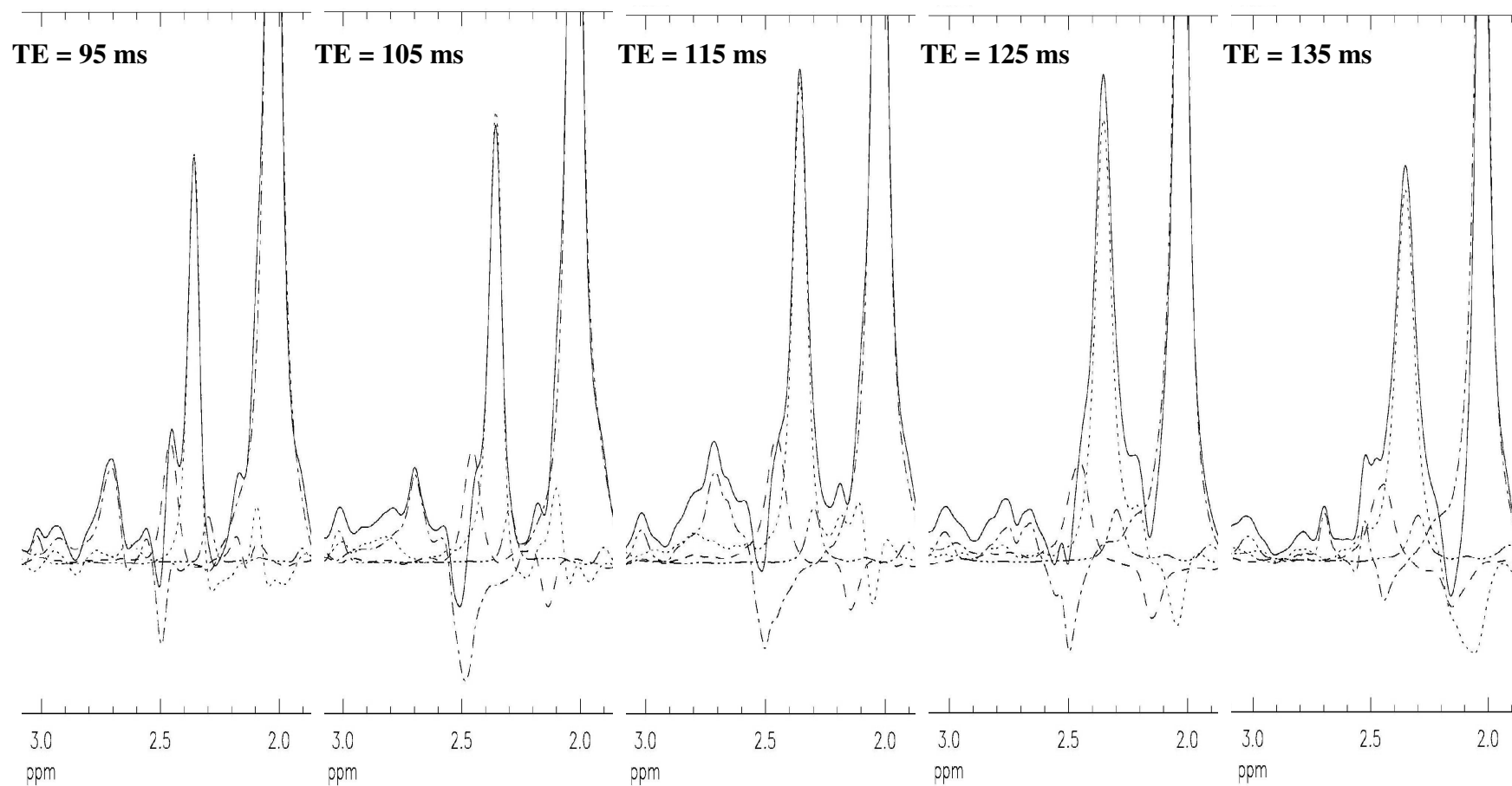


Fig. 4.2: PRESS spectra acquired on samples containing either glutamate, glutamine, NAA or GABA in solution at seven Tesla field strength. Echo times ranging from 95 ms to 135 ms were used. Glutamate has been plotted as dotted, glutamine as dashed and NAA as dash-dotted line. GABA has been printed as dash-dot-dot line and the sum of all spectra of as solid line. All spectra use the same y-scale. The highest glutamate content in the sum signal can be obtained using an echo time of 115 ms.

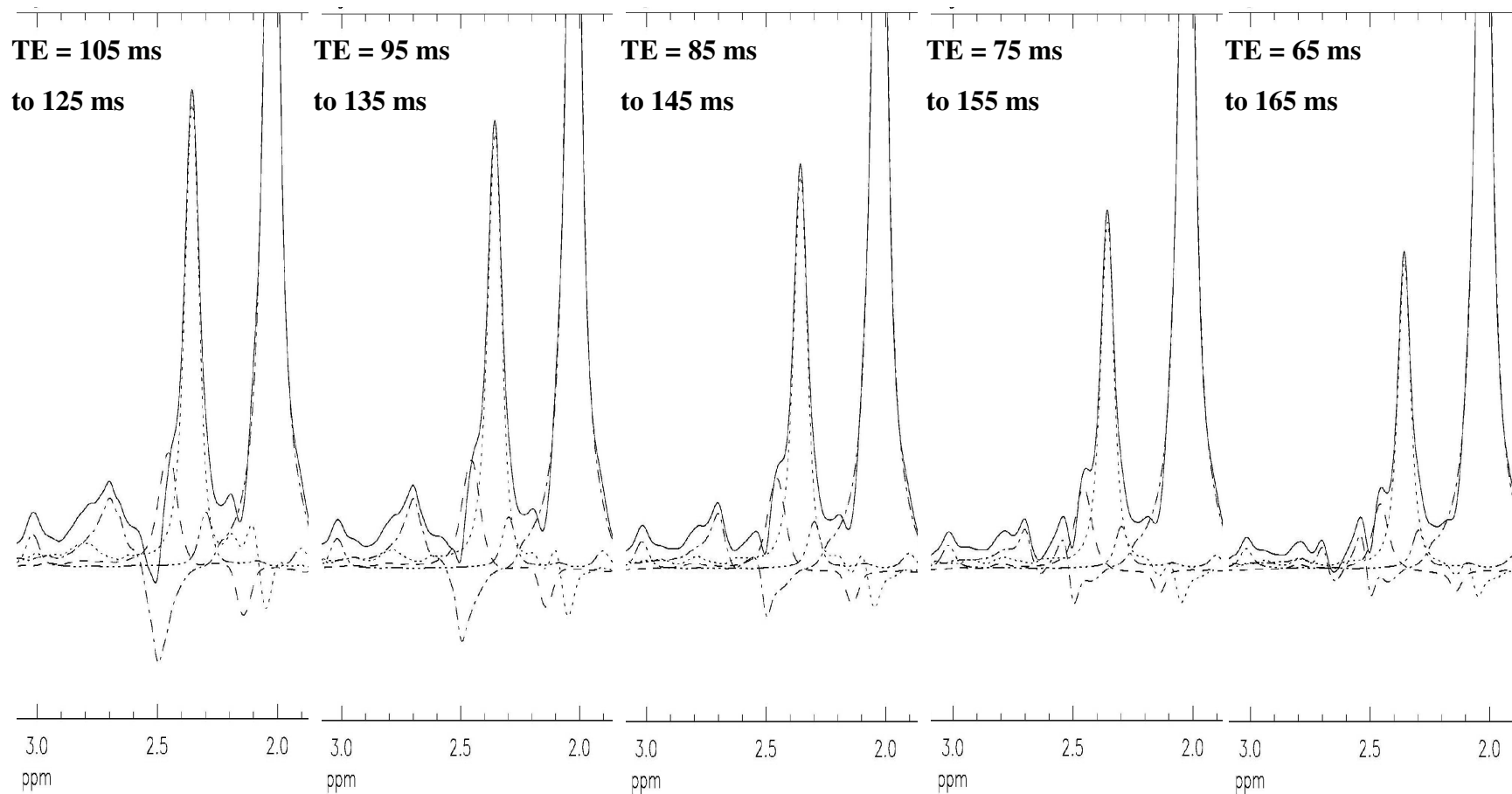


Fig. 4.3: TE averaged PRESS spectra using t_1 acquisition window lengths ranging from 20 ms to 100 ms, centered on an echo time of 115 ms. Samples containing in solution either glutamate, glutamine, NAA or GABA have been used. Glutamate has been plotted as dotted, glutamine as dashed and NAA as dash-dotted line. GABA has been printed as dash-dot-dot line and the sum of all metabolites as solid line. All spectra use the same y-scale. The sum signal contains almost exclusively glutamate, independent of the acquisition window length. At longer acquisition window lengths, less signal per unit time is acquired and the signal at 2.3 ppm is reduced.

4.2.3 Materials and methods *in vivo* experiments

The same spectrometer and configuration as described in section 4.2.3 has been used for the *in vivo* experiments, employing a surface coil for signal excitation and reception. A Sprague-Dawley rat was anesthetized by a gas mixture of air, O₂ and isoflurane. The animal was held in place by a stereotactic frame, the gas mixture was administered by a mask. The animal's temperature was maintained at 37°C by warm water circulation and verified by rectal temperature sensor. PRESS, TE averaged PRESS and VAPOR used the same pulseshapes and lengths as for the *in vitro* experiments described above.

Experiments started with the acquisition of scout images in the coronal, axial and sagittal planes. A volume of (4x4x4) mm³ was chosen well contained within the rat's brain structure. RF gain and shim adjustments were performed locally; shimming used an in-house developed routine based on FASTMAP (Gruetter 1993). All acquisitions started with eight dummy scans to achieve equilibrium magnetization and used a repetition time of 3 seconds. A spectral width of 5000 Hz was acquired on 4096 points. TE averaged PRESS used echotimes from 65 ms to 165 ms and step widths of 10 ms. These parameters correspond to the ones used for the *in vitro* spectrum of Fig. 4.3, right. Per echo time, 24 scans were averaged. PRESS used an echo time of 115 ms. Eleven spectra, averaging 24 scans per spectrum, were acquired. In both methods, the first echo time of the pulse sequence was kept at the smallest possible value of 12 ms as described for the *in vitro* experiments before. The acquisition duration for PRESS and TE averaged PRESS was about 14 minutes. PRESS and TE averaged PRESS used the same total number of scans. The PRESS spectra were acquired in packages of 24 scans to be able to apply individual frequency shift and phasing corrections as for TE averaged PRESS. Posttreatment used the IDL programming language. Seven Hertz exponential broadening and zero-filling to 8192 points was applied to all spectra. Each single spectrum of the PRESS and TE averaged PRESS experiment was corrected for 0th order phase and frequency shift using the NAA signal as reference. TE averaged PRESS and PRESS spectra were then calculated by adding the spectra of the respective acquisitions.

4.2.4 Results of *in vivo* experiments

Fig. 4.4 shows the PRESS and TE averaged PRESS spectrum acquired from a voxel situated in the rat brain (position not shown). Both spectra have been plotted at the same y-scale. Compared to the PRESS at 115 ms the TE averaged PRESS spectrum does not display an improved signal shape at 2.3 ppm. Peakshape and baseline near 2.3 ppm are comparable in both spectra. For the same acquisition duration however, TE averaged PRESS displays a reduced glutamate signal. Intensities for NAA at 2.0 ppm, total creatine at 3.0 ppm and total choline at 3.2 ppm are of comparable size in both spectra. Signals left of total choline are attenuated by water suppression.

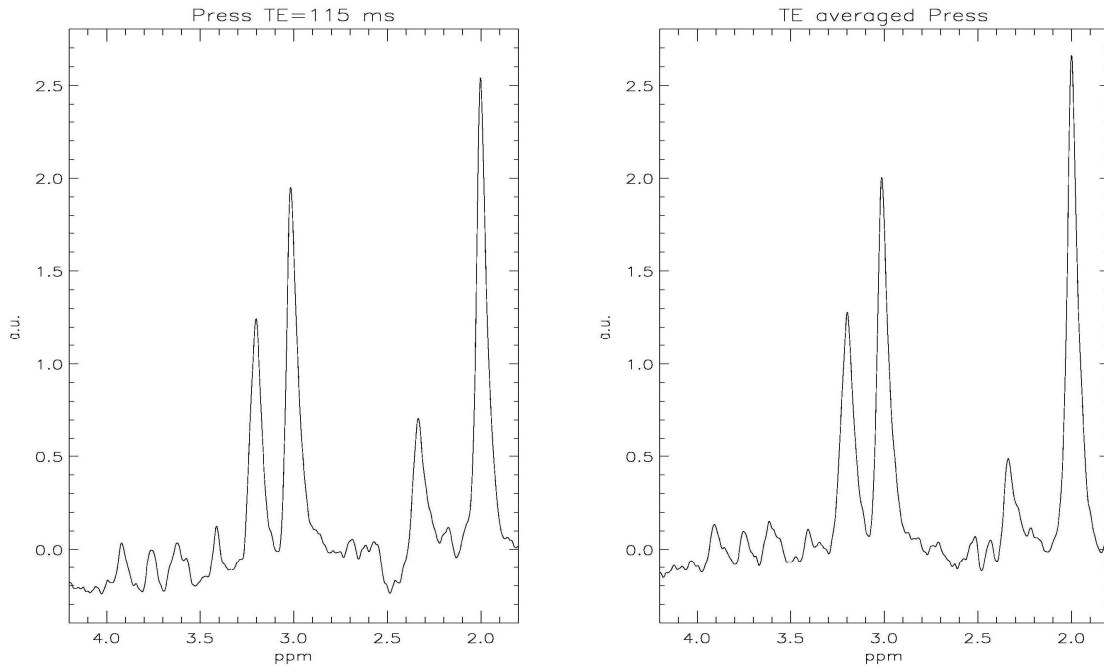


Fig. 4.4: PRESS spectrum (left) using an echo time of 115 ms and TE averaged PRESS spectrum (right) using a t_1 acquisition window length of 100 ms, centered on an echo time of 115 ms. Both spectra were acquired from a $(4 \times 4 \times 4)$ mm³ voxel situated in the rat brain (position not shown), using the same total acquisition duration and are plotted with the same y-scale. NAA, total creatine and total choline are visible at 2.0 ppm, 3.0 ppm and 3.2 ppm, signals above 3.4 ppm are attenuated by water suppression. The signal at 2.3 ppm is dominated by glutamate, as demonstrated by the *in vitro* spectra shown before. The TE averaged PRESS spectrum displays no improved spectral shape in the 2.3 ppm region as compared to the PRESS spectrum, but a reduced signal intensity of the 2.3 ppm peak.

4.2.5 Discussion *in vitro* and *in vivo* experiments

The optimal echo time for glutamate measurements at 7 Tesla using PRESS is 115 ms. At this echo time, the highest signal to noise ratio for a given total acquisition duration can be achieved. With respect to the linewidths simulated *in vitro*, corresponding to the linewidths typically observed *in vivo*, it is not possible to resolve glutamate from glutamine. Taking into account the physiological concentrations of the different metabolites, the contribution of gln, NAA and GABA to the total signal measured is although very small.

In TE averaged PRESS, the evolution of the glutamate signal in dependence of the echo time is well sampled using an echo time increment of 10 ms. As for PRESS, the contribution of gln, NAA and GABA to the total signal measured at 2.3 ppm is very small.

Using TE averaged PRESS, glutamate measurement can however not be significantly improved as compared to PRESS. The signal composition in a PRESS spectrum, acquired at an echo time of 115 ms and in a TE averaged PRESS spectrum, using a t_1 acquisition window from 65 ms to 165 ms, show no important difference. The ratio of glutamate to glutamine amplitude is only slightly higher for TE averaged PRESS with

an acquisition window from 65 to 165 ms than for PRESS at 115 ms. Still further increased t_1 acquisition windows for TE averaged PRESS lead to small reductions in the gln, NAA and GABA contributions but at the same time to important reductions in the signal intensity acquired per unit time for the peak at 2.3 ppm (data not shown). Because of T_2 relaxation, the spectra acquired at longer echo times do not add much information to the TE averaged PRESS spectrum, but add significantly less signal.

According to our *in vitro* results, TE averaged PRESS does not seem to be a favorable technique for *in vivo* applications at seven Tesla. Using very long t_1 acquisition windows, only a slight reduction of background underlying the glutamate signal can be achieved as compared to PRESS. The signal to noise ratio of such a TE averaged PRESS spectrum is however greatly reduced compared PRESS using the same acquisition duration. The precision gained in distinction of glutamate is then counterbalanced by the loss of precision in signal quantification due to noise.

Accordingly, spectra acquired *in vivo* from the rat's brain show no advantageous spectral shape using TE averaged PRESS as compared to PRESS. However, as predicted by *in vitro* experiments, the signal at 2.3 ppm is of reduced intensity in the TE averaged PRESS spectrum, using the same acquisition duration as for the PRESS spectrum.

4.3 Conclusion

According to our *in vivo* and *in vitro* experiences, TE averaged PRESS does not improve brain glutamate detection at seven Tesla field strength compared to a standard PRESS sequence. With respect to baseline definition and the possibility to acquire an unobstructed glutamate signal, no major improvements could be achieved as compared to PRESS using an optimized echo time. At the same time, PRESS permits the acquisition of more signal intensity per unit time. For a given experiment duration, this advantage can be used to achieve higher signal to noise ratio allowing improved peak quantification or higher localization precision by using a smaller acquisition volume.

Annex 8.3 describes numerical simulations performed to examine the influence of T_2 relaxation and shaped pulses on distinction of glutamate and glutamine with TE averaged PRESS at seven Tesla.

5 Study of glutamate levels in human Parkinson's disease

Ce chapitre décrit une étude sur la mesure de glutamate chez le patient Parkinsonien. La séquence « TE averaged PRESS » a été utilisée pour mesurer le glutamate dans le nucleus lentiforme des patients avant et après administration d'un traitement (L-DOPA). Les résultats sont comparés avec ceux obtenus chez le sujet sain.

5.1 Introduction

Glutamate is of high interest for research on Parkinson's disease (PD) as, according to current understanding, alteration of the glutamatergic transmission, is directly linked to striatal dopamine depletion (Morari, Marti et al. 1998; Schmidt 1998) and motor symptoms (Obeso, Rodriguez-Oroz et al. 2000) (introductory review of Parkinson's disease: (Hornykiewicz 2001)).

Dopamine denervation induces an increase in corticostriatal glutamate transmission (Meshul, Emre et al. 1999; Bruet, Windels et al. 2003). Several studies have suggested that dopamine lesion may also increase glutamate transmission in the basal ganglia output structures, especially the pallidum, presumably as a result of the abnormal activation of the subthalamic nucleus (Hirsch, Perier et al. 2000). Moreover, glutamate mediated mechanisms are also thought to play a role in the development of L-DOPA induced dyskinesias (Robelet, Melon et al. 2004). An increase of extracellular glutamate levels has been observed in the striatum of dopamine lesioned rats following either acute (Jonkers, Sarre et al. 2002) or repeated (Robelet, Melon et al. 2004) L-DOPA injections. On the other hand, as levodopa treatment significantly reduces motor symptoms in non dyskinetic patients, one could as well expect decreased glutamate levels following levodopa administration in these patients.

Only few MRS investigations have been conducted so far to assess glutamate on PD patients (Clarke, Lowry et al. 1997; Taylor-Robinson, Turjanski et al. 1999; Clarke and Lowry 2000) and only one of them included administration of an anti-Parkinsonian treatment (apomorphine, (Clarke, Lowry et al. 1997)). None of these studies could show alterations in the glutamate region of the spectrum at 2.3 ppm. However the sequences used were not optimized for glutamate detection i.e. the 2.3 ppm peak of the proton spectrum results from the overlap of resonance lines due to protons from glutamate but also from glutamine, n-acetylaspartate (NAA) and GABA. Any change in the glutamate levels might be masked by concomitant changes in the other metabolite contents.

In the present study, we have evaluated the potential of TE averaged PRESS (Hurd, Sailasuta et al. 2004) for the assessment of glutamate level changes in Parkinson's disease. TE averaged PRESS was preferred to double quantum filtering (Thompson and

Allen 1998) because of its relatively high signal yield and robustness (see chapter 3). We aimed at assessing glutamate level alterations in the lentiform nucleus of Parkinson patients in relation to administration of levodopa treatment and compared to healthy controls.

5.2 Patients and methods

Ten patients with Parkinson's disease according to the United Kingdom Parkinson's Disease Society Brain Bank criteria (Gibb and Lees 1988) and ten healthy volunteers have participated in this study and underwent two MRS exams each. All participants gave written consent before participation; the study was approved by the local ethic's committee (CCPPRB of the Grenoble university hospital). Patients participating in this study were recruited from the neurology department of the university hospital in Grenoble. Patients and healthy control persons underwent medical examination prior to acceptance in the protocol to ensure absence of contraindications to MR exams.

Patients were aged 60 ± 5 years with disease duration of 11 ± 3.5 years (range from 5 to 16 years). All patients were treated with levodopa at the time of this study and suffered from motor fluctuations. For the first exam, patients had not received levodopa for at least 12 hours (off-drug condition). The second exam was performed after administration of a supra-threshold levodopa dose, defined as the usual levodopa morning dose plus 20%, plus the levodopa dose equivalent to dopamine agonist drugs taken usually by the patient (Lang, Lozano et al. 1997). This dose corresponded to the dose necessary to achieve the best on-drug condition for the individual patient under the stressful condition of the exam. On-drug condition was verified by decrease of motor symptoms to a state typical for each individual patient. Motor signs in on- and off-drug condition had been evaluated in routine exams using the unified Parkinson's disease rating scale, motor section (UPDRS III), and are summarized in Table 5.1. The UPDRS in general is a rating tool to follow the longitudinal course of Parkinson's disease. Disease induced impairments affecting behavior, mood, activities of daily living and physical movement are evaluated. An increased score presents increased disability, 0 presents no disability. As well indicated in Table 5.1 are age, disease duration and levodopa equivalent daily dose (LEDD) used for chronic treatments.

The group of volunteers (mean age 56 ± 4 years) was matched in age with the group of patients and underwent two MRS exams under comparable conditions.

Table 5.1: Clinical details of the patient group having participated in this study. All patients presented motor fluctuations and were treated with levodopa. LEDD: levodopa equivalent daily dose, UPDRS: unified Parkinson's disease rating scale.

Patient ID	Age at exam [years]	Disease duration [years]	LEDD [mg/day]	UPDRS III motor score on-condition	UPDRS III motor score off-condition	Levodopa dose for exam in on-condition [mg]
1	56	9	700	6	27	275
2	67	12	600	22	45	200
3	64	16	1450	9	46	250
4	61	6	900	28	48	300
5	58	5	1000	17	33	400
6	56	10	1650	2	15	300
7	61	12	1400	15	45	250
8	50	12	1500	14	34	200
9	61	14	1650	15	42	200
10	64	14	1500	10	43	250

Exams were performed on a three Tesla whole body imager using TE averaged PRESS spectroscopy. Further details about the machine configuration and the sequence implementation have been presented in chapter 3. A standard quadrature head coil was used for signal excitation and reception.

To improve conditions for shimming, efforts were undertaken to approach the patient's putamen region to the magnet isocenter. In direction of the magnet axis (z-axis, head-foot axis) and in x-direction (left-right axis) this was achieved by positioning the patient's bed and displacement of the resonator. In the y-axis (anterior-posterior axis) however, off-center positions between one and four centimeters, depending on the patient, had to be accepted and led to reduced shim efficiency. The exam started with acquisition of scout images oriented in the three orthogonal planes defined by the machine coordinate system. MDEFT images, allowing acceptable gray matter – white matter contrast, were acquired from the region of the lentiform nucleus in order to place the voxel used for spectroscopy, see Fig. 5.1. Saggital images were oriented parallel to the inter-hemispherical plane, transverse images perpendicular to the saggital images and parallel to the axis defined by anterior and posterior commissures (ac and pc). Orientation of frontal images was thereby defined as orthogonal to the saggital and transverse images. The acquisition volume for spectroscopy measured 20 mm x 20 mm in the frontal plane and 30 mm in the anterior - posterior direction. Its axes were oriented parallel to the frontal, saggital and transverse plane. For reproducible positioning, we used always the transverse slice showing anterior (ac) and posterior (pc) commissures and the coronal slice showing the anterior commissure. The voxel position was defined by its distance to ac and pc, comparing to an anatomical atlas (*Atlas d'anatomie céphalique dans le plan neuro-oculaire (PNO)*, Thèse Médecine, 1983, Paris VI, Jean TAMRAZ), as image contrast was not always sufficient to well distinguish the lentiform nucleus. For final positioning, the voxel was rotated by 6° around its anterior-posterior axis to better fit the lentiform nucleus.

Calibrations of frequency and rf power were performed locally in a cube of 30 mm side length to account for voxel displacements due to differing chemical shifts of the

different metabolites. Local shimming used FASTMAP (Gruetter 1993) as implemented on our machine. Adjustment of the pulse power for VAPOR (Tkac, Starcuk et al. 1999) water suppression was refined manually, directly before start of the acquisitions. All acquisitions used a spectral width of 5000 Hz on 4096 points and eight step phase cycling (Henning 1992) during accumulations. A repetition time of 3 seconds was used. The unsuppressed water signal was acquired from the voxel and used for reference purposes, performing 8 dummy scans and accumulating the 8 following scans. The TE averaged PRESS spectrum was acquired in the following. TE averaged PRESS used a minimal echo time of 35 ms and a t_1 increment of 10 ms. Seventeen experiments (TE ranging from 35 ms to 195 ms) were acquired, accumulating 8 scans per experiment (for the notation of experiment, scan and t_1 increment please refer to chapter 3), after having performed 8 dummy scans to achieve equilibrium magnetization.

Data processing used the jMRUI software package (Naressi, Couturier et al. 2001). Each spectrum with a fixed echo time (called also experiment above) was corrected for 0th order phase and frequency shift using the NAA signal as reference. Then, these spectra were summed to give a TE averaged PRESS spectrum.

Total choline at 3.2 ppm (tCho; choline + phosphorylcholine + glycerophosphorylcholine with contributions of taurine and myoInositol), total creatine at 3.0 ppm (tCr; creatine + phosphocreatine), NAA at 2.0 ppm and the glutamate dominated signal at 2.3 ppm (glx; mainly glutamate with contributions of contributions of glutamine, NAA, GABA) were quantified in the time domain using AMARES (Vanhamme, van den Boogaart et al. 1997) as implemented in jMRUI. Linewidths of all peaks were constrained to the linewidth of the NAA signal, no global or individual phase adjustments were allowed in the model function. This restriction of adjustable parameters may increase the fit residual. Different tests showed however that best inter-subject reproducibility of glutamate assessment could be achieved for the healthy control group with this restricted parameter set. The reference spectrum of the unsuppressed water signal was quantified using AMARES as well. For the spectra shown in the results section, the fid was reduced to the first 2048 points, as the signal had already well decayed. Zero filling to 4096 points and seven Hertz exponential broadening were then applied to improve visualization.

The acquired data were as well evaluated to obtain a rough estimation of metabolite T_2 relaxation times in the basal ganglia region. HLSVD filtering to reduce the water signal, as implemented in MRUI, was applied to the individual experiments of the J-resolved acquisition. Spectra acquired with an echo time below 65 ms were rejected from further processing, as residual water and possible macromolecule contributions led to a deformed baseline. The signals of NAA, total creatine and choline were then quantified as described above, using AMARES. As data were acquired on a partially saturated spin system, signal amplitudes obtained by AMARES were corrected as (Traber, Block et al. 2004)

$$S'(TE) = \frac{S(TE)}{1 - 2 \exp[-(TR - TE/2)/T_1] + \exp(-TR/T_1)} \quad (5.1)$$

with $S'(TE)$ the corrected signal amplitudes, $S(TE)$ the data obtained from AMARES, TE the echo time used for acquisition of the respective data, TR the repetition time and T_1 the longitudinal metabolite relaxation time. Values for T_1 in the basal ganglia region were taken from the literature (Traber, Block et al. 2004). The plot of the corrected metabolite amplitudes $S'(TE)$ versus the echo time TE was then used to adjust a monoexponentially decaying function to obtain the transverse relaxation time T_2 .

5.3 Results

Fig. 5.1 shows a typical picture of the placement of the voxel used for spectroscopy in this study, centered on the lentiform nucleus.

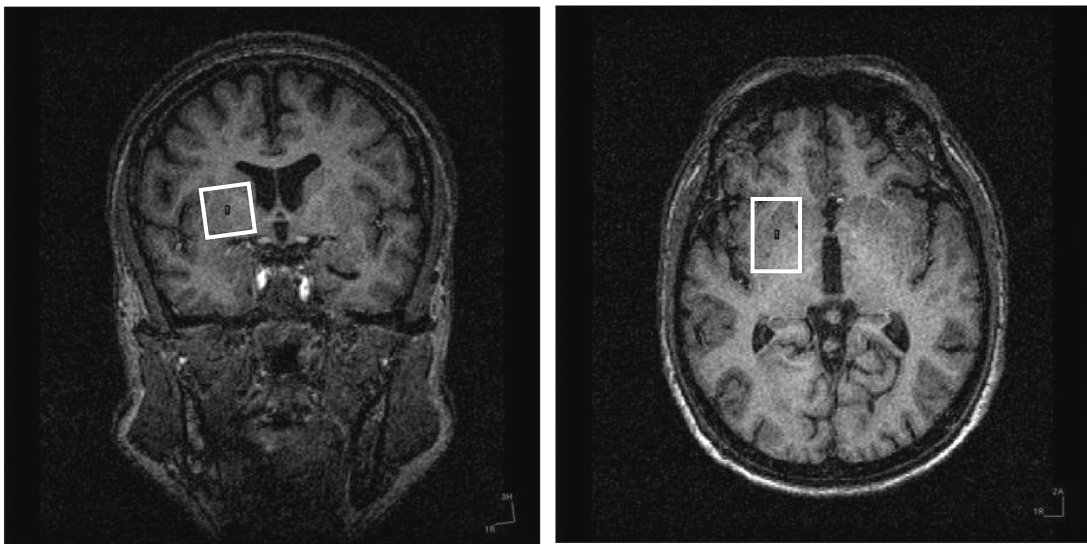


Fig. 5.1: Voxel size and position used for spectroscopy in this study. A volume measuring 20 mm x 20 mm in the frontal plane and 30 mm in the anterior-posterior direction was centered on the left lentiform nucleus, using anterior and posterior commissure as landmarks.

Linewidths obtained for the water signal in this study, ranged from 8 to 14 Hertz. For NAA, about the same values were obtained. Optimal shim settings as calculated by FASTMAP systematically surpassed limitations of our system and would have been from 120 up to 400% of the available currents. Examples for TE averaged spectra are shown in Fig. 5.2 for a healthy control person (bottom), a patient in off-drug condition (top) and for the same patient in on-drug condition (middle). The peaks were identified as: 2 ppm, NAA; 2.3 ppm, glx; 3 ppm, total creatine; 3.2 ppm, total choline. Only these peaks were used for quantification in AMARES, as signals above 3.2 ppm were affected by water suppression in some spectra. The signals at 3.7 ppm represent combined glutamate and glutamine and total creatine at 3.9 ppm.

The following figures display the quantification results for the glutamate dominated signal (Fig. 5.3), NAA (Fig. 5.4), total creatine (Fig. 5.5) and total choline (Fig. 5.6). The water amplitude from the same voxel has been used for normalization. Repeated measurements on the same subject (control or patient) are shown linked by a line to visualize evolution between exams.

Non parametric matched pairs tests (Wilcoxon) have been used for statistical evaluation of repeated exams on the same subject, unpaired Mann Whitney tests for comparison between the patient and control group. No correction for multiple comparisons was applied. Quality of the spectra in terms of metabolite quantification is given by the Cramer Rao lower boundaries (CRB) as calculated by jMRUI. These boundaries supply the minimal standard deviation one may obtain for peak quantification using an ideal model function.

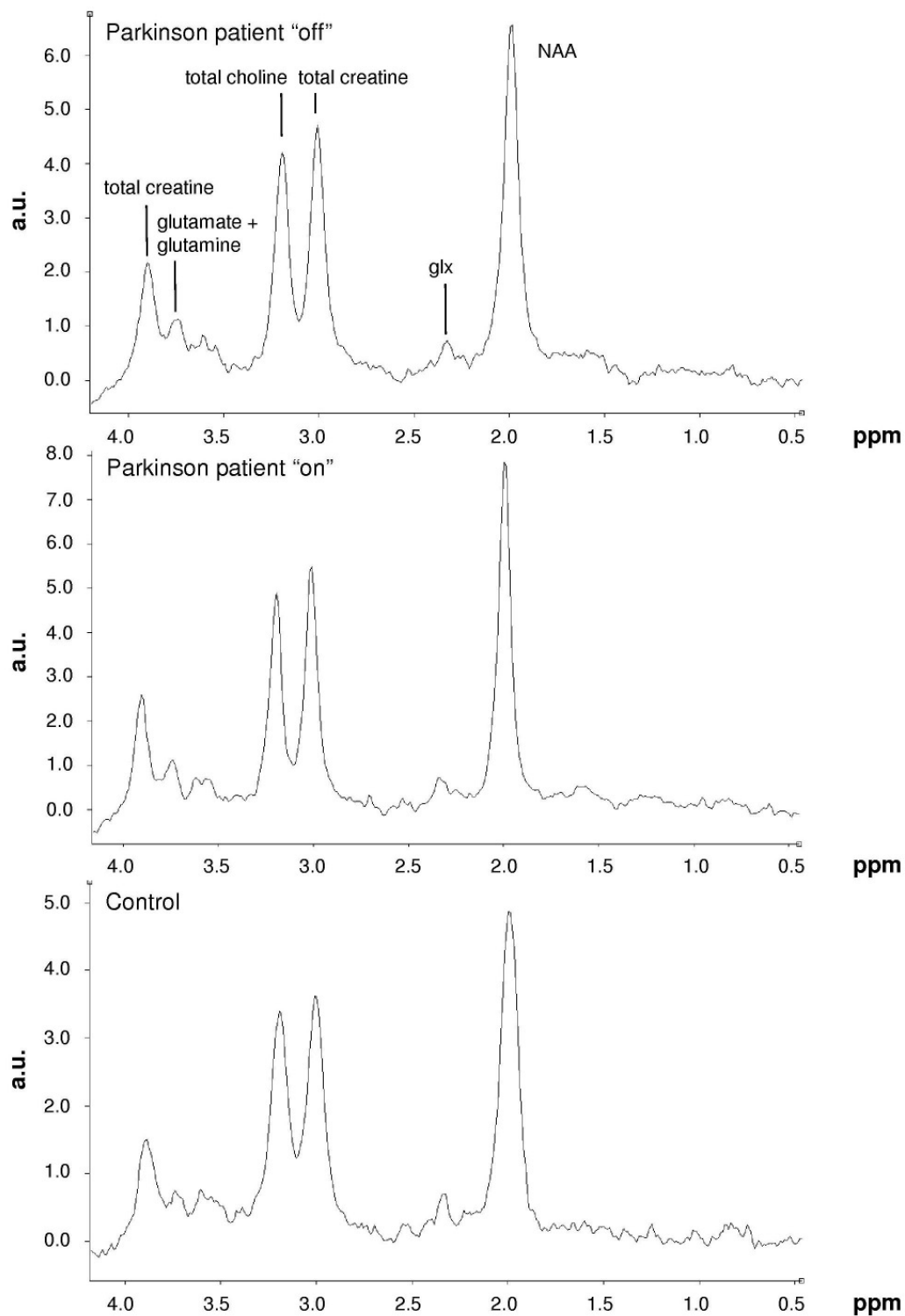


Fig. 5.2: TE averaged PRESS spectra obtained from a patient in off-condition (top), on-condition (middle) and a healthy control subject (bottom). Peaks are identified as indicated in the spectrum on top. As compared to spectra from the parietal lobe shown beforehand, the glutamate signal at 2.3 ppm is of less good visibility due to difficult shimming conditions. Signals at 2.0 ppm, 2.3 ppm, 3.0 ppm and 3.2 ppm were quantified using AMARES (Vanhamme, van den Boogaart et al. 1997).

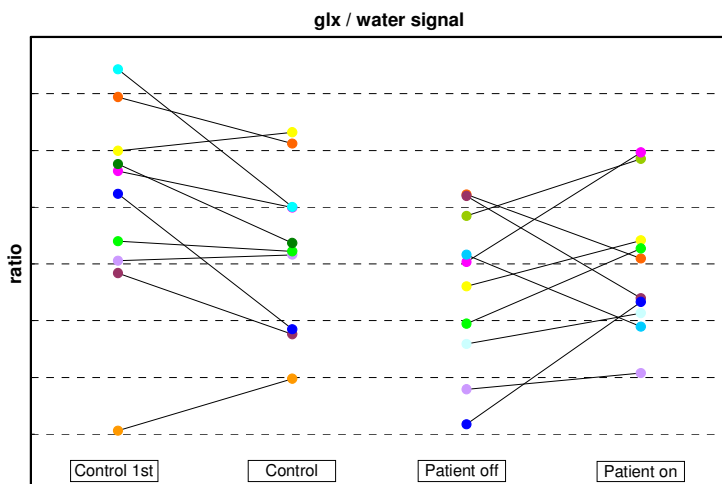


Fig. 5.3: Results obtained from quantification of the glx signal. The metabolite amplitude has been normalized with the water signal from the same acquisition volume. Repeated measurements are linked by a line to visualize evolution between exams. No statistically significant difference is found comparing patients in on- and off-drug condition. 1st and 2nd measurement on the control group have been averaged as statistically not different. Mean values of the control group show no statistically significant difference as compared to patient's on- or off-drug condition.

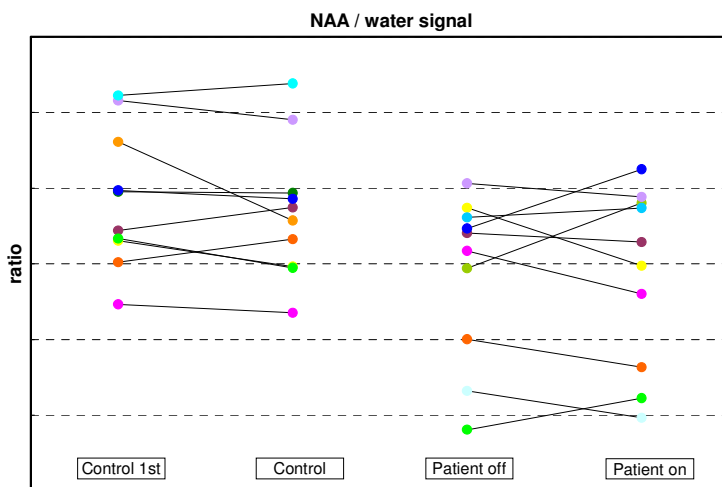


Fig. 5.4: Results obtained from quantification of the NAA signal. The metabolite amplitude has been normalized with the water signal from the same acquisition volume. Repeated measurements are linked by a line to visualize evolution between exams. No statistically significant difference is found comparing patients in on- and off-drug condition. 1st and 2nd measurement on the control group have been averaged as statistically not different. Mean values of the control group show no statistically significant difference as compared to patient's on- or off-drug condition.

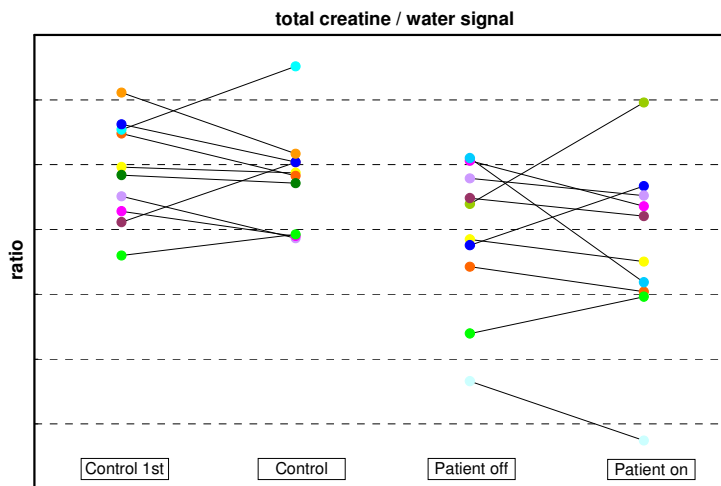


Fig. 5.5: Results obtained from quantification of the tCr signal. The metabolite amplitude has been normalized with the water signal from the same acquisition volume. Repeated measurements are linked by a line to visualize evolution between exams. No statistically significant difference is found comparing patients in on- and off-drug condition. 1st and 2nd measurement on the control group have been averaged as statistically not different. Reduction of tCr/water is statistically significant comparing control group to patients in on-condition ($p < 0.05$, Wilcoxon) and nearly significant comparing control group to patients in off-condition ($p = 0.052$).

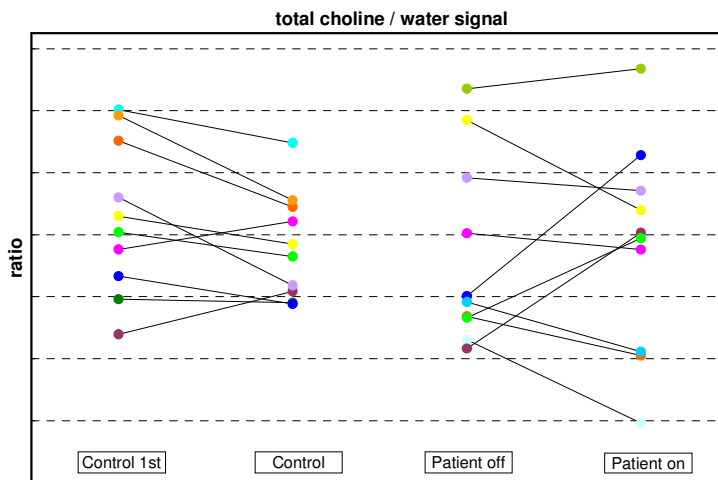


Fig. 5.6: Results obtained from quantification of the tCho signal. The metabolite amplitude has been normalized with the water signal from the same acquisition volume. Repeated measurements are linked by a line to visualize evolution between exams. No statistically significant difference is found comparing patients in on- and off-drug condition. 1st and 2nd measurement on the control group have been averaged as statistically not different. Mean values of the control group show no statistically significant difference as compared to patient's on- or off-drug condition.

Glutamate (glx signal):

For the glutamate to water ratio in our study, the CRB's ranged from 10 to 37% for the patient group and the control group. Repeated measurements on the control group (see Fig. 5.3) display variations in the determined glutamate level ranging from 2 up to 33%. For comparison with the patient group, results from the first and second exam of the control group were averaged for each subject, as they were not statistically different. Comparison between on- and off-drug conditions within the group of Parkinson patients revealed no statistical differences, as well as comparison of the means of the control group with on- or off-drug condition in the patient group. To compare with former studies (Taylor-Robinson, Turjanski et al. 1999), the glx/tCr ratio was as well evaluated, yielding the same non significant results as the glx/water ratio.

N-acetylaspartate:

As the strongest signal in the spectrum, Cramer Rao boundaries for NAA quantification were lower than for glutamate, ranging only between one and two percent. Repeated measurements in the control group show good reproducibility with intra subject alterations below 4% for all subjects but one. The mean for each subject of the control group was used for further comparisons, as exams were not significantly different. Differences between on- and off-drug conditions in the patient group were non significant, as well as comparing control group to on or off-drug values from patients. In Fig. 5.4, three patients, color coded in orange, green and light blue, seem to be distinct from the other patients. We could however not find any common criterion to form a subgroup of these patients.

Transverse relaxation times measured on NAA were of 229 ± 7 ms (mean \pm SEM) in the control group (mean of all exams), 241 ± 15 ms in the patient group in off-drug condition and 247 ± 21 ms in the patient group in on-drug condition.

Creatine (tCr signal):

Creatine CRB's are comparable to those obtained during NAA quantification, ranging between one and three percent. Intra subject alterations remain below 6% in repeated measurements in the control group. For comparison with the patient group, results from the first and second exam of the control group were averaged for each subject, as they were not statistically different. Differences between on- and off-drug conditions are statistically non-significant. Reduced creatine levels, assessed as cr/water, are found in the patient group as compared to the control group. Creatine is reduced by about 6%, being significant ($p < 0.05$) for the comparison of on-drug condition to the healthy control group and nearly significant for off-drug condition to healthy control group comparison ($p = 0.052$).

Transverse relaxation times measured on creatine were of 127 ± 3 ms (mean \pm SEM) in the control group (mean of all exams), 141 ± 6 ms in the patient group in off-drug condition and 141 ± 9 ms in the patient group in on-drug condition.

Choline (tCho signal):

Cramer Rao boundaries for choline quantification range between one and three percent as for the other singlet signals. Intra subject alterations are slightly higher than for creatine, displaying alterations below 10% for the control group measurements. Results from the first and second exam of the control group were averaged for each subject as they were not statistically different. No significant choline differences between on- and off-drug condition or comparing the control group with the patient group were found.

Transverse relaxation times measured on choline were of 198 ± 8 ms (mean \pm SEM) in the control group (mean of all exams), 209 ± 17 ms in the patient group in off-drug condition and 262 ± 48 ms in the patient group in on-drug condition.

No significant changes of the metabolite relaxation times were found comparing first and second exam of the control group, patients in on- and off-drug condition or measurements of the control group (averaged values of first and second exam for each subject) with patients in on- or off-drug condition.

5.4 Discussion

The aim of this study was to measure glutamate levels in patients affected by Parkinson's disease in off- and on-drug condition and to compare to healthy volunteers.

Even with an MRS sequence optimized for glutamate detection, we could not find significant glutamate (glx/water) changes in a voxel centered on the lentiform nucleus despite of clear changes in patient's motor performances following levodopa administration. Comparing patients to controls, no glutamate alterations could be found either.

Our study indicates that 1H MRS measurements of glutamate in PD patients do not reflect the increase in glutamate transmission implicated in the pathophysiology of PD or an alteration related to L-DOPA administration.

Some (Meshul, Emre et al. 1999; Jonkers, Sarre et al. 2002; Bruet, Windels et al. 2003), but not all (Robelet, Melon et al. 2004) microdialysis studies have reported important increases (+45 to 146%) of extracellular striatal glutamate after lesion of the nigrostriatal pathway in rats. Acute (Jonkers, Sarre et al. 2002) or repeated (Robelet, Melon et al. 2004) L-DOPA administrations were also shown to increase extracellular glutamate levels in the striatum of this model.

First our study has been not been performed on newly diagnosed patients but on patients with a disease duration and treatment ranging between 5 to 16 years. The long term treatment might interfere with glutamate measurements even after 12 hours of L-DOPA deprivation.

The targeted area for this study, the basal ganglia region, is a difficult area for MRS exams: Interfaces between brain mass, ventricles and skull base produce important magnetic field inhomogeneities. While water peak linewidths of about five to six Hertz could be achieved for exams as the one displayed in chapter 3.3, Fig. 3.5, linewidths throughout this study with up to 14 Hz were more than twice as large. Overall signal to noise ratio was thereby strongly reduced, complicating especially the detection of small signals as the glutamate peak. As a result, glutamate quantification yields important Cramer Rao boundaries and inter subject variability is high. As mentioned before, shim currents determined by FASTMAP could not always be realized in the necessary strength due to hardware limitations.

A further problem of the assessment of glutamate changes in our study is the size of the acquisition volume. The acquisition volume contains next to the putamen and the pallidum (where glutamate alterations could be expected) as well white matter and small portions of cerebral spin fluid. We can estimate that about 47 % of the voxel is filled with the putamen and another 11 % with the pallidum (GPi and GPe), assuming a volume of 5625 mm³ for the putamen, 478 mm³ for the internal and 808 mm³ for the external part of the globus pallidum (Yelnik 2002).

Most importantly however, MRS measures the total pool of glutamate which is around 10 mmolar in the brain (Govindaraju, Young et al. 2000) and represents mainly the intracellular pool, the extracellular glutamate levels being of the order of 2 to 3 μ mol (Fillenz 2005). An increase of extracellular glutamate, even of 140% if existent, cannot be detected by *in vivo* MRS because it is far below the detection sensibility of the method. In addition alterations of the extracellular glutamate pool are not necessarily linked to a significant change in the the total pool of glutamate. The synaptically released glutamate is rapidly removed from extracellular space by astrocytes. Glutamate participates in intermediary metabolism as well as cellular communication and serves as precursor for GABA. Therefore extracellular glutamate levels, playing a role in neurotransmission, are negligible in comparison with intracellular levels.

Our data indicate a trend to reduced tCr/water ratios in Parkinson patients (only a trend, as the control-patient off comparison is only nearly significant) which is not caused by a decrease of tCr transverse relaxation time, as indicate T₂ measurements. Concerning water relaxation time in putamen and pallidum, some studies suggest a decrease due to augmented iron deposition (Antonini, Leenders et al. 1993; Ye, Allen et al. 1996), some an increase (Graham, Paley et al. 2000; Kosta, Argyropoulou et al. 2005). Changing transverse relaxation due to iron deposition would presumably affect metabolite and water peak amplitudes in the same way. Brain edemas are generally not observed in PD, tissue water concentration should therefore remain unchanged with respect to healthy subjects. Our results may therefore indicate reduction of combined cerebral creatine/phosphocreatine concentrations putamen and pallidum of patients affected by Parkinson's disease.

Former MRS studies measuring NAA, creatine and choline signals in the lentiform nucleus of PD patients show a large variety of results, evaluating NAA/tCr, NAA/tCho and tCho/tCr ratios, see Table 5.2 and (Clarke and Lowry 2001). To compare, metabolite ratios (glx/tCr, NAA/tCho, NAA/tCr, tCho/tCr) have been calculated from the data of this study and have been tested for statistical significance as described above. No difference comparing on- to-off state in patients or patients to controls was found. Heterogeneity in results might be caused by different methodological approaches (field strength, echo time), but as well by differences in recruited patient groups (age, disease duration, treatment, disease progression and complications).

Average transverse relaxation times measured in the basal ganglia region for NAA, total creatine and total choline are in agreement with values present in the literature, being 221 ms for NAA, 143 ms for total creatine and 201 ms for total choline (Traber, Block et al. 2004).

5.5 Conclusion and perspectives

In the present study we have evaluated a new *in vivo* NMR spectroscopy sequence (Hurd, Sailasuta et al. 2004) optimized for the assessment of brain glutamate for research on Parkinson's disease. Glutamate levels measured on the Parkinson patient do not show concentration changes as compared to control values or in relation to levodopa administration.

¹H MRS measures the total pool of glutamate and does not provide a good reflect of the role of glutamatergic transmission in Parkinson's disease.

An important reason for high variability of measurements in this study was strong magnetic field inhomogeneity in the basal ganglia region, leading to broad linewidths and small peak intensities. Stronger shimming systems and use of higher order shims (up to third order) could substantially improve measurement conditions.

Table 5.2: Results of MRS studies targeting the striatal region of patients affected by Parkinson's disease. The symbol ↑ indicates finding of increased values; the symbol ↓ indicates finding of reduced values compared to controls. N.S. indicates absence of statistically significant difference.

Author	Controls (number, mean age)	PD patients (number, mean age)	Method (magn. field, echo time)	NAA	tCho	tCr	glx /water	glx /tCr	NAA /tCho	NAA/ tCr	tCho /tCr
This work	10 56 years	10 60 years	3 T TE av. PRESS	n.s. (relative to water)	n.s. (relative to water)	↓ (trend, relative to water)	n.s.	n.s.	n.s.	n.s.	n.s.
Clarke CE 2000	6 61 years	6 48 years	1.5T TE 20 ms	n.s. (absolute concentration)	↑ (absolute concentration)	n.s. (absolute concentration)		n.s.	↓	n.s.	↑
Taylor-Robinson SD 1999	12 49 years	12 57 years	1.5T TE 130 ms CSI					n.s.		n.s.	n.s.
Hoang TQ 1998	5 71 years	5 60 years	1.5T TE 30 ms	n.s. (absolute concentration)		n.s. (absolute concentration)					
Clarke CE 1997	5 53 years	5 58 years	1.5T TE 20 ms	n.s. (absolute concentration)	n.s. (absolute concentration)	n.s. (absolute concentration)		n.s.		n.s.	n.s.
Federico F 1997	10 63 years	12 57 years	1.5T TE 135 ms						n.s.	n.s.	n.s.
Tedeschi G 1997	11	10 50-72 years	1.5T TE 272 ms						n.s.	n.s.	n.s.
Ellis CM 1997	11 53 years	9, untreated 59 years	1.5 T TE 136 ms						↓	n.s.	n.s.
		7, treated 59 years							n.s.	n.s.	n.s.
Cruz CJ 1997	6 62 years	10 65 years	2 T TE 272 ms CSI						n.s.	n.s.	n.s.
Davie CA 1995	9 53 years	9 50 years	1.5T TE 270 ms							n.s.	n.s.
Holshouser BA 1995	89 62 years	91, treated 64 years	1.5T TE 135 ms						n.s.	n.s.	n.s.
	96 59 years	27, untreated 64 years							↓	n.s.	n.s.

6 Study of glutamate levels in a 6-OHDA rat model of Parkinson's disease

Ce chapitre décrit des mesures de glutamate sur le modèle animal de la maladie de Parkinson. La séquence « PRESS » à un temps d'écho de 136 ms a été utilisée à 7 Tesla pour mesurer le glutamate dans la partie dorsolatérale du striatum chez le rat avant et après lésion de la projection nigro-striatale à la 6-OHDA.

6.1 Introduction

Particular symptoms of human Parkinson's disease (PD) can be studied in rat animal models. A widely used model relies on the neurotoxin 6-hydroxydopamine (6-OHDA). After injection in the brain, this molecule is transported into the cell bodies and fibers of dopaminergic neurons and causes degeneration of their nerve terminals and eventually cell bodies. Neurotoxicity of 6-OHDA is based on inhibition of mitochondrial respiratory enzymes.

In human Parkinson's disease, mainly the dopaminergic nigrostriatal pathway is affected by neuronal degeneration. The animal model therefore relies on selective 6-OHDA lesions of this pathway. Selectivity is achieved by direct injection of the toxin into distinct parts of the nigrostriatal pathway. In currently used rat models, 6-OHDA is either injected in the substantia nigra pars compacta (SNc), the median forebrain bundle (MFB) (nerve bundle incorporating the axons of the neurons running from SNc to the striatum) or in the caudate putamen (CPu). The severity of the lesion, i.e. the percentage of dopaminergic neurons surviving after neurotoxin injection, depends strongly on the location of the injection. MFB injections produce the most severe reductions in SNc dopaminergic neurons and CPu dopamine levels, which may exceed neurodegeneration observed in human PD. Injections in SNc or CPu allow for more selectivity, for review see (Deumens, Blokland et al. 2002).

In the animal model as in human Parkinson's disease, death of the neurons projecting from SNc to the striatum is accompanied by striatal dopamine depletion. Lack of dopamine in the striatum is at the origin of several anatomical and functional modifications. Study of these modifications in the rat model allows thereby obtaining a better comprehension of the pathologic processes taking place in human Parkinson's disease.

Our principal interest in this study concerns the alteration of the striatal glutamate pool, which we want to assess *in vivo* using magnetic resonance spectroscopy. Current studies of glutamate in the rat model of PD mostly rely on anatomical exams or *in vivo* microdialysis experiments.

In the striatum, dopamine is generally taken to act as inhibitory modulator of glutamate release; this opinion is however still point of discussion ((Morari, Marti et al. 1998), review). Several research results indicate an increase of glutamatergic activity following striatal dopamine depletion.

Adaptive changes in striatal glutamatergic synapses have been found as a consequence of 6-OHDA lesion of the nigrostriatal pathway. Using electron microscopy, alterations in the number or length of asymmetric synapses containing a discontinuous or perforated postsynaptic density have been reported. An increase in this specific type of synapse is associated with increased synaptic activity. Nerve terminals of this synapse type were furthermore identified, using immunogold electron microscopy, to contain the neurotransmitter glutamate. One month following lesion, glu immunoreactivity within these nerve terminals significantly decreased. (Ingham, Hood et al. 1993; Meshul, Emre et al. 1999; Meshul, Cogen et al. 2000). These morphological changes suggest an increase of striatal glutamatergic activity.

Consistent with these results, increased concentrations of extracellular glutamate have been measured in the rat striatum following nigrostriatal 6-OHDA lesion (Meshul, Emre et al. 1999; Jonkers, Sarre et al. 2002; Bruet, Windels et al. 2003). Other studies failed however to measure such an increase (Corsi, Pinna et al. 2003; Galeffi, Bianchi et al. 2003; Robelet, Melon et al. 2004).

Common treatment of symptoms of Parkinson's disease relies on restoring striatal dopamine levels via administration of levodopa (L-dopa, L-Dihydroxyphenylalanine).

Levodopa is a precursor of dopamine. In the healthy brain, levodopa is synthesized from the amino acid tyrosine by the enzyme tyrosine hydroxylase. In the terminals of the dopaminergic neurons innervating the striatum, levodopa is then transformed to dopamine by DOPA decarboxylase. In the 6-OHDA treated rat or in human Parkinson's disease, death of dopaminergic neurons therefore leads to inability to produce striatal dopamine. For therapy, levodopa is administered orally or via injection together with inhibitors to prevent loss by extracerebral decarboxylase (in the gut and other peripheral tissues). Inhibitors of extracerebral decarboxylase are for example benserazide or carbidopa. In the striatum of the Parkinsonian brain (model or human disease), dopamine is formed from the administered L-Dopa in the remaining dopaminergic neuron nerve terminals, but also in other sites. Dopamine can also be formed in the nerve terminals of neurons producing serotonin and noradrenalin, as well as in some glial cells. Administration of levodopa therefore restores striatal dopamine levels. In most patients affected by Parkinson's disease, motor symptoms are strongly reduced or disappear following levodopa treatment. Levodopa treatment remains effective even in patients with severe loss of dopaminergic nerve terminals (for a general introduction to Parkinson's disease, see (Hornykiewicz 2001)).

By restoring dopamine levels in the striatum of 6-OHDA lesioned rats, restoring of normal glutamatergic activity could be expected as well (Morari, Marti et al. 1998). In some microdialysis experiments however, increased extracellular glutamate

concentrations have been observed after acute (Jonkers, Sarre et al. 2002) or chronic levodopa administration (Robelet, Melon et al. 2004) and could be related to developments of dyskinesia.

Only few studies have so far addressed the problem of glutamate measurement in the 6-OHDA rat model using magnetic resonance spectroscopy. MRS offers however interesting perspectives for research on Parkinson's disease.

As noninvasive tool, MRS allows long term studies on the same animal. This is particularly interesting for the monkey Parkinson model, which allows examining slow disease progression, taking usually place in human Parkinson's disease, as shown in (Brownell, Jenkins et al. 1998). Furthermore, MRS methods present great potential for transfer to clinical research and applications. As opposed to microdialysis, the combined extra- and intracellular glutamate pool is measured. Extracellular glutamate concentrations are however only present on a concentration scale of micromole (Fillenz 2005); intracellular glutamate concentrations are on the scale of millimole, see annex, Table 8.3. MRS glutamate signals therefore stem principally from an intracellular origin, and observable changes, as long as cells and synaptic activity are intact, must be interpreted as changes in intracellular glutamate.

A recent study measured striatal glutamate in the 6-OHDA lesioned rat using ^{13}C NMR spectroscopy (Chassain, Bielicki et al. 2005). Incorporation of $[2-^{13}\text{C}]$ acetate in the glutamate pool was significantly higher in lesioned rats than in control rats. Lesioned rats having received acute levodopa administration before acetate injection showed incorporation of $[2-^{13}\text{C}]$ acetate similar to intact control rats.

With the present study, we wanted to evaluate the potential of proton NMR spectroscopy for observing striatal glutamate changes in the 6-OHDA rat model of Parkinson's disease. Animals were examined before and after lesion of the nigrostriatal pathway and following acute levodopa administration. Non invasiveness of MRS allows us to follow up effects on the same animal.

6.2 Materials and methods

6.2.1 Experimental procedure

Twenty male Sprague Dawley rats (150 to 200 g, Janvier, France) were used for this study. Eight rats were examined in a first series, 12 rats in a second series. There was no essential difference in the experimental procedure of the first and second series, only a small change concerning the MRS acquisition parameters, as will be detailed later. Animals were housed under standard laboratory conditions (12h light/dark cycle) with food and water *ad libitum*. Protocols conformed to National Institutes of Health Guide for the Care and Use of Laboratory Animals (publication 865-23) and French Ministry of Agriculture regulations (decree n°87-848 of October 1987; authorization number: 380321, A3851610004 and B3851610003)

First MRS exams were performed on the intact rats (5-6 semaines, 150/200 gr). Animals were anesthetized with 5% isoflurane in air enriched with O₂ to 35%. Anesthesia was then maintained with 1 – 1.5% of isoflurane, administered by a mask. Rectal temperature was monitored throughout the experiment and maintained at 37°C with a heating pad under the abdomen. In the magnet, the rats were held in place by a stereotaxical frame. The exam started with acquisition of spin echo images (slice thickness 1mm) for voxel positioning. A 3 x 3 x 3 mm³ volume was chosen for MRS. The voxels were positioned to contain once the left, once the right dorsolateral striatum (see Fig. 6.1, Fig. 6.2), comparing to an in-house anatomical atlas relating MR images to anatomical brain cuts (C. Rémy). The dorsolateral part was chosen as the nigrostriatal afferents, which are affected by 6-OHDA lesion, primarily end here. The dorsolateral part represents the motor area of the striatum which is normally affected in Parkinson's disease.

To model Parkinson's disease, a (so called) complete lesion of the substantia nigra pars compacta (SNc) was induced unilaterally (Emilie Lacombe, INSERM U704, Grenoble) four days after the MR exam. Animals were anaesthetized by intraperitoneal injection of chloralhydrate (400 mg/kg body weight) and received desipramine (25 mg/kg, subcutaneous injection) to protect noradrenergic neurons. Secured in a stereotaxic apparatus, an unilateral lesion of dopaminergic neurons was induced by stereotaxic injection of 6-OHDA into the left SNc at the following coordinates: anterior 3mm; left 2mm; ventral 2.4mm from the midpoint of the interaural line, according to the brain atlas of Koenig and Klippel, 1963. Five milligram of 6-OHDA (6-hydroxydopamine hydrochloride stabilized with ascorbic acid) were dissolved in 1.67 ml of physiologic serum (NaCl 0.9%) to obtain a solution of 3 mg/ml 6-OHDA. Three microliters of this solution were injected into the left SNc at 0.5 µl/min using a syringe infusion pump. After injection, the canula was left in place for 5 minutes before being withdrawn. Lesion according to this protocol leads to nearly complete depletion of dopamine in the striatum. We use the complete lesion model because we suppose that severe lack of striatal dopamine should lead to the strongest alteration of the glutamate pool and to the most marked reaction of the brain to levodopa administration.

Rats underwent a second MRS exam 4 weeks post lesion. We chose to omit verification of the lesion by apomorphine rotation tests in order to elude priming of the animals to anti-Parkinsonian treatment. Effectiveness of the lesion was instead verified post-mortem, at the end of all exams, by antibody labeling of tyrosine hydroxylase (TH) on cytosections of the substantia nigra. As for the first experiment, animals were anesthetized with 4% isoflurane in air and anesthesia was then maintained with 1 – 1.5% of isoflurane in air enriched with O₂ to 35%. Catheters were introduced intraperitoneal (for later injection of benserazide and levodopa) and in the left femoral vein (for control of blood pressure and blood samples). Rats were tracheotomized and mechanically ventilated to ensure stable conditions during the relatively long period of anesthesia. Arterial pressure, ventilation and rectal temperature were monitored throughout the experiment to adapt anesthesia and ventilation when necessary, but not

recorded. As during the first MRS exam, rectal temperature was maintained at 37°C with a heating pad under the abdomen; rats were held in place by a stereotaxic frame in the magnet.

For MRS, a 3x3x3 mm³ voxel was positioned first on the right and then on the left striatum, reproducing as well as possible the positioning that had been chosen during pre-lesion acquisitions. Then, without moving the rat and maintaining all MR relevant calibrations (rf, shim, voxel position etc), rats received intraperitoneal injection of benserazide (0.5 ml, 12.5 mg/kg body weight) to inhibit extracerebral decarboxylase. After a delay of 30 minutes to let the benserazide take effect, levodopa was injected (50 mg/kg body weight) through the same catheter. MR spectra were acquired from the volume positioned on the left striatum during the following 3 hours. Further technical details concerning MRS will be given later in this text.

At the end of the *in vivo* MRS acquisitions, the anaesthetized rats were sacrificed by decapitation, the skull was opened and the brain removed. The brain was separated in an anterior and posterior part, the anterior part containing the striatum, the posterior part containing the substantia nigra. The anterior part was subsequently separated in left and right hemisphere and weighed. All brain parts were frozen as quickly as possible in liquid nitrogen. The posterior part was used for verification of the lesion by TH immunolabeling.

Next to the 6-OHDA rats, three intact rats of the same age were used for control purposes. Rats were anesthetized with 5% isoflurane in air enriched with O₂ to 35%. Animals were then sacrificed by decapitation and their brain removed and separated following the same protocol as for the Parkinsonian rats.

Absolute metabolite concentrations were determined from the anterior (left and right) brain parts of the 6-OHDA rats and the control rats, parts containing the striatum (Carine Chassain, QuaPA-STIM, INRA Clermont-Ferrand), using high resolution MRS. Technical details are given in the following text

6.2.2 *In vivo* MRS

The rats were placed in a 20 cm horizontal bore, 7 T magnet with actively shielded gradients (Magnex Scientific Ltd, Abington, UK), interfaced to a SMIS (Surrey medical imaging, Guildford, UK) console. A home made 25 mm surface coil was used for emission and reception. After voxel positioning, local adjustments of resonance frequency, rf power and shim (1st and 2nd order) were performed. Shimming was first done with a FASTMAP (Gruetter 1993) based protocol and then refined manually. Typical water resonance linewidths after shimming were 16 Hz. For localized spectroscopy we used PRESS with an echo time of 136 ms, preceded by a VAPOR (Tkac, Starcuk et al. 1999) water suppression module. First echo time was 12 ms to maximize the delay between last (180° pulse) crusher gradient and acquisition window.

A spectral width of 10 kHz was acquired on 1024 points, half the number of points before and the other half after the echo signal maximum. All acquisitions used a repetition time of 3 seconds, starting with eight dummy scans to establish steady state magnetization.

First and second series of experiments were slightly different with respect to signal accumulation. For the MR spectra of the first series, 128 scans were accumulated in a data block during acquisition. For the second series, only 32 scans were accumulated per data block. It is advantageous to accumulate as few as possible scans in a data block during acquisition, as this allows more precise correction of frequency shift and phase during postprocessing. Accumulating 32 scans was found to provide sufficient signal to noise ratio to apply correct phasing and frequency shift corrections.

During the first series of experiments, for the MRS exams “before lesion” and “after lesion - before levodopa injection”, a single block of 128 scans was acquired. These acquisitions were preceded by acquisition of the unsuppressed water signal for referencing purposes, using 8 accumulations after 8 dummy scans. After levodopa injection, during 2.5 to 3 hours, blocks of 128 scans were acquired and stored to disk for later treatment.

During the second series of experiments, 16 blocks of 32 scans were acquired for the MRS exams “before lesion” and “after lesion - before levodopa injection”. As for the first series, these acquisitions were preceded by acquisition of the unsuppressed water signal, using 8 accumulations. After levodopa injection, blocks of 32 scans were acquired during 3 hours.

It has been stated before (chapter 4) that the highest glutamate signal amplitude and the best estimation of glutamate can be obtained at an echo time of 115 ms. We have nevertheless chosen an echo time of 136 ms for several reasons. At 136 ms echo time, lactate presents a fully inverted doublet signal at 1.3 ppm which can easily be distinguished from neighboring lipid peaks. In healthy rats the lactate signal is barely visible. Hypoxic conditions lead to an increase in lactate. Easy visibility of the lactate signal is therefore favorable to monitor the rat’s condition in the magnet.

An echo time of 136 ms allows acquisition of a symmetrical time domain echo signal with an acquisition window length allowing still acceptable spectral resolution. An acquisition window duration of 102.4 ms (10 kHz, 1024 pts), after two times zerofilling, yields a spectral resolution of about 5 Hz per point, which is a minimum with respect to the obtained linewidth. At 115 ms the acquisition window would either have to be shorter or the echo signal would not be placed in the middle of the acquisition window. Symmetry in the time domain simplifies data handling in the spectral domain, for example with respect to 0th order phase correction, as the imaginary signal part is zero.

Experiments on model solutions to study the peak composition of the signal visible *in vivo* near 2.3 ppm have been performed using exactly the *in vivo* acquisition parameters; these are presented in the annex, section 8.4.

Furthermore, PRESS at 136 ms with the acquisition of a symmetrical echo, has been shown, within another research context present in our laboratory, to be a technique allowing the detection of brain glutamate alterations: It is known that excessive brain ammonium levels, for example produced artificially by infusion, lead to a decrease in brain glutamate (Fitzpatrick, Hetherington et al. 1989). This finding has been confirmed by work done in our laboratory (Provent, Kickler et al. 2005) using the above described PRESS sequence parameterization.

6.2.3 Postprocessing of *in vivo* spectra

Posttreatment used the IDL programming language (RSI, Boulder, CO). Exponential broadening of 9 Hz and zero-filling to 4096 points was applied before Fourier transformation. First order phase correction determined by the (theoretical) position of the spin echo maximum within the acquisition window was applied to all spectra (phase correction of π per spectral point). Spectra corresponding to accumulation of 128 scans (1st series of experiments) or 32 scans (2nd series of experiments) were then individually 0th order phase and frequency shift corrected using the NAA singlet as reference.

It has been described before that for the second series of experiments, for the MRS exams 'before lesion' and 'after lesion – before L-DOPA injection' acquisitions have been performed in 16 blocks of 32 scans. All the 16 scans corresponding to one MRS exam were in the following summed. Spectra of first and second series were then quantified.

For quantification, a sum of Lorentzian lineshapes was adjusted to the experimental data (real part of the spectrum) in the frequency domain. This model function incorporated Lorentzian lines to fit the following signals: 2.0 ppm (mainly n-acetylaspartate; referred to as NAA), 2.3 ppm (mainly glutamate with contributions of contributions of glutamine, NAA, GABA; referred to as glx), 3.0 ppm (creatine + phosphocreatine; referred to as total creatine (tCr)), 3.2 ppm (choline + phosphorylcholine + glycerophosphorylcholine with contributions of taurine and myoInositol; referred to as total choline (tCho)), 3.4 ppm (mainly Taurine, myo-Inositol). Adjustable parameters were linewidth, amplitude and position; the parameters were adjusted using IDL's built in function "curvefit". The signal at 3.4 ppm was included in the model function but not used for further statistical tests, as it was affected by water suppression in several spectra.

Alternatively, adjustment of model functions in the time domain using AMARES of MRUI has been tried, but was found less reliable, most probably due to difficulties with determination of the echo maximum within the acquisition window.

For a first (visual) evaluation of the MRS exams "after lesion – after L-DOPA injection" (spectra acquired during 2.5 to 3 hours post injection), spectra of the second

series were summed to blocks of 64 accumulations (sum of two consecutive spectra including each 32 accumulated scans) to ensure acceptable signal to noise ratio and then quantified as described above. Spectra of the first series, including 128 accumulated scans, were quantified directly.

For statistical evaluations, all post-injection spectra for each rat, omitting some particular spectra of poor quality, were summed and then quantified, as visually no evolution after levodopa injection was observed (see results section).

6.2.4 *In vitro* MRS

(Carine Chassain, QuaPA-STIM, INRA Clermont-Ferrand)

Solutions of the brain metabolites were obtained by perchloric acid (PCA) extracts: The striatal tissues were homogenized in 4% PCA using an ultrasound homogenizer and then centrifuged during 15 minutes at 4°C (9600 rotations per minute, rpm). The supernatant was retrieved and neutralized with K₂CO₃. Precipitates of KCL were separated by repeated centrifugation (4°C, 9600 rpm, 10 min). The supernatant was then lyophilized and resuspended in deuterated water (D₂O). The pH was adjusted to 7.4 ppm and the sample stored at -20°C. For quantification of absolute metabolite concentrations, the sample was placed in an NMR tube next to a tube containing a 5 mM TSP solution. Spectra were obtained at 9.4 Tesla field strength with a standard pulse-acquire sequence (number of averages 128, repetition time 9.1 sec).

6.2.5 Postprocessing of *in vitro* spectra

Spectra were processed using the MRUI software package (Naressi, Couturier et al. 2001). Corrupted first points due to digital filtering were removed of each FID. Spectra were then phased to 1st and 0th order and baseline corrected. Assignment of the different resonances was performed based on values from the literature (Govindaraju, Young et al. 2000). The identified peaks were then quantified using AMARES (Vanhamme, van den Boogaart et al. 1997). As prior knowledge, only peak positions and a common linewidth of 2 Hz were entered. Individual and global phases were kept fixed. Peak amplitudes for each metabolite and TSP, as determined by AMARES, were divided by the number of resonating protons giving rise to the respective resonance lines. Absolute metabolite concentrations were then obtained relating to the known TSP concentration and knowing the tissue weight from which the PCA abstract was obtained. For visualization in Fig. 6.7, one Hertz exponential broadening was applied.

6.2.6 Statistics

A two way within subjects analysis of variance was conducted to evaluate the effect of 6-OHDA lesion on the metabolite signals (glx/NAA, tCr/NAA and tCho/NAA) measured *in vivo* in ipsi- and contralateral hemisphere. NAA was used for normalization as, supported by results obtained *in vitro*, we assumed it stable after lesion in these experiments (see results section for NAA). The within subjects factors were brain hemisphere with two levels (left, right) and time with two levels (before lesion, after lesion). Non parametric matched pairs tests (Wilcoxon) were conducted to follow up interaction and main effects where significant.

To evaluate the results obtained after levodopa injection (acquisitions accumulated during 2.5h to 3h) non parametric matched pairs tests were used as well. We compare the metabolite ratios obtained from the left hemisphere after lesion – before levodopa injection with the ones obtained after injection.

For statistical treatment of the absolute metabolite concentrations obtained *in vitro*, a non parametric (Mann-Whitney) test was used to compare data from ipsi- and contralateral hemisphere.

6.3 Results

The experiments could be successfully completed on 10 animals, 3 of 8 animals during the first series and 7 of 12 animals during the second series of experiments. During the first series, 2 animals died after lesion and 2 during the second MRS session; during the second series 2 animals died after lesion and 3 during the second MRS session. The experimental procedure of repeated anesthesia exerts considerable strain on the animals. Premature deaths during the second MR exam occurred mostly directly after introduction of anesthesia. The group size for statistical analysis of the *in vivo* experiments was nine, as one rat of the first series had to be excluded due to technical problems during acquisition. Group size for statistical analysis of the *in vitro* experiments was ten.

On all animals which underwent the complete protocol, 6-OHDA lesion was successful as verified by TH immunolabeling.

Voxel position *in vivo*, spectra *in vivo* and *in vitro*

In this paragraph we present images visualizing the voxel position used for *in vivo* spectroscopy and spectra acquired from the respective brain regions, followed by spectra acquired *in vitro* on PCA extracts.

Fig. 6.1 and Fig. 6.2 are representative for placement of the volume used for spectroscopy when centered on the left dorsolateral striatum. Fig. 6.1 shows the voxel

used for the pre-lesion exam, Fig. 6.2 the voxel used for the post-lesion exam on the same animal. Due to experimental problems, the voxel position may vary up to 0.8 mm in the left-right direction from the depicted position. The volume remains however well within the striatal region.

Fig. 6.3 shows the spectrum acquired before lesion from the left hemisphere, the spectrum acquired after lesion from the same hemisphere of the same animal is displayed in Fig. 6.4. For quantification, a model function (solid line) has been adjusted to the signals at 2.0 ppm, 2.3 ppm, 3.0 ppm, 3.2 ppm and 3.4 ppm (see Methods section), as can be seen in Fig. 6.5. The fit residual (solid line) together with the spectrum (dotted line) is displayed in Fig. 6.6. The model function fits well to the observed peaks, only minor contributions remain (unfitted) in the residual. Quantification results and statistics will be described later in this text, together with observations concerning changes in the spectral region at 1.3 ppm.

Fig. 6.7 shows an example of a high resolution *in vitro* spectrum obtained from a PCA extract of the striatal tissue (left hemisphere, ipsilateral, anterior part) of a 6-OHDA treated rat. Peak assignments have been performed according to (Govindaraju, Basus et al. 1998) and are as indicated in the figure caption.

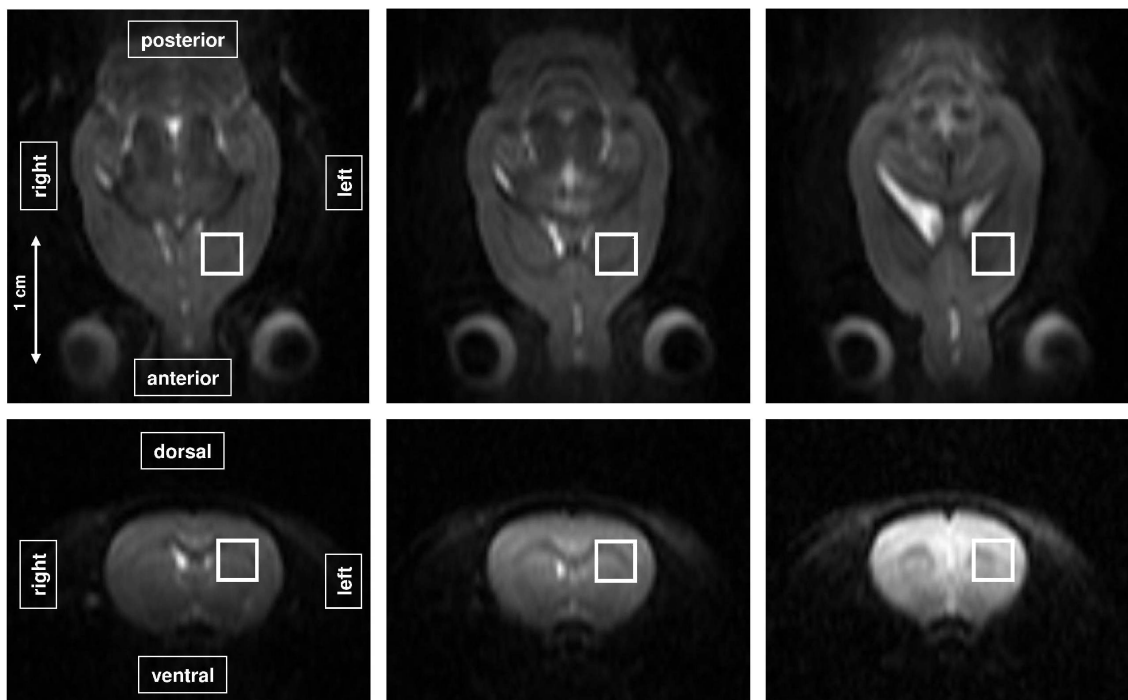


Fig. 6.1: Placement of the $(3 \times 3 \times 3) \text{ mm}^3$ voxel used for spectroscopy in this study. The acquisition volume is centered on the left dorsolateral striatum. All images were acquired before lesion with a slice thickness of 1mm. The scale, as indicated, is the same for all images in horizontal and vertical dimension. The spectrum acquired from this position is shown in Fig. 6.3.

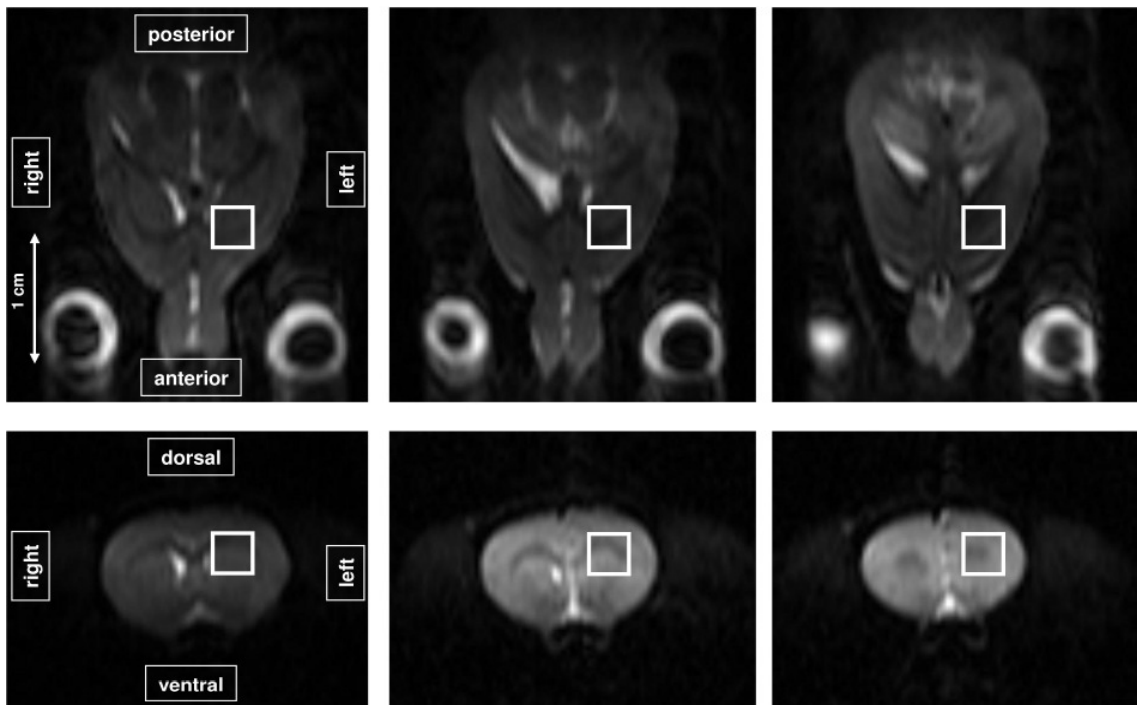


Fig. 6.2: Placement of the $(3 \times 3 \times 3) \text{ mm}^3$ volume used for spectroscopy, centered on the left dorsolateral striatum of the same rat shown in Fig. 6.1 but after 6-OHDA lesion. All images were acquired with a slice thickness of 1mm. The scale, as indicated, is the same for all images in horizontal and vertical dimension. The spectrum acquired from this position is shown in Fig. 6.4.

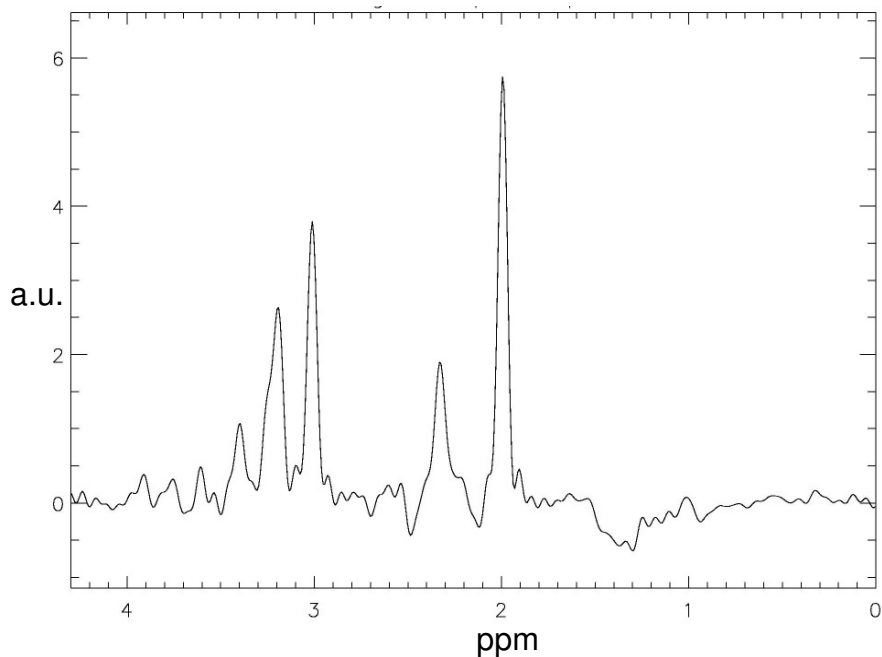


Fig. 6.3: *In vivo* PRESS spectrum acquired with an echo time of 136 ms from the voxel shown in Fig. 6.1 (left hemisphere, pre-lesion). Signals are identified as (compare to Fig. 6.7): 2.0 ppm; mainly N-acetylaspartate (NAA), 2.3 ppm; mainly glutamate with contributions of glutamine, NAA, GABA (glx), 3.0 ppm; creatine + phosphocreatine (tCr), 3.2 ppm; choline + phosphorylcholine + glycerophosphorylcholine with contributions of taurine and myo-Inositol (tCho), 3.4 ppm; mainly Taurine, myo-Inositol.

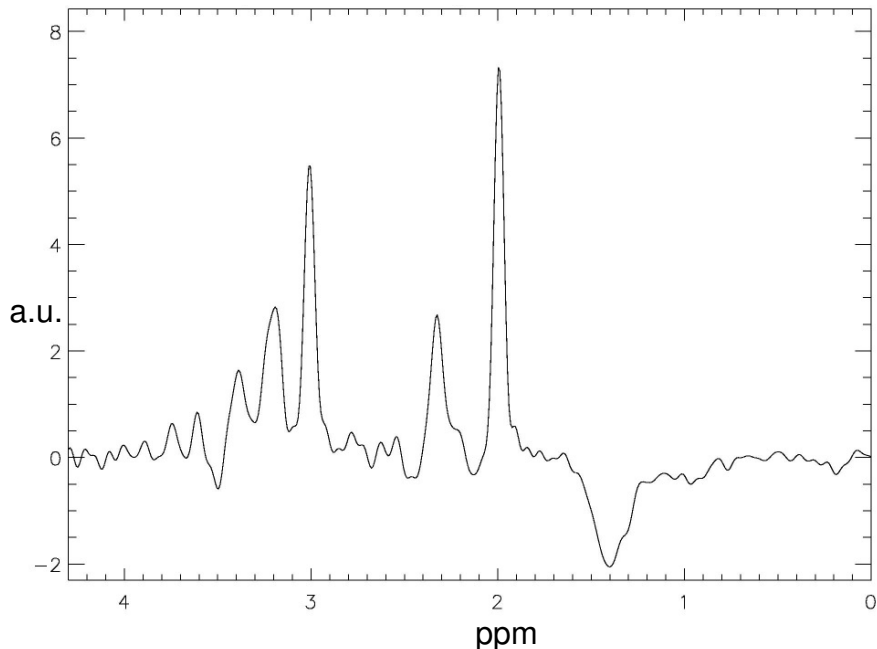


Fig. 6.4: *In vivo* PRESS spectrum acquired with an echo time of 136 ms from the voxel shown in Fig. 6.2. This spectrum has been acquired from the same rat and the same hemisphere (left) as the one shown in Fig. 6.3 but after 6-OHDA lesion of the left nigrostriatal pathway. Peak identifications are as in Fig. 6.3. Changes are visible in the spectral region of 1.3-1.4 ppm as compared to Fig. 6.3 and are associated with an increase in lactate.

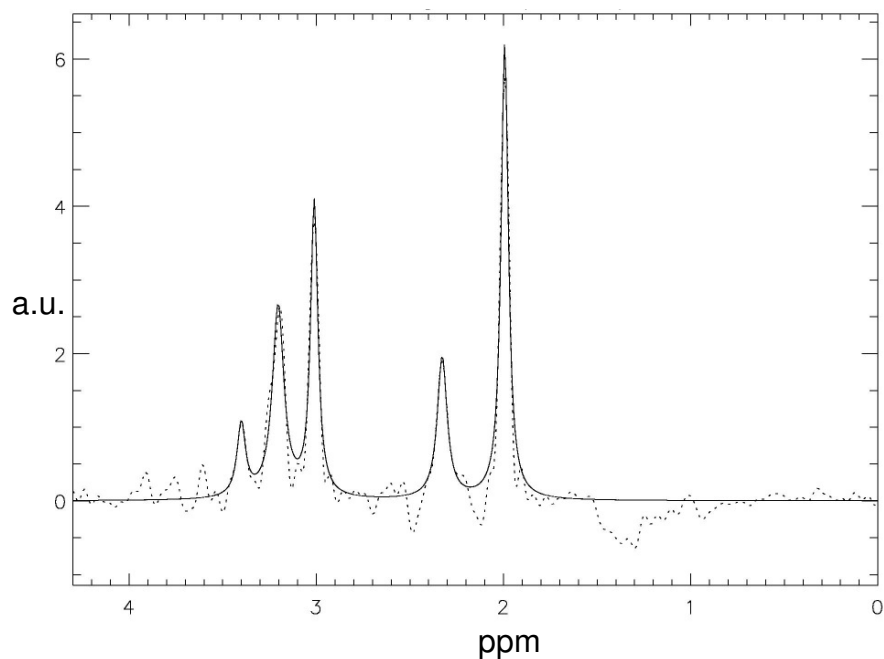


Fig. 6.5: Adjustment of a model function to the spectrum of Fig. 6.3 (solid line). A sum of five Lorentzian lineshapes was adjusted in the frequency domain to the peaks visible at 2.0 ppm, 2.3 ppm, 3.0 ppm, 3.2 ppm and 3.4 ppm. Fitted parameters were position, linewidth and peak amplitude. The spectrum is shown as dotted line.

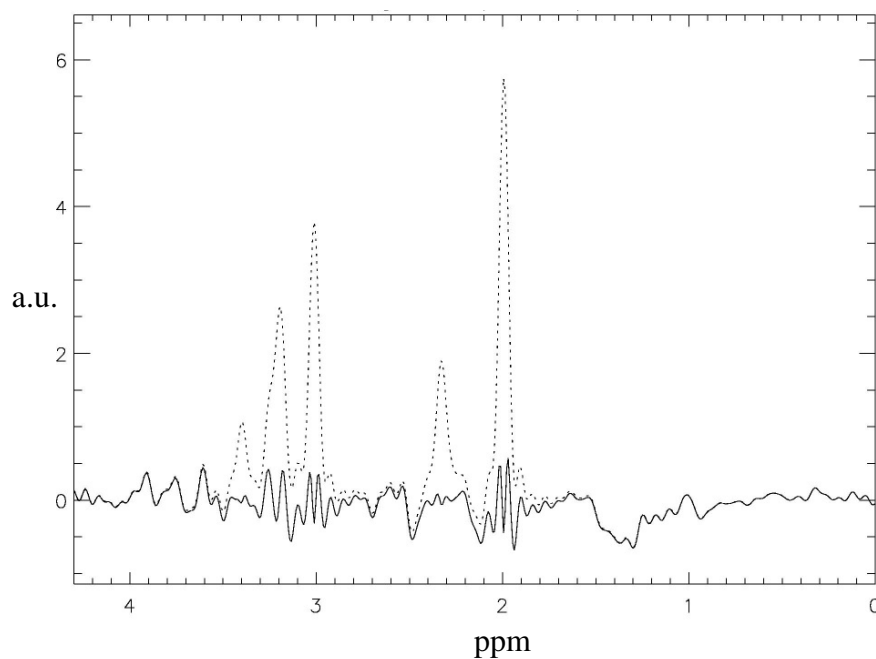


Fig. 6.6: Residual (spectrum minus fitted model function, solid line) of the fit shown in Fig. 6.5. The spectrum is shown as dotted line (compare to Fig. 6.3).

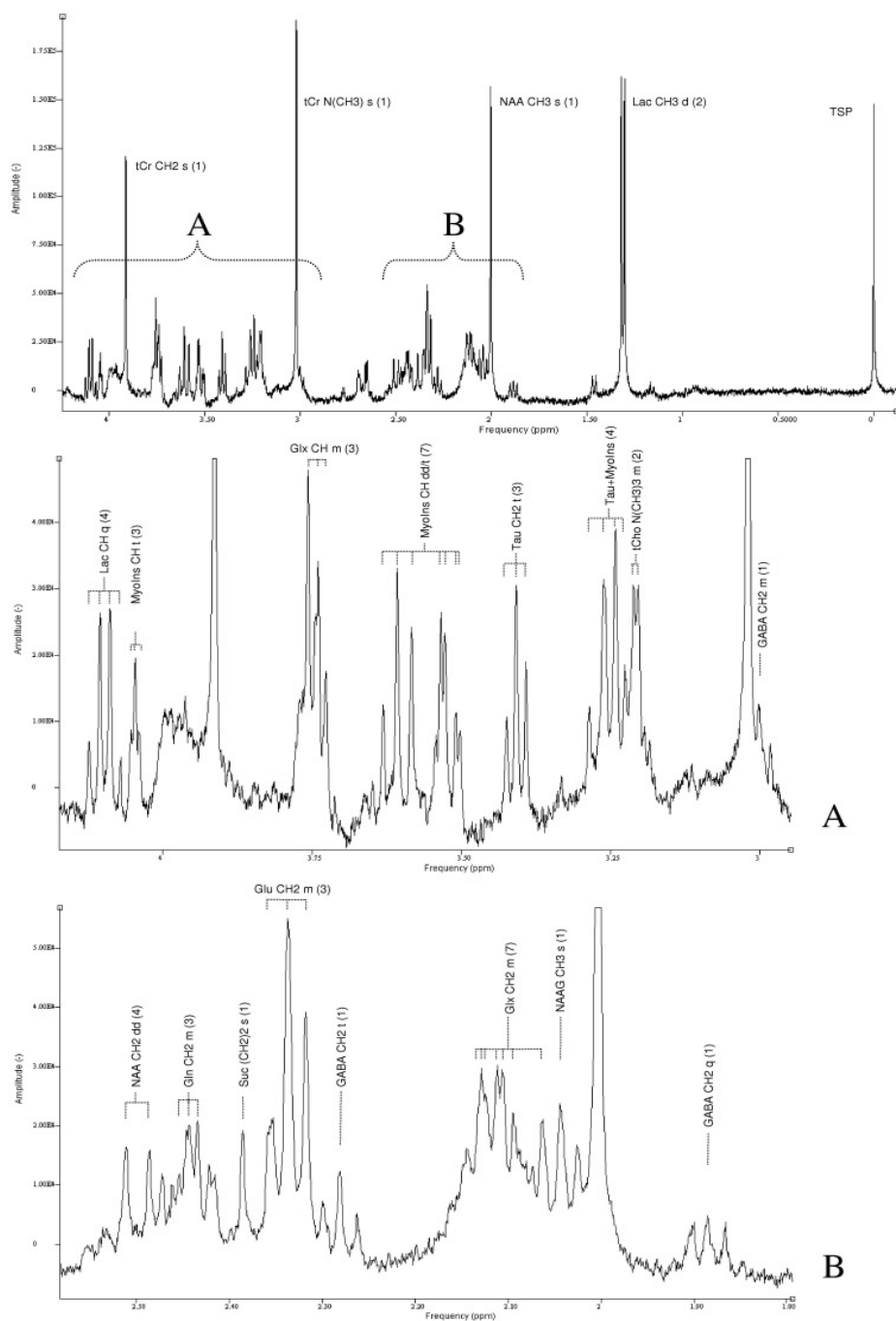


Fig. 6.7: High resolution *in vitro* spectrum obtained from a PCA extract of the striatal tissue (left hemisphere, anterior part) of a 6-OHDA treated rat. Peak assignments have been performed according to (Govindaraju, Basus et al. 1998). Abbreviations used for metabolites are: tCr, total creatine (creatine + phosphocreatine); NAA, n-acetylaspartate; Lac, lactate; TSP, trimethylsilylpropionic acid (reference); MyoIns, myoinositol; Glx, glutamate+glutamine; Tau, taurine; tCho, total choline (choline+phosphorylcholine, glycerophosphorylcholine); GABA, gamma-aminobutyric acid; Gln, glutamine; Glu, glutamate; Suc, succinate; NAAG, n-acetylaspartylglutamate. Abbreviations used for signal structures are: s, singlet; d, doublet; dd, doublet of doublets; t, triplet; q, quadruplet; m, multiplet. Indicated between brackets is the number of Lorentzian lines used for fitting of the indicated structure with AMARES. For visualization, 1 Hz exponential broadening was applied.

Statistics and visual evaluation *in vivo* and *in vitro*

In the following we describe the results obtained from statistical analysis. Graphs for visualization of the data are shown at the end of this paragraph.

Glutamate (*in vivo* and *in vitro*)

Fig 6.8 (top) shows the values obtained from quantification of the signal visible *in vivo* at 2.3 ppm (about 80% glutamate, next to glutamine, NAA and GABA, see annex 8.4), normalized with the NAA signal amplitude. Values were obtained from the exams “left hemisphere (ipsilateral) before lesion”, “left hemisphere after lesion”, “left hemisphere after lesion and levodopa injection” (from spectra accumulated during 2.5 to 3 hours, see results below), “right hemisphere (contralateral) before lesion” and “right hemisphere after lesion”. Values obtained from the same animal and the same hemisphere are shown linked by a line to visualize evolution.

Two way ANOVA shows no significant main effect or interaction for the within subject factors time (lesion) and hemisphere, evaluating the measurements obtained before lesion and after lesion-before levodopa injection.

Fig. 6.9 (top, left) visualizes the evolution of the 2.3 ppm signal after levodopa injection. Shown are the quantification results obtained from 10 rats, three from the first (upper three lines) and seven from the second (lower seven lines) series of experiments. For the first series, each point corresponds to the peak area obtained from a spectrum accumulating 128 scans. For the second series, each point corresponds to 64 scans. The points associated with negative time correspond to spectra acquired before any injection. These serve as reference. For each rat, all peak areas have been normalized with respect to the average peak area determined on all pre-injection spectra. Timepoint zero minutes corresponds to injection of levodopa and is preceded by a thirty minutes delay, which followed injection of benserazide. For presentation, results obtained from the different rats have been separated vertically. Visually, no change or evolution in the 2.3 ppm peak following levodopa injection may be observed. All post-injection spectra (for each rat) have therefore been summed and glx was quantified in this sum spectrum. Statistical evaluation used the data obtained from this sum spectrum.

Wilcoxon matched pairs test between the groups “left hemisphere after lesion” and “left hemisphere after lesion and levodopa injection” shows no significant influence of levodopa injection on glx/NAA.

Fig. 6.10 (left) shows absolute glutamate concentrations (mmole/kg wet weight of brain tissue) determined using high resolution NMR spectroscopy from extracts of the brain parts containing mainly the striatum. The left column shows values obtained from the right (contralateral) side, the right column values obtained from the left (ipsilateral) side of the 6-OHDA rats. Glutamate concentrations show no significant difference between ipsi- and contralateral side.

Total creatine (*in vivo* and *in vitro*)

Fig 6.8 (middle) shows the values obtained *in vivo* from quantification of combined creatine and phosphocreatine, normalized with the NAA signal (see description of glutamate graphic for details of the presentation).

Two way ANOVA shows no significant main effect or interaction for the within subject factors time (lesion) and hemisphere, evaluating the measurements obtained before lesion and after lesion-before levodopa injection.

In the same way as for the glutamate signal, Fig. 6.9 (top, right) shows the evolution of tCr after levodopa injection. Visually, no effect of the injection on the peak area may be seen. As for glutamate, all post-injection spectra for each rat have therefore been summed and the sum was used for tCr quantification.

Wilcoxon matched pairs test between the groups “left hemisphere after lesion” and “left hemisphere after lesion and levodopa injection” shows no significant influence of levodopa injection on tCr/NAA, but a trend to a slight increase ($p = 0.055$).

Absolute combined creatine/phosphocreatine concentrations as obtained from high resolution NMR are displayed in Fig. 6.10 (right). As for glutamate, ipsi- and contralateral side present no statistically significant differences.

Total choline (*in vivo* and *in vitro*)

Fig 6.8 (bottom) visualizes the values measured for total choline (choline + phosphorylcholine + glycerophosphorylcholine with contributions of taurine and myoInositol) *in vivo*, normalized with the NAA signal.

The hemisphere main effect was significant ($p = 0.023$) as well as the hemisphere * time interaction effect ($p = 0.044$). This means that differences in mean tCho/NAA ratios between left and right hemisphere significantly differ between pre- and post-lesion state. The test associated with the time main effect was not significant ($p = 0.34$). Wilcoxon matched pairs tests were conducted to follow up the significant interaction: The contralateral hemisphere does not show significantly different tCho/NAA ratios between pre- and post-lesion (Wilcoxon: $p = 0.77$), whereas the ipsilateral hemisphere shows an almost significant decrease (Wilcoxon: $p = 0.066$) by about 18% (decrease of group mean) as compared to its pre-lesion value.

Fig. 6.9 (bottom, left) shows the evolution of tCho after levodopa injection. Visually, no effect of the injection on the peak area may be seen. As described for glx and tCr, all post-injection spectra have therefore been summed for each rat and tCho was determined from the sum spectrum. Wilcoxon matched pairs test between the groups “left hemisphere after lesion” and “left hemisphere after lesion and levodopa injection” shows no significant influence of levodopa injection on tCho/NAA.

Absolute concentrations of combined choline, phosphorylcholine and glycerophosphorylcholine obtained *in vitro* on extracts are shown in Fig. 6.11 (top, left). Values from ipsi- and contralateral hemisphere are not significantly different.

NAA (only *in vitro*, as used as reference *in vivo*)

In vitro, no statistically significant difference (Wilcoxon: $p = 0.43$) between NAA concentrations of ipsi- and contralateral hemisphere of the 6-OHDA treated rats can be observed (Fig. 6.11, top, right). For the experiments described in this chapter, we assume that NAA levels are not affected by 6-OHDA lesion and use the NAA signal as reference for *in vivo* experiments. This point will be further discussed in the following section.

GABA (only *in vitro*)

In 5 of the 9 animals GABA was higher on the ipsilateral than on the contralateral side (Fig. 6.11, 2nd from top, left). The mean value of all animals was 71% higher after lesion, and a Wilcoxon test showed a trend with $p = 0.065$.

Taurine (only *in vitro*)

In 7 of the 9 animals taurine was lower on the ipsilateral than on the contralateral side (Fig. 6.11, 2nd from top, right). The mean value of all animals was 14% lower after lesion, and a Wilcoxon test showed a trend with $p = 0.084$.

Glutamine, NAAG and myoInositol (only *in vitro*)

No statistically significant differences between the ipsilateral and contralateral hemisphere of the 6-OHDA rats could be found for glutamine, NAAG and myoInositol, see Fig. 6.11.

Lactate region (only *in vivo*)

Changes in the region of 1.3 ppm to 1.4 ppm have been observed following lesion. A well formed peak as in Fig. 6.3 and Fig. 6.4 is not always visible. Changes will therefore be reported only qualitatively. Strong signals in the spectral region 1.3-1.4 ppm have been observed post-lesion in the left hemisphere of six of the nine animals. One of these rats already showed a relatively strong but nevertheless smaller peak before lesion. In four of these rats, strong signals in the same spectral region could as well be observed post-lesion in the right hemisphere.

In summary

No significant change of glutamate (glx/NAA signal) or total creatine (tCr/NAA) signal could be observed *in vivo* following lesion; the total choline signal (tCho/NAA) shows a trend to decrease ipsilateral. No significant influence of levodopa administration on any of the measured metabolite signals could be observed.

In vitro, GABA shows a trend to higher values, whereas taurine shows a trend to lower in the ipsilateral hemisphere as compared to the contralateral hemisphere.

Increased signals were observed in the region of the lactate resonance following lesion.

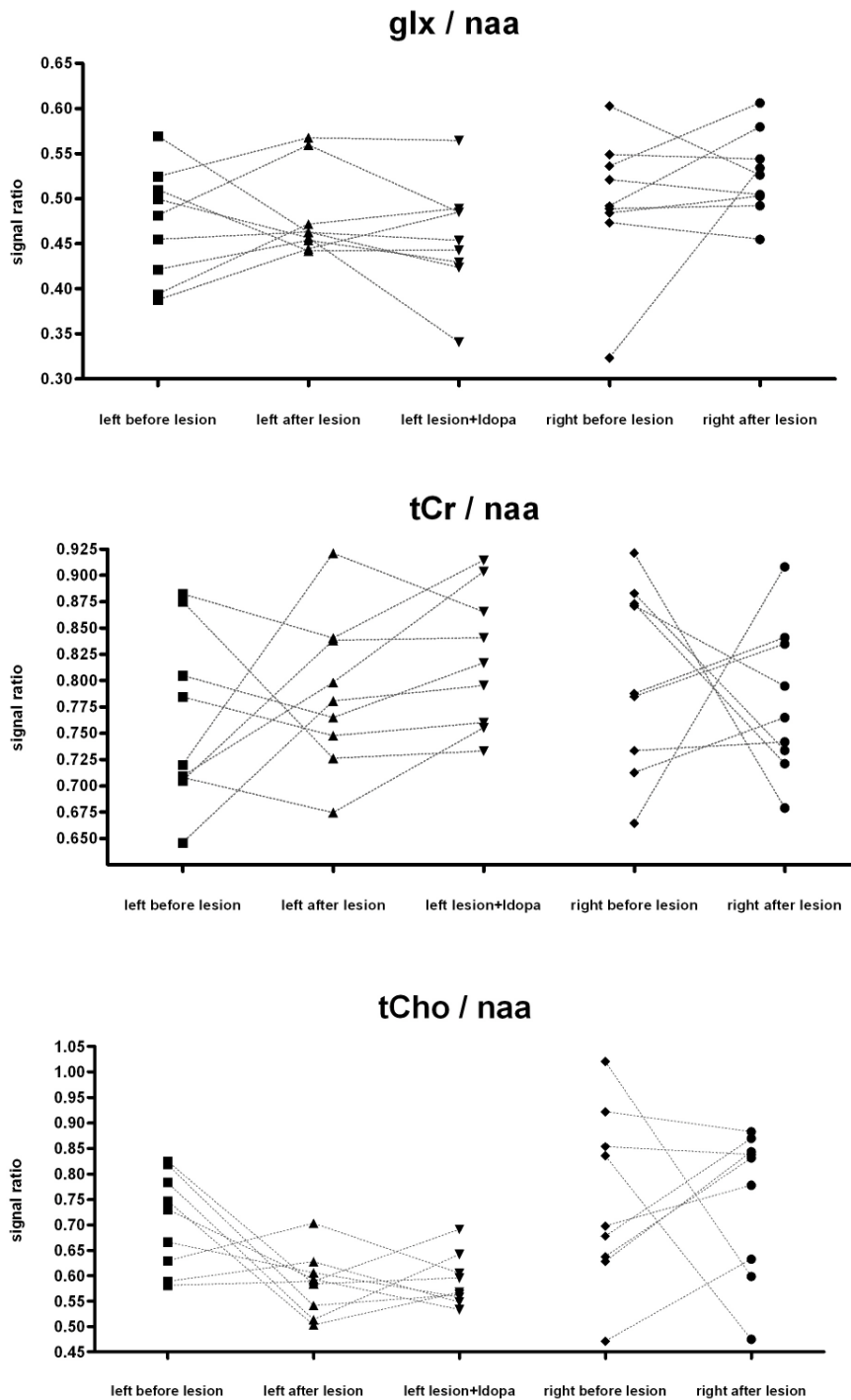


Fig 6.8: Results obtained for glx, tCr and tCho from quantification of the *in vivo* spectra, normalized with the value obtained for NAA. Values from each animal originate from the exams “left hemisphere (ipsilateral) before lesion”, “left hemisphere after lesion”, “left hemisphere after lesion and levodopa injection” (from spectra accumulated during 2.5 to 3 hours), “right hemisphere (contralateral) before lesion” and “right hemisphere after lesion”. Results from the same animal and the same hemisphere are linked by a line to visualize evolution. For tCho/NAA, two way ANOVA shows a significant hemisphere main effect ($p = 0.023$) and a significant interaction effect ($p = 0.044$). The contralateral hemisphere does not show significantly different tCho/NAA ratios between pre- and post-lesion (Wilcoxon: $p = 0.77$), whereas the ipsilateral hemisphere shows a trend to decrease (Wilcoxon: $p = 0.066$) by about 18% as compared to its pre-lesion value.

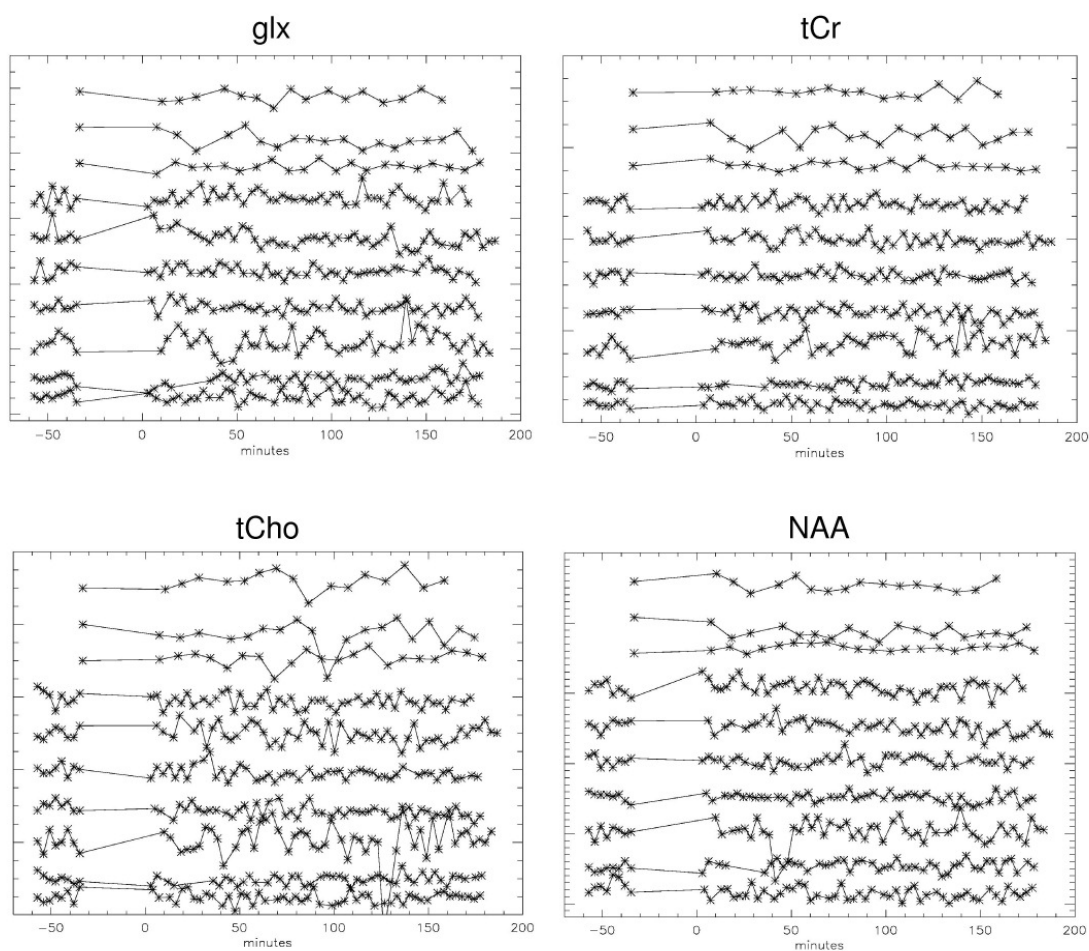


Fig. 6.9: Evolution of the glx, tCr, tCho and NAA signal after levodopa injection. Shown are the quantification results obtained from 10 rats, three from the first (upper three lines) and seven from the second (lower seven lines) series of experiments. For the first series, each point corresponds to the peak area obtained from a spectrum accumulating 128 scans. For the second series, each point corresponds to a spectrum accumulating 64 scans. The points at negative time are associated to spectra acquired before any injection. These serve as reference. For each rat, all peak areas have been normalized with respect to the average peak area determined on all pre injection spectra. Timepoint zero minutes corresponds to injection of levodopa and is preceded by a thirty minutes delay, which followed injection of benserazide. For presentation, results obtained from the different rats have been separated vertically. No signal change during the 2.5 to 3 hours following levodopa injection can be observed visually.

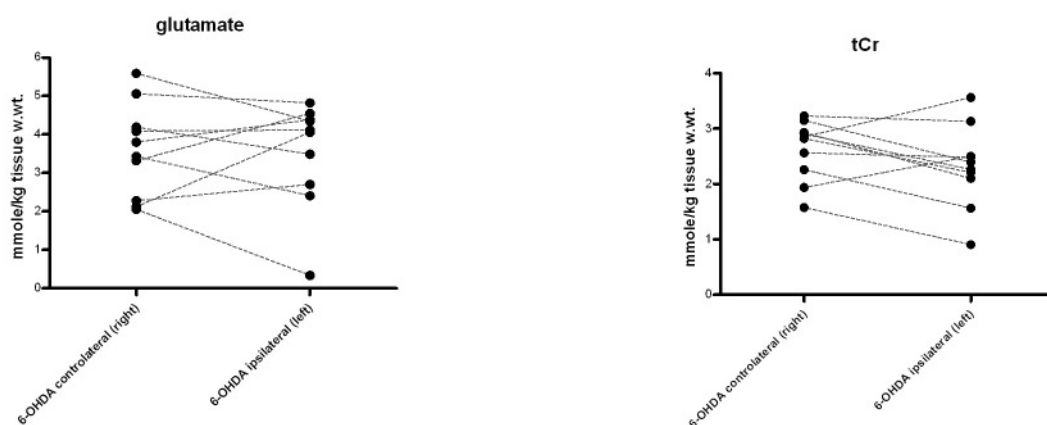


Fig. 6.10: Absolute concentrations (mmole/kg wet weight of brain tissue) of metabolite PCA extracts from brain tissue of the 6-OHDA treated rats. The anterior left or right brain part, divided as described in the method's section, was used for extracts, which were then examined using high resolution NMR spectroscopy. The left column shows values obtained from the right (contralateral) side, the right column values obtained from the left (ipsilateral to lesion) side. Measurements from the same animal are connected by a line. Statistical comparisons show no significant difference between left and right hemisphere values (Wilcoxon).

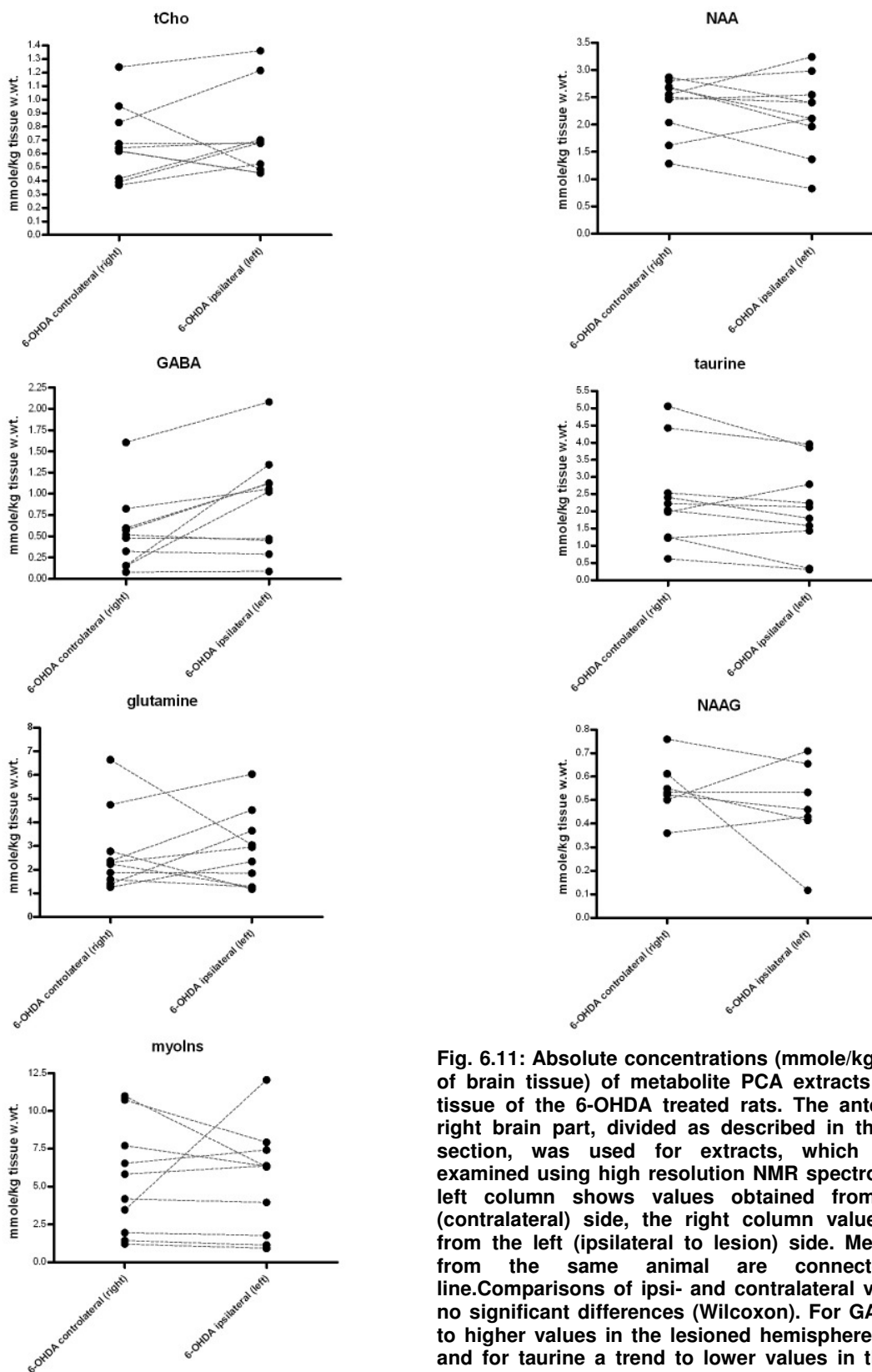


Fig. 6.11: Absolute concentrations (mmole/kg wet weight of brain tissue) of metabolite PCA extracts from brain tissue of the 6-OHDA treated rats. The anterior left or right brain part, divided as described in the method's section, was used for extracts, which were then examined using high resolution NMR spectroscopy. The left column shows values obtained from the right (contralateral) side, the right column values obtained from the left (ipsilateral to lesion) side. Measurements from the same animal are connected by a line. Comparisons of ipsi- and contralateral values show no significant differences (Wilcoxon). For GABA a trend to higher values in the lesioned hemisphere ($p = 0.065$) and for taurine a trend to lower values in the lesioned hemisphere ($p = 0.084$) is observed, comparing to the contralateral side.

6.4 Discussion

General aspects

Premature death of animals during this series of experiments is elevated. Experiments could only be pursued successfully on 10 animals from a total of 20 animals. Administration of anesthesia by a mask instead of tracheotomy could be considered to circumvent stressful surgery and risks.

Compared to values from the literature (see Table 8.2 annex), absolute metabolite concentrations determined *in vitro* on the controlateral side of the 6-OHDA treated rats are low. Low values by about a factor 3.5 as compared to the literature for total creatine, total choline, NAA, glutamate and glutamine were measured on control rats as well (data not shown). Taurine values from controls are coherent with the literature, but GABA concentrations are lower by a factor five. Low values could be explained by losses during extract preparation or incomplete integration of multiplets in the spectrum. As the same experimental protocol was used for all samples, we may however assume that relative differences between hemispheres of the 6-OHDA rats are still valid information.

The NAA signal was used for referencing *in vivo*. NAA in the brain is located almost exclusively within neurons (Hakumäki, Ala-Korpela et al. 1997); decrease is often associated with neuronal loss (see for (Sager, Laursen et al. 1999) example). Of the nigrostriatal neurons, the striatum incorporates the axons whereas the cell body is situated in the substantia nigra. It can be assumed that degeneration of the axons following 6-OHDA injection does not lead to an important NAA decrease, as in volume, they present only a small part of the striatum. No concentration alterations between ipsi- and contralateral hemisphere of the 6-OHDA treated rats could be found *in vitro*. Even though it is difficult to use the contralateral hemisphere as control, as cross effects may exist, absence of ipsi-/contralateral impairment may support our hypothesis for NAA. Furthermore, absolute NAA concentrations determined on the three control animals show values resembling to contra- and ipsilateral side of the 6-OHDA treated rats (data not shown). In the present study, we could not use the water signal for referencing (as done in chapter 5) as it was not unchanged following lesion. Determining the water signal intensity within the spectroscopy region on images, increased intensities following lesion were found. This increase could be due to inflated ventricle volumes, but image quality is not sufficient to pursue exact comparisons.

Influence of unilateral 6-OHDA lesion on glutamate and other metabolites

Our aim in this study was to determine whether it would be possible to measure alterations of striatal glutamate concentrations following 6-OHDA lesion of the nigrostriatal pathway and whether it would be possible to measure a change of this glutamate concentration following administration of levodopa.

Statistical evaluation of the data acquired *in vivo* from the striatum does not allow stating a change in the glx/NAA signal ratio following lesion of the nigrostriatal pathway in the same hemisphere. As well, no influence of levodopa administration on glx can be demonstrated. *In vivo* ^1H MRS measurements of glutamate in our study do not reflect the increase in glutamatergic activity measured by other studies in this model of Parkinson's disease or an alteration related to levodopa administration. Our results suggest that nigrostriatal deafferentiation does not have an important effect on the total quantity of glutamate present within cell and synapses.

According to *in vitro* experiments (Fig. 8.4), the MRS measured signal should be well representative of glutamate, overlapping contributions of other metabolites or opposite changes of gln and gaba might however mask subtle alterations of glutamate.

Changes of increased glutamatergic activity related to nigrostriatal deafferentiation and/or levodopa injection reported in the literature rely mostly on measurements of extracellular glutamate (Meshul, Emre et al. 1999; Jonkers, Sarre et al. 2002; Bruet, Windels et al. 2003) or on vesicular activity (Meshul, Emre et al. 1999) and might depend on small changes in the experimental protocol, as increased extracellular glutamate was not observed systematically (Corsi, Pinna et al. 2003; Galeffi, Bianchi et al. 2003; Robelet, Melon et al. 2004). Increased incorporation of a ^{13}C label to glutamate has been reported as well (Chassain, Bielicki et al. 2005). A single study reports an increased glx/cr signal in the striatum of the cat ten days following MPTP lesion (Podell, Hadjiconstantinou et al. 2003), displaying however spectra difficult to interpret. No changes of combined intra- and extracellular glutamate could be shown in the lesioned striatum one month following 6-OHDA denervation using chromatographic methods (Tanaka, Nijima et al. 1986).

MRS measures the total pool of glutamate which is around 10 mM in the brain (see Table 8.2) and presents mainly the intracellular pool, as extracellular glutamate levels are on the order of 2 to 3 μM . Increases of extracellular glutamate between 45% and 146%, which have been measured in some microdialysis studies (Meshul, Emre et al. 1999; Jonkers, Sarre et al. 2002; Bruet, Windels et al. 2003) are far below the detection sensitivity of *in vivo* MRS. Furthermore, alterations of the extracellular glutamate pool are not necessarily linked to significant changes in the total pool of glutamate.

The *in vitro* measurements of glutamate represent metabolite concentrations in animals following 6-OHDA lesion, levodopa administration and prolonged anesthesia of 3 hours. Absence of statistical difference between ipsi- and contralateral hemisphere may be due to levodopa administration but may as well indicate that, if concentration alterations of total glutamate occur, they are on the order of μM and below detection sensitivity of our MRS protocol.

Our data show a trend of decreased tCho ipsilateral following lesion. Some former studies have reported increased tCho/NAA ratios or increased absolute tCho in human PD (Holshouser, Komu et al. 1995; Ellis, Lemmens et al. 1997; Clarke and Lowry 2000) or increased tCho/tCr in the MPTP monkey model (Brownell, Jenkins et al.

1998). The peak labeled “tCho” observed in proton MRS is a combined signal of choline and choline containing compounds (phosphocholine, glycerophosphocholine) as well as taurine and myoInositol. Depending on experimental parameters (field strength, TR and TE), the relative contributions of these metabolites to the observed peak changes, which may explain different results obtained in our study as compared to literature. Furthermore, the observed changes may be a secondary effect to neurotoxin administration or disease and not related to striatal dopamine depletion. Therefore, changes observed for tCho may well differ between different animal models and human PD. Decrease of the tCho signal may be indicative of membrane degradation, as glycerophosphocholine and phosphocholine play a central role in membrane phospholipid metabolism (Hakumäki, Ala-Korpela et al. 1997).

In vivo, we found increased striatal lactate levels post-lesion in some of the ipsilateral (six animals) and the contralateral (four animals) hemispheres. Similar alterations have been described before in the MPTP cat (Podell, Hadjiconstantinou et al. 2003) and monkey (Brownell, Jenkins et al. 1998) model. Lactate is an indicator of anaerobic oxidation and degenerative changes. Presence in left and right striata might indicate that even though 6-OHDA injection was performed unilaterally, both hemispheres react to neurotoxin administration.

A trend to decreased taurine and increased GABA has been observed ipsilateral. Decreased taurine may contribute to the trend observed for tCho *in vivo*, but comparisons are difficult, as the *in vitro* data represent a state of the animals after levodopa administration and prolonged anesthesia.

Increased GABA one month following lesion has been observed before in the 6-OHDA model using chromatographic methods (Tanaka, Nijima et al. 1986). In the reported study, mean GABA concentrations were found increased to 128% comparing lesioned to contralateral side. Increase of 171% measured in our study is slightly higher but still well comparable. Sprouting of GABAergic nerve terminals following lesion has been suggested as explanation.

6.5 Conclusion and perspectives

Glutamate levels measured by MRS in the 6-OHDA rat model do not display alterations following lesion of the nigrostriatal pathway. MRS measures the total pool of (extra- and intracellular) glutamate and is not a good reflect of increased glutamatergic activity demonstrated in the same model by other methods.

A trend of ipsilateral changes in GABA and taurine has been observed *in vitro*. It would be interesting to perform the same *in vitro* experiments on 6-OHDA lesioned animals omitting levodopa injection and to compare to control animals. If the observed trend can be confirmed, it would be interesting to pursue *in vivo* measurements with methods optimized for GABA and/or taurine detection.

7 General conclusion and perspectives (English and French)

Français

L'objectif du travail était l'implémentation de méthodes de spectroscopie RMN *in vivo* pour la mesure du glutamate et l'application de ces méthodes dans le cadre de la recherche sur la maladie de Parkinson.

Dans des spectres acquis dans des champs magnétiques jusqu'à 3 Tesla et utilisant les méthodes actuellement disponibles, les raies de glutamate, glutamine, NAA et GABA se chevauchent. Utilisant des temps d'écho courts, le chevauchement est marqué mais grâce à l'abondance d'information contenu dans les spectres et grâce à des méthodes de traitement optimisées, les signaux des différents métabolites peuvent être différenciés (Boumezbeur, Besret et al. 2005; Jang, Lee et al. 2005). D'autres approches pour la mesure de glutamate ciblent la minimisation des signaux résonnant au voisinage de glutamate (Pan, Mason et al. 1996; Hurd, Sailasuta et al. 2004; Mayer and Spielman 2005; Schulte, Trabesinger et al. 2005). Au sein de ce dernier groupe de méthodes et en vue d'une application chez le patient, une approche de filtre à double quanta (Thompson and Allen 1998) et une approche liée à la spectroscopie bidimensionnelle (TE averaged PRESS (Hurd, Sailasuta et al. 2004)) ont été implémentées et évaluées à 3 Tesla. Comparé à la méthode de filtrage à double quanta, la méthode de « TE averaged PRESS » permettait une meilleure distinction de glutamate des autres métabolites ainsi que l'acquisition de spectres présentant un meilleur rapport de signal sur bruit, compte tenu des temps d'acquisition utilisés. La mise en place s'est avérée simple et de bons résultats ont pu être obtenus immédiatement. Les spectres acquis dans le lobe pariétal de volontaires sains présentent un signal bien visible, dominé par glutamate. Dans les spectres acquis dans des régions cérébrales plus profondes du nucleus lentiforme le signal de glutamate était moins bien mesurable à cause de fortes inhomogénéités magnétiques provoquées par les interfaces entre tissu cérébral, os et liquide encéphalo-rachidien des ventricules. Pour des examens de spectroscopie dans cette région du cerveau, des systèmes de shims puissants, permettant éventuellement un ajustement de contributions jusqu'au troisième ordre, serait souhaitable. Les méthodes de « TE averaged PRESS » (Hurd, Sailasuta et al. 2004), « CSSF » (Schulte, Trabesinger et al. 2005) et « CT-PRESS » (Mayer and Spielman 2005) sont proches, et la reconstruction de spectres selon ces trois techniques devrait être possible à partir d'une seule acquisition. Il serait ainsi intéressant de comparer directement ces trois approches et éventuellement d'apporter des améliorations en les combinant.

La méthode « TE averaged PRESS » a aussi été évalué à 7 Tesla, sur un imageur petit animal. A cette intensité de champ, « TE averaged PRESS » ne permet pas d'améliorer la mesure de glutamate par rapport à une séquence « PRESS » standard utilisant un

temps d'écho de 115 ms ou 136 ms. A champ élevé, le comportement des systèmes de spins est simplifié et les spectres acquis à un temps d'écho approprié montrent déjà un signal largement dominé par glutamate. A des champs de 7 Tesla, les meilleurs résultats peuvent sans doute être obtenus utilisant des méthodes de temps d'écho court en combinaison avec une procédure de shims optimisées. « PRESS » à temps d'écho long permet pourtant déjà une bonne estimation de glutamate si d'autres techniques ne sont pas disponibles. Un développement intéressant serait l'évaluation d'une séquence de filtrage à double quanta pour l'édition du signal de GABA ou de la taurine à 7 Tesla. L'évolution simplifiée de systèmes de spins à 7 Tesla pourrait faciliter l'optimisation du paramétrage d'un tel filtre.

Comparant le patient Parkinsonien et le sujet sain, aucun changement de glutamate total n'a pu être mis en évidence. De même, les niveaux de glutamate mesurés chez le rat avant et après lésion à la 6-OHDA ne présentaient pas de différence significative. L'administration de levodopa n'avait aucune influence mesurable sur les taux de glutamate, ni chez le malade ni chez le rat lésé. La plupart des études montrant une activation des systèmes glutamatergiques dans le cadre de la maladie de Parkinson reposent sur la mesure du glutamate extracellulaire (Meshul, Emre et al. 1999; Jonkers, Sarre et al. 2002; Bruet, Windels et al. 2003; Robelet, Melon et al. 2004). Les signaux mesurés par spectroscopie par résonance magnétique ne permettent pas de distinguer entre les contributions extra- et intracellulaire. Ainsi, ils représentent majoritairement la concentration intracellulaire de glutamate qui est de l'ordre de 10 millimole (Govindaraju, Young et al. 2000), la concentration extracellulaire étant de l'ordre de 2 à 3 micromole (Fillenz 2005). Nos résultats suggèrent que les altérations de la neurotransmission glutamatergique dans le cadre de la maladie de Parkinson, si présent, ne sont pas accompagnées d'un changement important du taux combiné de glutamate intra- et extracellulaire.

Chez le patient, une tendance de diminution de la créatine totale a été mesurée, dans le modèle animal une tendance de diminution de la choline totale suivant lésion. Les résultats d'études chez le patient présentés dans la littérature ne sont pas cohérentes et il est difficile de conclure (Clarke and Lowry 2001). D'après nos connaissances, aucune étude en spectroscopie RMN chez le rat 6-OHDA n'a encore été publiée. Un plus grand nombre de mesures est nécessaire pour confirmer les tendances observées pour créatine totale et choline totale chez le patient et le petit animal. Le rôle exact de la choline et de la créatine dans le cadre de la maladie de Parkinson n'est pas clair. Une diminution est généralement associée à la dégénération neuronale et à la dissociation de membranes. Les causes de la mort neuronale dans la maladie de Parkinson et dans le modèle 6-OHDA chez le rat sont probablement très différentes, ce qui pourrait expliquer la différence entre les observations rapportées pour le patient et pour l'animal. Les mesures effectuées sur des extraits PCA des rats 6-OHDA montrent des taux réduits de taurine et des taux augmentés de GABA du côté de la lésion par rapport au côté non

lésé. Des études complémentaires sont nécessaires pour confirmer ces observations et pour comparer par rapport à des animaux non lésés. Si une altération des taux de GABA et de taurine était confirmée, la mesure de ces métabolites *in vivo*, utilisant par exemple une séquence de filtrage, pourrait offrir une perspective intéressante.

English

The objective of this work was the implementation of *in vivo* MRS methods for glutamate measurement and their application to research on Parkinson's disease.

In spectra acquired at field strengths up to 3 Tesla, glutamate, glutamine, NAA and GABA signals overlap using currently available acquisition methods. Overlap in short echo time spectra is strong, but high information content allows disentangling of metabolite signals during posttreatment (Boumezbeur, Besret et al. 2005; Jang, Lee et al. 2005). Other approaches try to minimize the contributions of signals overlapping with glutamate (Pan, Mason et al. 1996; Hurd, Sailasuta et al. 2004; Mayer and Spielman 2005; Schulte, Trabesinger et al. 2005). Of the latter methods, for applications on the patient, we have evaluated a double quantum filter method (Thompson and Allen 1998) and an approach related to two-dimensional (2D) spectroscopy (TE averaged PRESS (Hurd, Sailasuta et al. 2004)) on a 3 T whole body imager. TE averaged PRESS showed better distinction of glutamate from its background and allowed acquisition of spectra with better signal to noise ratio at comparable acquisition duration. It was easier to implement and easier to use than the double quantum filter method. Spectra acquired on the parietal lobe of volunteers show a well visible glutamate dominated signal. In spectra from deeper brain regions like the lentiform nucleus, glutamate was less well measurable due to strong magnetic field inhomogeneities caused by interfaces between brain tissue, bone mass and ventricles. In summary, TE averaged PRESS was found to be an easy to implement and easy to use, robust technique allowing acquisition of spectra with a signal largely dominated by glutamate. For spectroscopy exams on deep brain structures, strong shimming systems and maybe shimming of up to third order is necessary to obtain satisfactory results. Spectra of several recently proposed approaches for glutamate measurement (TE averaged PRESS (Hurd, Sailasuta et al. 2004), CSSF (Schulte, Trabesinger et al. 2005), CT-PRESS (Mayer and Spielman 2005)) could be obtained by different reconstructions from the same data set, and it would be interesting to compare approaches or maybe even to combine the approaches to improve glutamate measurement.

TE averaged PRESS was as well implemented and evaluated on a 7 T MRI dedicated to small animal research. At seven Tesla field strengths, TE averaged PRESS does not improve glutamate measurement as compared to a standard PRESS sequence using an echo time of 115 ms or 136 ms. Because of the higher field strength, coupling evolution is simplified as compared to three Tesla and PRESS spectra with an appropriate echo time already display a signal largely dominated by glutamate. At these (high) field strengths, best results can be obtained with short echo time methods, combined with

effective shimming (Tkac, Andersen et al. 2001). Standard PRESS spectra may however allow a good estimation of glutamate alterations, if short TE methods are not available. It might be interesting to evaluate double quantum filter editing for GABA measurement (see below) at 7 T field strengths, as reduced strong coupling behavior could facilitate optimization of such sequences.

Changes in combined extra- and intracellular glutamate could not be observed comparing patients to healthy volunteers or comparing untreated to 6-OHDA lesioned rats. Administration of levodopa did not alter measured glutamate levels in patients or in the 6-OHDA treated animals. Most evidence of activation of glutamate systems in the basal ganglia refers to extracellular or synaptic glutamate and is interpreted as increased glutamatergic transmission (Meshul, Emre et al. 1999; Jonkers, Sarre et al. 2002; Bruet, Windels et al. 2003; Robelet, Melon et al. 2004). MRS measures the total pool of glutamate which is around 10 mmolar in the brain (Govindaraju, Young et al. 2000) and represents mainly the intracellular pool, the extracellular glutamate levels being on the order of 2 to 3 μmol (Fillenz 2005). Our results indicate that changes in glutamate transmission in the striatum as response to dopamine depletion or to levodopa administration are not reflected by important changes of the total glutamate pool.

In the Parkinson patient a tendency of decreased total creatine has been measured; in the animal model a tendency of decreased total choline. Human MRS studies in the literature present incoherent results and it is difficult to draw clear conclusions (Clarke and Lowry 2001). Proton MRS studies of the 6-OHDA rat model have (to our knowledge) not been published before. Creatine decrease in human PD as well as choline decrease in the animal model should be confirmed by increasing the number of measurements. Implication of the metabolites readily measured by *in vivo* MRS (total choline, total creatine, NAA) in Parkinson's disease is not clear, but decrease of these metabolites is often related to neuronal death and membrane degeneration. Principles underlying degeneration of dopaminergic neurons in the animal model and in Parkinson's disease are probably very different, which may explain the above mentioned differences found in this work between human PD and animal model. In PCA extracts of the 6-OHDA lesioned rats decreased taurine and increased GABA levels were found ipsilateral as compared to the contralateral side. Further studies should try to confirm this observed tendency and as well compare to untreated control animals. Results might offer an interesting perspective for further studies, as GABA and taurine could be measured, for example, *in vivo* using editing sequences.

8 Annex

8.1 Chemical shifts and coupling constants of some brain metabolites

In this section, chemical shifts and coupling constants for glutamate, glutamine, n-acetylaspartate (NAA) and γ -aminobutyric acid have been summarized, as taken from (Govindaraju, Young et al. 2000). Index numbers for the spins are as labeled in the graphical representation of the molecules in Fig. 1.1, chapter 1. As can be seen from the chemical shift values, the preferable spectral region for glutamate measurement is situated near 2.3 ppm. At 3.7 ppm glutamate and glutamine overlap almost inseparably. The last two columns to the right in Table 8.1 give information about the coupling behavior at 3 Tesla and at 7 Tesla field strengths. Coupling behavior between two spins, I and S, may be considered as weak if

$$|\nu_I - \nu_S| \gg J_{IS} \quad (8.1)$$

Here, ν_I and ν_S correspond to the resonance frequency of the spin labeled I or S, J_{IS} indicates the coupling constant between I and S. In the two columns to the right of Table 8.1, the ratio $\frac{|\nu_I - \nu_S|}{J_{IS}}$ has been calculated for the two spins indicated in the corresponding line of the table. In general, the spectral pattern of coupled spins corresponds well enough to that of weakly coupled spins if this ratio is bigger than ten. Values smaller than or close to ten have been indicated in Table 8.1. At 3 Tesla field strength the spin groups of glu, gln, NAA and GABA resonating in the targeted chemical shift range near 2.3 ppm have to be considered strongly coupled. At 7 Tesla, glutamine (as glutamate) is at the limit to weak coupling behavior for most of its spins. GABA may be considered weakly coupled, but the two spins of NAA resonating at 2.5 ppm and 2.7 ppm remain strongly coupled.

Table 8.1: Chemical shifts and coupling constants for glutamate, glutamine, n-acetylaspartate (NAA) and γ -aminobutyric acid (GABA) (Govindaraju, Young et al. 2000). The two columns to the right give information about the coupling behavior (strong or weak) at 3 Tesla and 7 Tesla field strengths. Couplings to be considered as strong or at the limit to strong coupling have been distinguished by bold italic digits.

Metabolite	spin I index	spin S index	$\delta(I)$ [ppm]	$\delta(S)$ [ppm]	J [Hz]	coupling at 126 MHz, 3 T	coupling at 298 MHz, 7 T
glutamate	2	3	3,7433	2,0375	7,331	29,3	69,3
	2	3'	3,7433	2,12	4,651	44,0	104,0
	3	3'	2,0375	2,12	14,849	<i>0,7</i>	<i>1,7</i>
	3	4'	2,0375	2,352	8,406	<i>4,7</i>	<i>11,1</i>
	3'	4'	2,12	2,352	6,875	<i>4,3</i>	<i>10,1</i>
	3	4	2,0375	2,3378	6,413	<i>5,9</i>	14,0
	3'	4	2,12	2,3378	8,478	<i>3,2</i>	<i>7,7</i>
	4	4'	2,3378	2,352	15,915	<i>0,1</i>	<i>0,3</i>
glutamine	2	3	3,753	2,129	5,847	35,0	82,8
	2	3'	3,753	2,109	6,5	31,9	75,4
	3	3'	2,129	2,109	14,504	<i>0,2</i>	<i>0,4</i>
	3	4'	2,129	2,454	6,347	<i>6,5</i>	15,3
	3'	4'	2,109	2,454	9,209	<i>4,7</i>	<i>11,2</i>
	3	4	2,129	2,432	9,165	<i>4,2</i>	<i>9,9</i>
	3'	4	2,109	2,432	6,324	<i>6,4</i>	15,2
	4	4'	2,432	2,454	15,371	<i>0,2</i>	<i>0,4</i>
NAA aspartate moiety	2	3	4,3817	2,6727	3,861	55,8	131,9
	2	3'	4,3817	2,4863	9,821	24,3	57,5
	3	3'	2,6727	2,4863	15,592	<i>1,5</i>	<i>3,6</i>
	NH	2	7,8205	4,3817	6,4	67,7	160,1
GABA	2	3	3,0128	1,889	5,372	26,4	62,3
	2	3'	3,0128	1,889	7,127	19,9	47,0
	2'	3	3,0128	1,889	10,578	13,4	31,7
	2'	3'	3,0128	1,889	6,982	20,3	48,0
	3	4	1,889	2,284	7,755	<i>6,4</i>	15,2
	3	4'	1,889	2,284	7,432	<i>6,7</i>	15,8
	3'	4	1,889	2,284	6,173	<i>8,1</i>	19,1
	3'	4'	1,889	2,284	7,933	<i>6,3</i>	14,8

8.2 Metabolite concentrations in the rat brain: Literature values

A literature research was performed to find reference values for the concentration of different metabolites in the rat brain. From values published by different authors, average values were calculated and used for the evaluation of *in vitro* experiments and simulations. The values of Table 8.3 represent an approximation for average concentrations found in the brain, in specific structures concentrations may differ.

Table 8.2: Values for concentrations of different metabolites as found in the literature for the rat brain, not distinguishing between different brain structures.

Author	(Hawkins, Miller et al. 1973)	(Hindfelt and Siesjo 1971)	(Hindfelt, Plum et al. 1977)	(Marcucci, Mussini et al. 1966)
Unit	mmol/kg w.wt	mmol/kg w.wt	mmol/kg w.wt	mmol/kg w.wt
Analysis	removed brain, enzymatic	removed brain, enzymatic	cranial funnel, enzymatic	removed brain, gas chromatography
[glu]	11.6 ± 0.1	11.82 ± 0.018	10.66 ± 0.28	Not available
[gln]	6.71 ± 0.2	Not available	5.36 ± 0.67	Not available
[NAA]	Not available	Not available	Not available	9.48
[GABA]	Not available	Not available	1.65+/- 0.13	Not available

Author	(Miyake and Kakimoto 1981)	(Perry, Hansen et al. 1981)	(Sager, Laursen et al. 1999)	(Remy, Arus et al. 1994)
Unit	mmol/kg w.wt	mmol/kg w.wt	mmol/kg w.wt	mmol/kg w.wt.
Analysis	removed brain, gas chromatography	removed brain, chromatography	removed brain, HPLC	removed brain, NMR PCA extract
[glu]	Not available	11.29 +/-0.37	Not available	Not available
[gln]	Not available	4.51 +/- 0.15	Not available	Not available
[NAA]	9.19	Not available	7.96 +/- 1.43	Not available
[GABA]	Not available	1.79 +/- 0.07	Not available	Not available
[tau]	Not available	3.92 +/- 0.17	Not available	Not available
[MyoIns]	Not available	Not available	Not available	5.82 +/- 0.27
[tCho]	Not available	Not available	Not available	1.27 +/- 0.28

Author	(Veech, Harris et al. 1973)	(Ponten, Ratcheson et al. 1973)
Unit	mmol/kg w.wt	mmol/kg w.wt
Analysis	freeze blowing	cranial funnel
tCr	9.17 +/- 0.12	10.56 +/- 0.18

Table 8.3: Rat brain metabolite concentrations assumed in this work, as calculated from Table 8.2. The mean values for each metabolite have been determined.

Metabolite	glu	gln	NAA	GABA	tau	myoIns	tCho	tCr
mmol / kg w.wt.	11.3	5.5	8.9	1.7	3.92	5.82	1.27	9.87

8.3 TE averaged PRESS at 7 Tesla: Numerical simulations

Our *in vitro* experiments conducted at seven Tesla field strength, as presented in chapter 4, show that TE averaged PRESS does perform less well than predicted by numerical simulations (Hurd, Sailasuta et al. 2004). In this section we use numerical simulations to study the influence of different parameters on the quality of TE averaged PRESS spectra.

8.3.1 Materials and Methods

Simulations were performed using the C++ library Gamma (Smith, Levante et al. 1994) under GNU's gcc in a Linux environment. Simulation of the PRESS sequence used shaped pulses and simulated signal acquisition from a volume selected within a larger sample. Spoiler gradients are difficult to program because of the limited number of spin systems that can be simulated within the sample volume. Our simulator used exocycle phase cycling of the refocusing pulses instead to remove signal originating from not refocused magnetization in the spectrum.

Calculations simulated an acquisition volume of $(15 \text{ mm})^3$ selected within a cubic sample of 6 cm side length and seven Tesla magnetic field strength. The sample contained $(64)^3$ spin systems, allowing to achieve a spatial resolution of about 1 mm. We simulated 3 lobe sinc pulses of 1.18 ms length for excitation and of 0.9 ms for refocusing. An acquisition spectral width of 5000 Hz on 4096 points was assumed. TE averaged PRESS spectra were calculated by adding 40 PRESS spectra with echo times starting at 35 ms and incremented by 10 ms from one PRESS spectrum to the next. The echo time increment was equally separated between first and second echo time. TE averaged PRESS spectra using these parameters were calculated from the molecules of glutamate, glutamine, NAA and GABA. Chemical shift and J-coupling values for glu and gln were taken from (Thompson and Allen 1998), for NAA and GABA from (Govindaraju, Young et al. 2000). To shorten calculation time, the uncoupled spins of NAA resonating at 2.0 ppm were excluded in the calculation of the NAA spectrum. An exponential signal decay corresponding to a linewidth of 19 Hz in f_2 was simulated by multiplication of the signal with the corresponding exponential function. To study the influence of T_2 relaxation in t_1 , TE averaged PRESS spectra were calculated from this data set once without simulating relaxation in t_1 , once assuming a T_2 of 170 ms (de Graaf 1998).

Further calculations were performed simulating the rf pulses as ideal rotation operators instead of simulating shaped pulses. For these spectra, no T_2 decay in t_1 was assumed.

The spectra calculated from the different molecules were weighed with the *in vivo* metabolite concentration assumed for the respective molecule (see section 8.2). We assume a concentration of 11.3 mmol/kg w.wt for glutamate, 5.5 mmol/kg w.wt for

glutamine, 8.9 mmol/kg w.wt for NAA and 1.7 mmol/kg w.wt for GABA. In all spectra, the y-scale has been chosen to set the glutamate signal to the intensity of one.

On a PC with a Pentium 3 GHz processor, calculation of one PRESS spectrum using shaped pulses and volume selection took about one hour.

8.3.2 Results

In the following figures, glutamate has been plotted as dotted, glutamine as dashed and NAA as dash-dotted line. GABA has been printed as dash-dot-dot line and the sum of all metabolites as solid line. The preeminent singlet signal of NAA at 2 ppm is missing as this spin group was not included in the simulations.

Fig. 8.1 shows the spectra simulated with ideal rotation operators as rf pulses and no T_2 decay in t_1 . Almost no glutamine signal is visible in the spectrum; the sum signal (solid line) is dominated by contributions of glutamate and GABA. Fig. 8.2 shows the results of calculations using shaped pulses and simulating the acquisition from a volume selected within a larger sample. No T_2 decay in t_1 was assumed. As compared to Fig. 8.1, a well visible glutamine signal is present in the spectrum. Fig. 8.3 uses the same data set as Fig. 8.2, but here a T_2 of 170 ms in t_1 has been simulated. This exponential apodization in t_1 leads to an even more pronounced glutamine signal, as compared to Fig. 8.2. The spectra of glutamate, GABA and NAA exhibit only small changes as compared to glutamine.

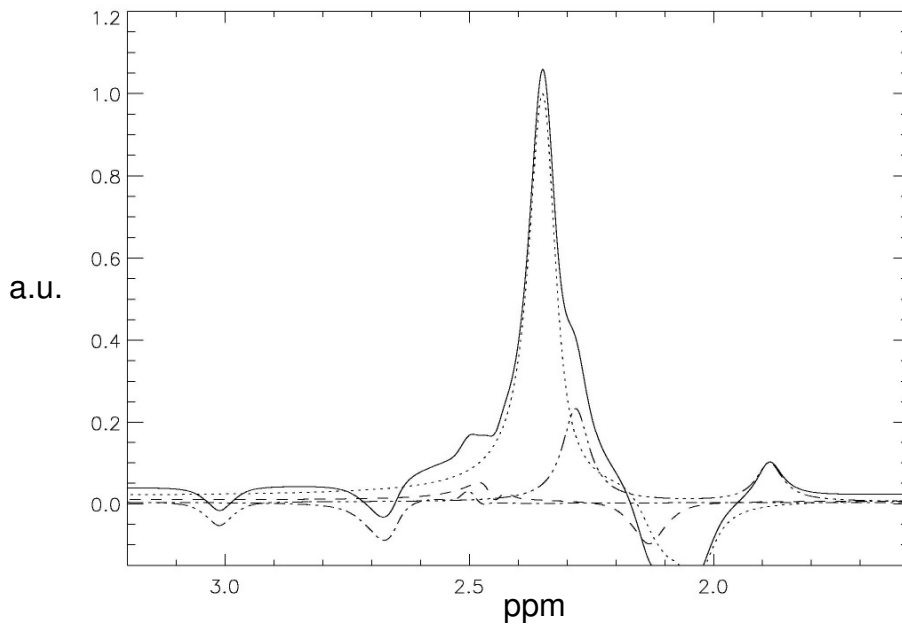


Fig. 8.1: TE averaged PRESS spectra simulated for glutamate (dotted), glutamine (dashed), NAA (dash-dot) and GABA (dash- 3 dots), assuming ideal rotation operators for rf pulses and no T_2 decay in t_1 at seven Tesla field strength. Almost no glutamine signal is visible; the sum signal (solid line) contains almost only glutamate with a contribution of GABA. The NAA singlet at 2.0 ppm has been excluded from simulations to shorten duration of calculations.

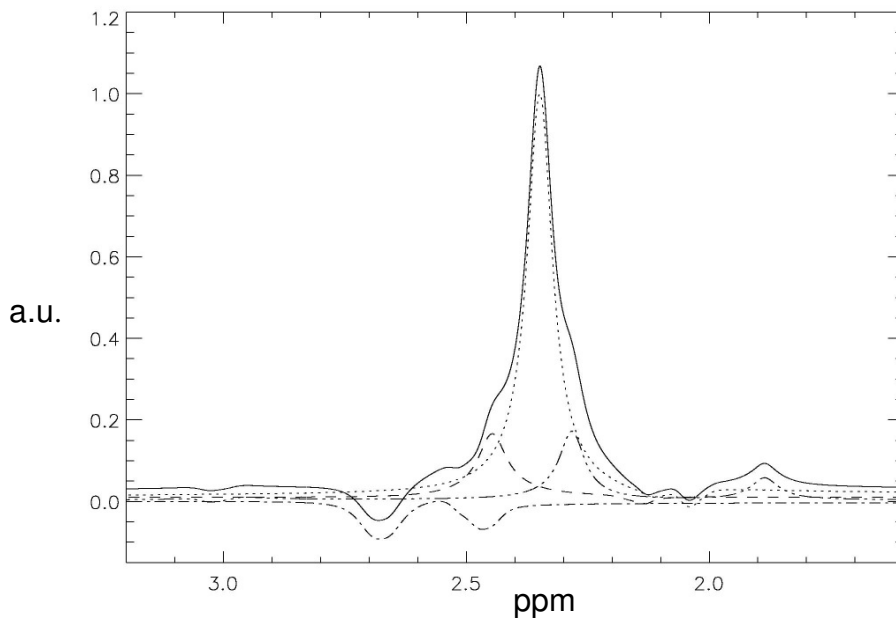


Fig. 8.2: TE averaged PRESS spectra simulated for glutamate (dotted), glutamine (dashed), NAA (dash-dot) and GABA (dash- 3 dots). Shaped pulses and acquisition from a cube within a larger sample volume at 7 Tesla field strength was simulated. No T_2 decay in t_1 was assumed. A well visible glutamine signal is present in the spectrum between 2.4 and 2.5 ppm (dashed line), next to the preminent glutamate signal at 2.35 ppm. The sum of glu, gln, NAA and GABA is presented as solid line. Volume selection and possibly coherence transfer caused by shaped pulses result in increased glutamine contribution.

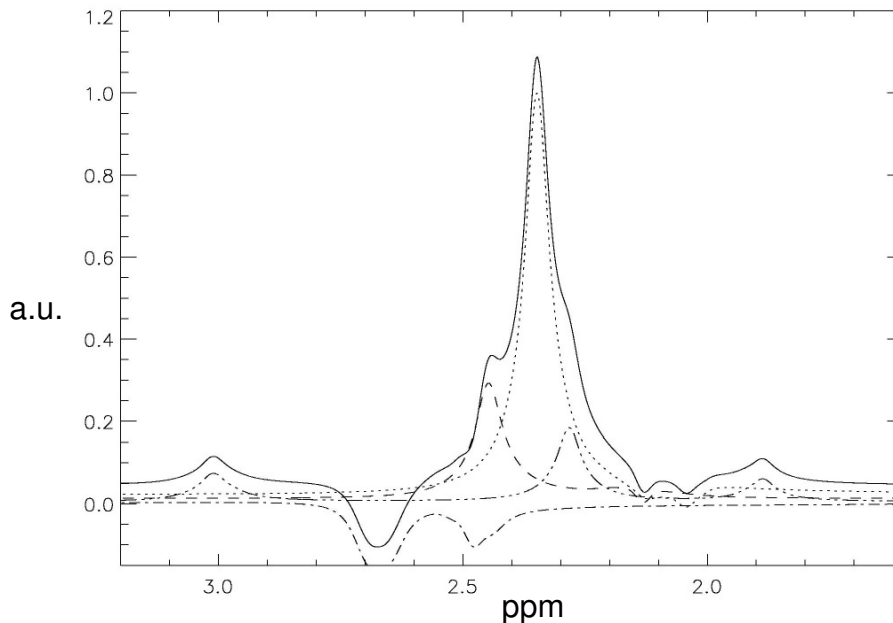


Fig. 8.3: Spectrum using the same data set as for Fig. 8.2, but simulating a T_2 of 170 ms in t_1 . An increased glutamine signal as compared to Fig. 8.2 is visible between 2.4 and 2.5 ppm. The sum of glu, gln, NAA and GABA is presented as solid line. Increase in T_2 relaxation increases the glutamine content in the spectrum.

8.3.3 Discussion

The results presented in this section help to understand how shaped pulses and T_2 relaxation influence TE averaged PRESS spectra, especially the possibility to measure an unobstructed glutamate signal.

Different authors have described the influence of shaped pulses on the evolution of coupled spins (Slotboom and Mehlkopf 1994; Thompson and Allen 1999; Thompson and Allen 2001). Shaped pulses alter the coupling evolution because of coherence transfer taking place during their application. Of further influence is the volume selection. The volumes selected for spin groups presenting different chemical shifts of the same molecule do not coincide. Volumes in which only some, but not all spins of the molecule, have been excited, experience altered coupling evolution as compared to the rest of the voxel. As can be seen comparing Fig. 8.1 and Fig. 8.2, these effects diminish the possibility to acquire an unobstructed glutamate signal using the TE averaged PRESS sequence. A contingent of magnetization exists for glutamine that does not evolve in t_1 and remains on the $f_1 = 0$ axis if shaped pulses and volume selection are used. Transverse relaxation (T_2) reduces resolution in the f_1 dimension. A part to the glutamine signal getting stronger in the TE averaged spectrum of Fig. 8.3 as compared to Fig. 8.2 can be imagined as tail from a glutamine cross peak, extending towards the $f_1 = 0$ axis with increased T_2 relaxation.

8.4 Press at 7 Tesla and an echo time of 136 ms: Experiments on metabolites in solution

In this section, results from *in vitro* experiments at 7 Tesla field strengths performed on metabolite solutions of glutamate, glutamine, NAA or GABA are presented. The same acquisition parameters as for the study described in chapter 6 have been used. The spectrum shown in this section should give information about the peak composition observed *in vivo* during the animal study.

8.4.1 Materials and methods

Experiments on samples containing in solution either glutamate, glutamine, NAA or GABA (phosphate buffer containing 100 mmol/l metabolite, 0.2 mmol/l chelated Gadolinium complex, 37 mmol/l TSP) have been performed as described in further detail in section 4.2.1. As for the *in vivo* experiments of chapter 6, we have used an echo time of 136 ms, acquiring the complete echo signal on 1024 points with a bandwidth of 10 kHz. The signal of 64 scans was accumulated during acquisition.

Postprocessing used the IDL programming language. Zero filling to a total of 4096 points was performed on both sides of the echo signal, followed by exponential broadening and first and second order phase correction. Differences between the metabolite spectra concerning linewidth (for example caused by differing shim quality), signal intensity (for example caused by slightly different coil loading factors) and frequency shift were corrected using the TSP signal as reference, see section 4.2.1. To compare to *in vivo* acquisitions, all spectra were then broadened with the same exponential function to obtain a linewidth of 22 Hz on the NAA singlet peak.

The spectra of glu, gln, NAA and GABA and their sum have been plotted assuming an *in vivo* concentration of 11.3 mmol/kg w. wt. for glu, 5.5 mmol/kg w. wt. for gln, 8.9 mmol/kg w. wt. for NAA and 1.7 mmol/kg w. wt. for GABA.

8.4.2 Results

Fig. 8.4 shows the spectra of glutamate, glutamine, NAA and GABA as well as their sum. The sum of these metabolites, forming a peak near 2.3 ppm (thin black line), should be comparable to the signal peak visible *in vivo* at the same position, compare to chapter 5. This sum signal contains mainly glutamate, but as well small contributions of glutamine and GABA. Contribution of NAA is less pronounced. As well visible is a contribution of glutamate to the signal measured at 2 ppm, dominated by NAA.

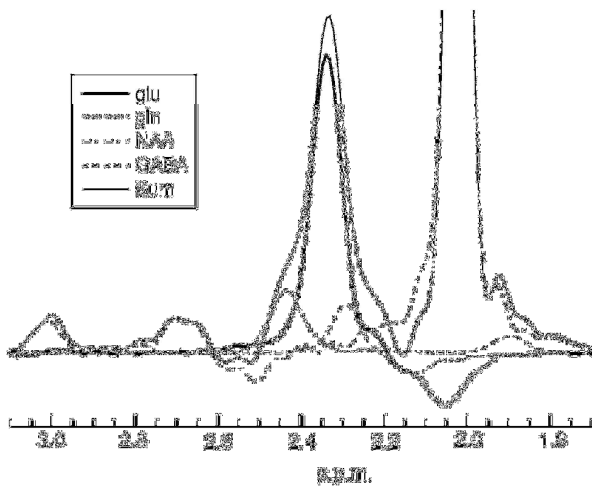


Fig. 8.4: Press spectra acquired at an echo time of 136 ms on samples containing either glutamate, glutamine, NAA or GABA. The sum peak (thin solid line) contains almost exclusively glutamate.

8.4.3 Discussion

The relative contributions of glu, gln, NAA and GABA to the signal visible in *in vivo* spectra may differ from the representation shown in Fig. 8.4. Relative concentrations assumed for the plot, as taken from the literature, may be different *in vivo* and depend on the examined brain region. Differences may furthermore be introduced by relaxation times T_1 and T_2 differing between *in vivo* and *in vitro* conditions. Acquisitions performed *in vivo* at 7 T field strengths and using a repetition time of 3 seconds work on partially saturated systems. Signals from metabolites with long T_1 are therefore weaker than signals from metabolites with shorter T_1 , even if present at the same concentration. *In vivo*, at 7 Tesla, T_1 values of different metabolites are however similar (de Graaf 1998). *In vitro*, because of the contrast agent added to the metabolite solution at high concentration, saturation effects should be negligible.

Relative peak amplitudes between metabolites vary as well due to different transverse relaxation times. As for T_1 , values for T_2 of different metabolites *in vivo* are similar (de Graaf 1998). *In vitro*, as the chemical environment in solution is the same for all metabolites, T_2 values should be close as well. Fig. 8.4 should therefore provide an acceptable approximation of *in vivo* conditions.

According to Fig. 8.4, PRESS spectra acquired at an echo time of 136 ms allow good estimation of glutamate, although its quantity is overestimated due to contributions of glutamine and GABA. About 80% of the peak surface of the signal at 2.3 ppm is due to glutamate.

Ideally, glutamate, glutamine, NAA and GABA should be separated for reliable glutamate measurement. PRESS spectra at an echo time of 136 ms allow however a good estimation.

9 References

- Abe, K., H. Terakawa, et al. (2000). "Proton magnetic resonance spectroscopy of patients with parkinsonism." Brain Res Bull **52**(6): 589-95.
- Antonini, A., K. L. Leenders, et al. (1993). "T2 relaxation time in patients with Parkinson's disease." Neurology **43**(4): 697-700.
- Baik, H. M., B. Y. Choe, et al. (2003). "Proton MR spectroscopic changes in Parkinson's diseases after thalamotomy." Eur J Radiol **47**(3): 179-87.
- Boumezbeur, F., L. Besret, et al. (2005). 1H NMR quantification of 11 metabolites in the brain at 3 Tesla. Proc. Intl. Soc. Magn. Reson. Med.
- Bowen, B. C., R. E. Block, et al. (1995). "Proton MR spectroscopy of the brain in 14 patients with Parkinson disease." AJNR Am J Neuroradiol **16**(1): 61-8.
- Brownell, A. L., B. G. Jenkins, et al. (1998). "Combined PET/MRS brain studies show dynamic and long-term physiological changes in a primate model of Parkinson disease." Nat Med **4**(11): 1308-12.
- Bruet, N., F. Windels, et al. (2003). "Neurochemical mechanisms induced by high frequency stimulation of the subthalamic nucleus: increase of extracellular striatal glutamate and GABA in normal and hemiparkinsonian rats." J Neuropathol Exp Neurol **62**(12): 1228-40.
- Camicioli, R. M., J. R. Korzan, et al. (2004). "Posterior cingulate metabolic changes occur in Parkinson's disease patients without dementia." Neurosci Lett **354**(3): 177-80.
- Chase, T. N., J. D. Oh, et al. (2000). "Antiparkinsonian and antidyskinetic activity of drugs targeting central glutamatergic mechanisms." J Neurol **247 Suppl 2**: II36-42.
- Chassain, C., G. Bielicki, et al. (2005). "Cerebral glutamate metabolism in Parkinson's disease: an in vivo dynamic (13)C NMS study in the rat." Exp Neurol **191**(2): 276-84.
- Choi, I. Y., S. P. Lee, et al. (2004). "Single-shot two-echo technique for simultaneous measurement of GABA and creatine in the human brain in vivo." Magn Reson Med **51**(6): 1115-21.
- Choi, I. Y., S. P. Lee, et al. (2005). "In vivo single-shot three-dimensionally localized multiple quantum spectroscopy of GABA in the human brain with improved spectral selectivity." J Magn Reson **172**(1): 9-16.
- Clarke, C. E. and M. Lowry (2000). "Basal ganglia metabolite concentrations in idiopathic Parkinson's disease and multiple system atrophy measured by proton magnetic resonance spectroscopy." Eur J Neurol **7**(6): 661-5.
- Clarke, C. E. and M. Lowry (2001). "Systematic review of proton magnetic resonance spectroscopy of the striatum in parkinsonian syndromes." Eur J Neurol **8**(6): 573-7.

- Clarke, C. E., M. Lowry, et al. (1997). "Unchanged basal ganglia N-acetylaspartate and glutamate in idiopathic Parkinson's disease measured by proton magnetic resonance spectroscopy." Mov Disord **12**(3): 297-301.
- Corsi, C., A. Pinna, et al. (2003). "Adenosine A2A receptor antagonism increases striatal glutamate outflow in dopamine-denervated rats." Eur J Pharmacol **464**(1): 33-8.
- Cruz, C. J., M. J. Aminoff, et al. (1997). "Proton MR spectroscopic imaging of the striatum in Parkinson's disease." Magn Reson Imaging **15**(6): 619-24.
- Davie, C. A., G. K. Wenning, et al. (1995). "Differentiation of multiple system atrophy from idiopathic Parkinson's disease using proton magnetic resonance spectroscopy." Ann Neurol **37**(2): 204-10.
- de Graaf, R. A. (1998). In vivo NMR spectroscopy, Wiley.
- Deumens, R., A. Blokland, et al. (2002). "Modeling Parkinson's disease in rats: an evaluation of 6-OHDA lesions of the nigrostriatal pathway." Exp Neurol **175**(2): 303-17.
- Du, F., W. J. Chu, et al. (2004). "In vivo GABA detection with improved selectivity and sensitivity by localized double quantum filter technique at 4.1T." Magn Reson Imaging **22**(1): 103-8.
- Ellis, C. M., G. Lemmens, et al. (1997). "Changes in putamen N-acetylaspartate and choline ratios in untreated and levodopa-treated Parkinson's disease: a proton magnetic resonance spectroscopy study." Neurology **49**(2): 438-44.
- Ernst, R., G. Bodenhausen, et al. (1987). Principles of nuclear magnetic resonance in one and two dimensions, Oxford Science Publications.
- Federico, F., I. L. Simone, et al. (1997). "Proton magnetic resonance spectroscopy in Parkinson's disease and atypical parkinsonian disorders." Mov Disord **12**(6): 903-9.
- Fillenz, M. (2005). "In vivo neurochemical monitoring and the study of behaviour." Neurosci Biobehav Rev **29**(6): 949-62.
- Firbank, M. J., R. M. Harrison, et al. (2002). "A comprehensive review of proton magnetic resonance spectroscopy studies in dementia and Parkinson's disease." Dement Geriatr Cogn Disord **14**(2): 64-76.
- Fitzpatrick, S. M., H. P. Hetherington, et al. (1989). "Effects of acute hyperammonemia on cerebral amino acid metabolism and pH_i in vivo, measured by ¹H and ³¹P nuclear magnetic resonance." J Neurochem **52**(3): 741-9.
- Galeffi, F., L. Bianchi, et al. (2003). "The effect of 6-hydroxydopamine lesions on the release of amino acids in the direct and indirect pathways of the basal ganglia: a dual microdialysis probe analysis." Eur J Neurosci **18**(4): 856-68.
- Geen, H. and R. Freeman (1991). "Band-selective radiofrequency pulses." Journal of Magnetic Resonance **93**: 93-141.
- Gibb, W. R. and A. J. Lees (1988). "The relevance of the Lewy body to the pathogenesis of idiopathic Parkinson's disease." J Neurol Neurosurg Psychiatry **51**(6): 745-52.
- Govindaraju, V., V. J. Basus, et al. (1998). "Measurement of chemical shifts and coupling constants for glutamate and glutamine." Magn Reson Med **39**(6): 1011-3.

- Govindaraju, V., K. Young, et al. (2000). "Proton NMR chemical shifts and coupling constants for brain metabolites." NMR Biomed **13**(3): 129-53.
- Graham, J. M., M. N. Paley, et al. (2000). "Brain iron deposition in Parkinson's disease imaged using the PRIME magnetic resonance sequence." Brain **123 Pt 12**: 2423-31.
- Gruetter, R. (1993). "Automatic, localized in vivo adjustment of all first- and second-order shim coils." Magn Reson Med **29**(6): 804-11.
- Hakumäki, J. M., M. Ala-Korpela, et al. (1997). "¹H nuclear magnetic resonance spectroscopy: noninvasive neurochemistry for basic research and clinical applications." Current topics in Neurochemistry **1**: 59-85.
- Hawkins, R. A., A. L. Miller, et al. (1973). "The acute action of ammonia on rat brain metabolism in vivo." Biochem J **134**(4): 1001-8.
- Henning, J. (1992). "The application of phase rotation for localized in vivo proton spectroscopy with short echo times." J Magn Reson **96**: 40-49.
- Hindfelt, B., F. Plum, et al. (1977). "Effect of acute ammonia intoxication on cerebral metabolism in rats with portacaval shunts." J Clin Invest **59**(3): 386-96.
- Hindfelt, B. and B. K. Siesjo (1971). "Cerebral effects of acute ammonia intoxication. II. The effect upon energy metabolism." Scand J Clin Lab Invest **28**(3): 365-74.
- Hirsch, E. C., C. Perier, et al. (2000). "Metabolic effects of nigrostriatal denervation in basal ganglia." Trends Neurosci **23**(10 Suppl): S78-85.
- Hoang, T. Q., S. Bluml, et al. (1998). "Quantitative proton-decoupled ³¹P MRS and ¹H MRS in the evaluation of Huntington's and Parkinson's diseases." Neurology **50**(4): 1033-40.
- Holshouser, B. A., M. Komu, et al. (1995). "Localized proton NMR spectroscopy in the striatum of patients with idiopathic Parkinson's disease: a multicenter pilot study." Magn Reson Med **33**(5): 589-94.
- Hornykiewicz, O. (2001). "Parkinson Disease." Nature Encyclopedia of Life Sciences.
- Hu, M. T., S. D. Taylor-Robinson, et al. (1999). "Evidence for cortical dysfunction in clinically non-demented patients with Parkinson's disease: a proton MR spectroscopy study." J Neurol Neurosurg Psychiatry **67**(1): 20-6.
- Hurd, R., N. Sailasuta, et al. (2004). "Measurement of brain glutamate using TE-averaged PRESS at 3T." Magn Reson Med **51**(3): 435-40.
- Ingham, C. A., S. H. Hood, et al. (1993). "Morphological changes in the rat neostriatum after unilateral 6-hydroxydopamine injections into the nigrostriatal pathway." Exp Brain Res **93**(1): 17-27.
- Jang, D. P., J. M. Lee, et al. (2005). "Interindividual reproducibility of glutamate quantification using 1.5-T proton magnetic resonance spectroscopy." Magn Reson Med **53**(3): 708-12.
- Jonkers, N., S. Sarre, et al. (2002). "MK801 suppresses the L-DOPA-induced increase of glutamate in striatum of hemi-Parkinson rats." Brain Res **926**(1-2): 149-55.
- Jouvensal, L., P. G. Carlier, et al. (1996). "Practical implementation of single-voxel double-quantum editing on a whole-body NMR spectrometer: localized monitoring of lactate in the human leg during and after exercise." Magn Reson Med **36**(3): 487-90.

- Keltner, J. R., L. L. Wald, et al. (1997). "In vivo detection of GABA in human brain using a localized double-quantum filter technique." *Magn Reson Med* **37**(3): 366-71.
- Keltner, J. R., L. L. Wald, et al. (1998). "A localized double-quantum filter for the in vivo detection of brain glucose." *Magn Reson Med* **39**(4): 651-6.
- Kim, H. and P. S. Allen (2003). *Brain metabolite discrimination in proton spectroscopy: Illustration with myo-inositol*. ISMRM, Toronto.
- Kish, S. J., A. Rajput, et al. (1986). "Elevated gamma-aminobutyric acid level in striatal but not extrastriatal brain regions in Parkinson's disease: correlation with striatal dopamine loss." *Ann Neurol* **20**(1): 26-31.
- Kosta, P., M. I. Argyropoulou, et al. (2005). "MRI evaluation of the basal ganglia size and iron content in patients with Parkinson's disease." *J Neurol*.
- Lang, A. E., A. M. Lozano, et al. (1997). "Posteroventral medial pallidotomy in advanced Parkinson's disease." *N Engl J Med* **337**(15): 1036-42.
- Lee, H. K., A. Yaman, et al. (1995). "Homonuclear J-refocused spectral editing technique for quantification of glutamine and glutamate by ¹H NMR spectroscopy." *Magn Reson Med* **34**(2): 253-9.
- Lei, H. and J. Peeling (1999). "A localized double-quantum filter for in vivo detection of taurine." *Magn Reson Med* **42**(3): 454-60.
- Lucetti, C., P. Del Dotto, et al. (2001). "Proton magnetic resonance spectroscopy (1H-MRS) of motor cortex and basal ganglia in de novo Parkinson's disease patients." *Neurol Sci* **22**(1): 69-70.
- Marcucci, F., E. Mussini, et al. (1966). "Distribution of N-acetyl-L-aspartic acid in rat brain." *J Neurochem* **13**(11): 1069-70.
- Marino, M. J., O. Valenti, et al. (2003). "Glutamate receptors and Parkinson's disease: opportunities for intervention." *Drugs Aging* **20**(5): 377-97.
- Mayer, D. and D. M. Spielman (2005). "Detection of glutamate in the human brain at 3 T using optimized constant time point resolved spectroscopy." *Magn Reson Med* **54**(2): 439-42.
- McLean, M. A., A. L. Busza, et al. (2002). "In vivo GABA+ measurement at 1.5T using a PRESS-localized double quantum filter." *Magn Reson Med* **48**(2): 233-41.
- Meshul, C. K., J. P. Cogen, et al. (2000). "Alterations in rat striatal glutamate synapses following a lesion of the cortico- and/or nigrostriatal pathway." *Exp Neurol* **165**(1): 191-206.
- Meshul, C. K., N. Emre, et al. (1999). "Time-dependent changes in striatal glutamate synapses following a 6-hydroxydopamine lesion." *Neuroscience* **88**(1): 1-16.
- Miyake, M. and Y. Kakimoto (1981). "Developmental changes of N-acetyl-L-aspartic acid, N-acetyl-alpha-aspartylglutamic acid and beta-citryl-L-glutamic acid in different brain regions and spinal cords of rat and guinea pig." *J Neurochem* **37**(4): 1064-7.
- Morari, M., M. Marti, et al. (1998). "Reciprocal dopamine-glutamate modulation of release in the basal ganglia." *Neurochem Int* **33**(5): 383-97.
- Naressi, A., C. Couturier, et al. (2001). "Java-based graphical user interface for the MRUI quantitation package." *Magma* **12**(2-3): 141-52.

- Obeso, J. A., M. C. Rodriguez-Oroz, et al. (2000). "Pathophysiology of levodopa-induced dyskinesias in Parkinson's disease: problems with the current model." Ann Neurol **47**(4 Suppl 1): S22-32; discussion S32-4.
- Obeso, J. A., M. C. Rodriguez-Oroz, et al. (2000). "Pathophysiology of the basal ganglia in Parkinson's disease." Trends Neurosci **23**(10 Suppl): S8-19.
- O'Neill, J., N. Schuff, et al. (2002). "Quantitative ¹H magnetic resonance spectroscopy and MRI of Parkinson's disease." Mov Disord **17**(5): 917-27.
- Pan, J. W., G. F. Mason, et al. (1996). "Spectroscopic imaging of human brain glutamate by water-suppressed J-refocused coherence transfer at 4.1 T." Magn Reson Med **36**(1): 7-12.
- Perry, T. L., S. Hansen, et al. (1981). "Postmortem changes of amino compounds in human and rat brain." J Neurochem **36**(2): 406-10.
- Pfeuffer, J., I. Tkac, et al. (1999). "Toward an in vivo neurochemical profile: quantification of 18 metabolites in short-echo-time (¹H) NMR spectra of the rat brain." J Magn Reson **141**(1): 104-20.
- Podell, M., M. Hadjiconstantinou, et al. (2003). "Proton magnetic resonance imaging and spectroscopy identify metabolic changes in the striatum in the MPTP feline model of parkinsonism." Exp Neurol **179**(2): 159-66.
- Ponten, U., R. A. Ratcheson, et al. (1973). "Optimal freezing conditions for cerebral metabolites in rats." J Neurochem **21**(5): 1127-38.
- Provencher, S. W. (1993). "Estimation of metabolite concentrations from localized in vivo proton NMR spectra." Magn Reson Med **30**(6): 672-9.
- Provent, P., N. Kickler, et al. (2005). In vivo H1 NMR spectroscopy shows that a brief infusion of ammonium can cause an increase in lactate in rat brain that is rapid, reversible and repeatable. 22th annual meeting of European Society for Magnetic Resonance In Medicine and Biology, Basel (CH), ESMRMB.
- Remy, C., C. Arus, et al. (1994). "In vivo, ex vivo, and in vitro one- and two-dimensional nuclear magnetic resonance spectroscopy of an intracerebral glioma in rat brain: assignment of resonances." J Neurochem **62**(1): 166-79.
- Richter, W. and S. W. Warren (2000). "Intermolecular multiple quantum coherences in liquids." Concepts Magn Reson **12**(6): 396-409.
- Robelet, S., C. Melon, et al. (2004). "Chronic L-DOPA treatment increases extracellular glutamate levels and GLT1 expression in the basal ganglia in a rat model of Parkinson's disease." Eur J Neurosci **20**(5): 1255-66.
- Ross, B. D., T. Q. Hoang, et al. (1999). "In vivo magnetic resonance spectroscopy of human fetal neural transplants." NMR Biomed **12**(4): 221-36.
- Sager, T. N., H. Laursen, et al. (1999). "N-Acetylaspartate distribution in rat brain striatum during acute brain ischemia." J Cereb Blood Flow Metab **19**(2): 164-72.
- Schmidt, W. J. (1998). "Dopamine-glutamate interactions in the basal ganglia." Amino Acids **14**(1-3): 5-10.
- Schubert, F., J. Gallinat, et al. (2004). "Glutamate concentrations in human brain using single voxel proton magnetic resonance spectroscopy at 3 Tesla." Neuroimage **21**(4): 1762-71.

- Schubert F, S. F., Rinneberg H (2001). Determination of glutamate in human brain at 3 Tesla using PRESS and a multiple quantum filter. Proc. Intl. Soc. Mag. Reson. Med 9.
- Schulte, R. F., A. H. Trabesinger, et al. (2005). "Chemical-shift-selective filter for the in vivo detection of J-coupled metabolites at 3T." Magn Reson Med **53**(2): 275-81.
- Shen, J., D. L. Rothman, et al. (2002). "In vivo GABA editing using a novel doubly selective multiple quantum filter." Magn Reson Med **47**(3): 447-54.
- Slotboom, J. and A. F. Mehlkopf (1994). "The Effects of Frequency-Selective RF Pulses on J-Coupled Spin 1/2 Systems." J Magn Reson A **108**: 38-50.
- Smith, S. A., T. O. Levante, et al. (1994). "Computer simulations in magnetic resonance. An object oriented programming approach." J Magn Reson A **106**: 75-105.
- Swanson, L. W. (1998/1999). Brain maps: Structure of the rat brain, 2nd edition. Amsterdam, Elsevier.
- Tanaka, Y., K. Nijjima, et al. (1986). "Changes in gamma-aminobutyrate, glutamate, aspartate, glycine, and taurine contents in the striatum after unilateral nigrostriatal lesions in rats." Exp Neurol **91**(2): 259-68.
- Taylor-Robinson, S. D., N. Turjanski, et al. (1999). "A proton magnetic resonance spectroscopy study of the striatum and cerebral cortex in Parkinson's disease." Metab Brain Dis **14**(1): 45-55.
- Tedeschi, G., I. Litvan, et al. (1997). "Proton magnetic resonance spectroscopic imaging in progressive supranuclear palsy, Parkinson's disease and corticobasal degeneration." Brain **120** (Pt 9): 1541-52.
- Thompson, R. B. and P. S. Allen (1998). "A new multiple quantum filter design procedure for use on strongly coupled spin systems found in vivo: its application to glutamate." Magn Reson Med **39**(5): 762-71.
- Thompson, R. B. and P. S. Allen (1999). "Sources of variability in the response of coupled spins to the PRESS sequence and their potential impact on metabolite quantification." Magn Reson Med **41**(6): 1162-9.
- Thompson, R. B. and P. S. Allen (2001). "Response of metabolites with coupled spins to the STEAM sequence." Magn Reson Med **45**(6): 955-65.
- Tkac, I., P. Andersen, et al. (2001). "In vivo 1H NMR spectroscopy of the human brain at 7 T." Magn Reson Med **46**(3): 451-6.
- Tkac, I., Z. Starcuk, et al. (1999). "In vivo 1H NMR spectroscopy of rat brain at 1 ms echo time." Magn Reson Med **41**(4): 649-56.
- Traber, F., W. Block, et al. (2004). "1H metabolite relaxation times at 3.0 tesla: Measurements of T1 and T2 values in normal brain and determination of regional differences in transverse relaxation." J Magn Reson Imaging **19**(5): 537-45.
- Trabesinger, A. H. and P. Boesiger (2001). "Improved selectivity of double quantum coherence filtering for the detection of glutathione in the human brain in vivo." Magn Reson Med **45**(4): 708-10.
- Trabesinger, A. H., O. M. Weber, et al. (1999). "Detection of glutathione in the human brain in vivo by means of double quantum coherence filtering." Magn Reson Med **42**(2): 283-9.

- Vanhamme, L., A. van den Boogaart, et al. (1997). "Improved method for accurate and efficient quantification of MRS data with use of prior knowledge." J Magn Reson **129**(1): 35-43.
- Veech, R. L., R. L. Harris, et al. (1973). "Freeze-blowing: a new technique for the study of brain in vivo." J Neurochem **20**(1): 183-8.
- Wilman, A. H. and P. S. Allen (1993). "In Vivo NMR Detection strategies for γ -Aminobutyric Acid, Utilizing Proton Spectroscopy and Coherence-Pathway Filtering with Gradients." J Magn Reson A **101**: 165-71.
- Wilman, A. H. and P. S. Allen (1995). "Yield enhancement of a double-quantum filter sequence designed for the edited detection of GABA." J Magn Reson B **109**(2): 169-74.
- Ye, F. Q., P. S. Allen, et al. (1996). "Basal ganglia iron content in Parkinson's disease measured with magnetic resonance." Mov Disord **11**(3): 243-9.
- Yelnik, J. (2002). "Functional anatomy of the basal ganglia." Mov Disord **17 Suppl 3**: S15-21.
- Zhong, K. and T. Ernst (2004). "Localized in vivo human ¹H MRS at very short echo times." Magn Reson Med **52**(4): 898-901.
- Ziegler, A., M. Izquierdo, et al. (1995). "Optimization of homonuclear two-dimensional correlation methods for in vivo and ex vivo NMR." J Magn Reson B(107): 10-18.